Characterizing the Dynamics of Otto Glacier, Ellesmere Island, Canadian High Arctic: 1992-2020

by

Monika Wagner

A thesis

presented to the University of Waterloo

in fulfilment of the

thesis requirement for the degree of

Master of Science

in

Geography

Waterloo, Ontario, Canada, 2023

Author's Declaration

I hereby declare that I am the sole author of this thesis. This is a true copy of the thesis, including any required final revisions, as accepted by my examiners.

I understand that my thesis may be made electronically available to the public.

Abstract

The mass loss observed from glaciers in the Canadian Arctic is unprecedented over recent decades (Hugonnet et al., 2021) and is the third largest contributor to global sea level rise (Derksen et al., 2019). One way in which glaciers lose mass to the ocean is through dynamic discharge, which involves the calving of icebergs to the ocean. Glacier dynamics in the Canadian Arctic have undergone limited study, especially surge-type glaciers, which oscillate between periods of fast flow and slow flow. Detailed studies of individual surge-type glaciers can enhance knowledge of how and why glaciers surge. As such, this thesis analyzed the surge cycle of Otto Glacier on northern Ellesmere Island in Nunavut, Canada, from 1992-2020. The analysis included velocity measurements from 1992-2020, which used data from optical and radar imagery. Three phases were identified for the study period: the fast flow phase (1992-2008), the deceleration phase (2009-2017), and the quiescent phase (2018-2020). Maximum velocities occurred within the lowermost ~6 km of the glacier during the fast flow phase (700-1300 m/yr), and minimum velocities (1-80 m/yr) were noted along the entire glacier during the quiescent phase. Terminus extent, analyzed with optical and radar imagery, advanced by 1545 m during the fast flow phase, and retreated by 1408 m by the end of the quiescent phase. Rates of glacier surface elevation change, obtained from pre-generated elevation products by Hugonnet et al. (2021), showed surface elevation lowering in the lowermost ~6 km of the glacier and thickening upglacier that was progressive over the study period. Analysis of bedrock topography found a v-shaped sill spanning ~4-8 km upglacier from the terminus, which was inferred to have influenced terminus retreat, glacier thickness, and subsequently velocity variability. The findings provide a detailed characterization of the surge cycle phases for Otto Glacier and suggest a possible surge mechanism, which has not previously been explored in depth.

Acknowledgements

I would first like to acknowledge my supervisors, Dr. Ellsworth LeDrew and Dr. Wesley Van Wychen, who provided me the guidance necessary to conduct this research. Without their support, timely edits, and meetings, this thesis would not have been possible. I was also supported by their facilitation of conference and field work opportunities, which provided me valuable professional experience.

I would also like to express great appreciation to my lab group and friends, Courtney Bayer, Kristie Shannon, Natalija Nikolić, Danielle Hallé, and Lauren Samo, all of whom helped me learn the skills needed for data processing and analysis. This took time from their personal schedules for which I am very grateful. I would also like to acknowledge my colleagues and friends in the Cryosphere Office in the Faculty of Environment at the University of Waterloo who I worked with every day. They dedicated time to helping me troubleshoot software problems and automate data processing for which I am very appreciative.

Table of Contents

List of Figures

List of Tables

List of Equations

List of Abbreviations

AMI	Active Microwave Instrument
ASTER	Advanced Spaceborn Thermal Emission and Reflection Radiometer
auto-RIFT	Autonomous repeat image feature tracking
CReSIS	Centre for Remote Sensing of Ice Sheets
DEM	Digital elevation model
ERS	European Remote Sensing System
HH	Horizontal-horizontal
HV	Horizontal-vertical
InSAR	Synthetic Aperture Radar interferometry
MCoRDS	Multichannel Coherent Data Depth Sounder
m/yr	Meters per year
NCC	Normalized cross correlation
NDC	Normalized displacement coherence
MLI	Multi look image
R2	RADARSAT2
REMA	Reference Elevation Model of Antarctica
RGI	Randolph Glacier Inventory
SAR	Synthetic Aperture Radar
SLC	Single look complex
TanDEM-X	Terra SARX add on for Digital Elevation Measurement
VH	Vertical-horizontal
VV	Vertical-vertical
w.e./yr	Water-equivalent per year

Chapter 1 - Introduction

1.1 Overview and Research Objectives

A significant increase in global air temperature at a rate of 0.03°K/yr has been reported over the 2000-2019 period (Hugonnet et al., 2021), resulting in environmental consequences across the Arctic (Fisher et al., 2012). Specifically, Arctic air temperatures are warming faster than regions elsewhere, which is attributed to 'Arctic amplification' and may be related to an increase in pole-ward heat advection in response to rising global temperatures (Fisher et al., 2012). The increase in temperatures has been associated with environmental consequences for Canada as a whole. For example, snow cover in Canada since 1981 has decreased between 5% and 10% per decade as a result of later snow initiation and early spring melt (Mudryk et al., 2018). It is projected that snow cover duration is very likely to decline into the end of the century, with stabilized snow loss under a medium emission scenario and persistent loss under a high emission scenario (Brown et al., 2017). Sea ice has also thinned since 1968 and summer sea ice cover has declined at a rate of 5%-20% per decade across the Canadian Arctic (Canadian Ice Service Digital Archive as cited in Derksen et al., 2019). It is very likely that increasing temperatures under all emission scenarios will result in continued summer reductions in sea ice across the Canadian Arctic (Derksen et al., 2019), especially under the high emission scenario, where widespread reduction in sea ice cover is expected for summer (ice melt season) and fall (ice formation season) (Mudryk et al., 2018). By the summer of 2050, it is very likely that most Canadian Arctic marine regions will be sea-ice free (Derksen et al., 2019). The duration of seasonal lake ice cover has also declined across Canada for the past 50 years due to early spring break up and later ice formation in the fall (Brown and Duguay, 2010; Wang et al., 2012). Under a medium emission scenario, spring lake ice breakup will likely occur 10 to 25 days earlier by mid-century, and ice formation in the fall is likely to be 5-15 days later (Brown and Duguay, 2010; Dibike et al., 2012). Permafrost stability is also at risk. Over the past 40 years, permafrost temperature has increased by 0.3°C to 0.5°C per decade in the high Arctic (Romanovsky et al., 2017). Increase in mean air

temperature overlying permafrost is projected under all emission scenarios, which will continue driving permafrost thaw into mid-century (Derksen et al., 2019).

The projected changes in the cryosphere are of serious concern to humans and natural ecosystems. For example, seals and polar bears rely on sea ice for breeding and feeding (Derksen et al., 2019). Sea ice cover affects algae growing season, water temperatures, oxygen levels, passageways used by wildlife to cross water bodies (Derksen et al., 2019). Breakup of sea/lake ice impacts shipping and offshore operations (Pizzolato et al., 2016). Freshwater supply from snow and glaciers is relevant to human economy, agriculture, and drinking water security (Sturm et al., 2017). Melting of ice roads interferes with transportation (Sturm et al., 2016). Cryosphere instability also contributes to hazards such as spring flooding, avalanches, and landscape instability due to permafrost thaw (AMAP, 2017). Permafrost thaw also releases greenhouse gases contributing to climate change (Olefeldt et al., 2016). Cryosphere stability is also foundational to the traditional ways of life for Indigenous communities particularly in the North (Derksen et al., 2019).

Glaciers in Canada have undergone unprecedented mass loss over recent decades (Hugonnet et al., 2021) and are the third largest contributors to global sea level rise (Derksen et al., 2019). From 2000 to 2019, global glacier mass loss accelerated by 48 +/- 16 Gt/yr per decade (Hugonnet et al., 2021). During this period, glacier mass loss was 47% larger than mass loss from the Greenland Ice Sheet and 200% larger than mass lost from the Antarctic Ice Sheet (Hugonnet et al., 2021). Figure 1-1 provides global glacier mass loss trends. Alaska accounts for 25% of mass lost during 2000-2019, followed by the Greenland Periphery contributing 13%, and Arctic Canada North and South each contributing 10% (Hugonnet et al., 2021). The Antarctic, Subantarctic, High Mountain Asia, and Southern Andes contribute 8% each. In the Southern Arctic (Alaska, Arctic Canada South, southern Greenland Periphery, Iceland, Scandinavia), mass loss was nearly triple that of more northerly latitudes at 0.74 +/- 0.1 m w.e./yr (Hugonnet et al., 2021). Non-polar regions experienced mass loss of 0.69 +/-0.11 m w.e./yr on average (except High Mountain Asia which

lost 0.22 +/- 0.05 m w.e./yr) (Hugonnet et al., 2021). The Antarctic and Subantarctic had the least mass loss at 0.17 +/- 0.04 m w.e./yr (Hugonnet et al., 2021). The pattern of glacier mass loss is coincident with increases in global temperature. The observed increase in air temperature at a rate of 0.03°K/yr for the 2000-2019 period is associated with a glacier mass balance sensitivity to temperature of -0.27 m w.e./yr/°K (Hugonnet et al., 2021). This association suggest that the glacier mass loss is a response to anthropogenic climate warming (Box et al., 2018; Hugonnet et al., 2021). Persistent changes to the cryosphere into midcentury are virtually certain, since temperatures are projected to increase under all emission scenarios (Derksen et al., 2019). Under a moderate emission scenario, glaciers across the Western Cordillera are projected to lose 74% to 96% of their volume by late century (Derksen et al., 2019). Subsequent decline in glacial meltwater to rivers and streams is projected for the mid-century, with later impacts on freshwater availability for humans (Derksen et al., 2019). Most small ice caps and ice shelves in the Canadian Arctic are projected to be gone by the end of century (Derksen et al., 2019).

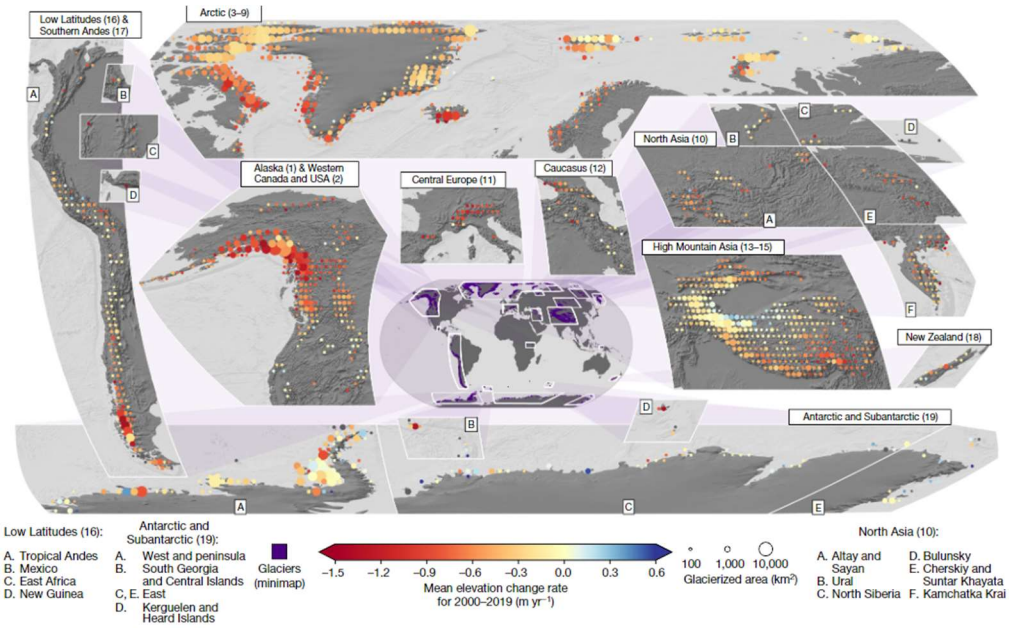

Figure 1-1: Global glacier mean elevation change rates from 2000 to 2019 from Hugonnet et al. (2021). Tiles of 1° × 1° below 60° latitude, 2° × 1° between 60° and 74° latitude, and 2° × 2° above 74° latitude, therefore representing similar surface areas of approximately 10,000 km^2. Discs are scaled with glacierized area for each tile. Grey is used to colour discs if less than 50% of the surface is covered by observations or if the 95% confidence interval is larger than 1 m/yr (only applies to 0.4% of the glacierized area).

Global sea level has risen over the past century and has accelerated in recent decades (Dieng et al., 2017). For example, from 2006-2015, the rate of global mean sea level rise was ~3.6 mm/yr, whereas between the years 1901-1990, global mean sea level rise rate was ~1.4 mm/yr (IPCC, 2019). The Arctic as a whole has been identified as the largest source of land ice to global sea level rise over 2003-2014 and continues to accelerate to the present day, where Arctic contribution to sea level rise increased from 0.13 mm/yr over 1955-1995 to 0.47 +/- 0.19 mm/yr over 1971-2017 (3.6 times more than 1955-1995) (Box et al., 2018). Ice sheet and glacier mass loss have been deemed the primary sources of sea level rise and is also accelerating (IPCC, 2019). Specifically, global glacier mass loss is estimated to have contributed 21+/-3% of the sea level rise that occurred over 2000-2019 (after the Greenland and Antarctic Ice Sheets) (Hugonnet et al., 2021). Global sea level rise threatens coastal communities, infrastructure, and agriculture (Gingerich et al., 2017), and impacts marine ecosystems (Frainer et al., 2017). Therefore, studying changes in glaciers, particularly in the Arctic, is of paramount importance.

Glaciers and ice sheets largely lose mass either by surface melt and run off or frontal ablation, which includes calving of ice mass into the ocean (termed dynamic discharge) as well as ocean driven melt at the glacier front. Dynamic discharge has been the dominant source of mass loss in Antarctica (Gardner et al., 2018; Mouginot et al., 2014a). As an example, ice discharge in the Amundsen Sea Embayment (Antarctica) increased by 77% since the 1970s mainly due to acceleration of four glaciers and subsequent increase in dynamic discharge to the ocean (Mouginot et al., 2014b). In Greenland, dynamic discharge has accounted for 36% of mass lost in 2005-2009 and 32% of mass lost from 2009-2012 (Enderlin et al., 2014). From 1991-2015, ~40% of mass lost from the Greenland Ice Sheet was due to dynamic discharge (Van Den Broeke et al., 2016). In the Canadian Arctic, dynamic discharge accounted for 52% of glacier mass lost from 1991-2005 (Millan et al., 2017). From 2005-2014, dynamic discharge accounted for only 10% of glacier mass loss (Millan et al., 2017). Though dynamic discharge accounted for the minority of ice lost in

the Canadian Arctic in the recent years, individual regions can experience substantial mass loss due to the acceleration of one or a few glaciers (Millan et al., 2017; Van Wychen et al., 2020).

Most glacier motion patterns in the Canadian Arctic have remained consistent in the last two decades, apart from a few glaciers that display marked variability in motion patterns (Van Wychen et al., 2020). A variety of glacier motion patterns have been observed in the Canadian Arctic. In general, glaciers in this region have been found to either accelerate continuously (Van Wychen et al., 2016; Van Wychen et al., 2022), accelerate at regular intervals (e.g. surging, pulsing) (Copland et al., 2003; Van Wychen et al., 2016), or show expected seasonal speed changes (Van Wychen et al., 2016). Although these patterns have been identified, efforts to quantify the reasons and mechanisms that drive variability in glacier motion has been much less successful. Particularly elusive are the mechanisms driving surge-type glaciers, a class of flow pattern that cycles between periods of fast glacial flow (surge phase) and of slow flow (quiescent phase) (Jiskoot, 2011). While many observations of surges have been reported in the Canadian Arctic (Copland et al., 2003; Van Wychen et al., 2016), studies dedicated to precise characterization of oscillations in glacier flow are lacking. Yet, understanding surge mechanisms, in addition to typical glacier acceleration/deceleration patterns, are essential for understanding the full nature of glacier dynamics both in Canada and elsewhere, as glacier acceleration can substantially increase ice discharge to the ocean (Millan et al., 2017).

Studies dedicated to individual surge-type glaciers allow for in-depth analysis on how and why surges occur in the Canadian Arctic (Lauzon, 2022; Van Wychen et al., 2022). For example, a study of Split Lake Glacier (Van Wychen et al., 2022) proposed that it has been slowly surging since the 1950s (unusually long for a surge phase), and a study dedicated to Iceberg Glacier proposed relationships between tributary location and speed changes, and the influence of the enthalpy balance theory (Lauzon, 2022). Otto Glacier, located on Northern Ellesmere Island, is a prime example of an under-studied surge-type glacier. Otto Glacier was first reported to have surged between 1950-1964, as evident by crevassing and terminus

advance observed in aerial photos and is one of the first identified surge-type glaciers in the Canadian Arctic (Hattersley-Smith, 1964, 1969). Surge behavior was also observed in 1991 with terminal speeds >800 m/yr (Millan et al., 2017), and again in 1999 based on observations of surface crevassing (Copland et al., 2003). In 2013, Otto Glacier was observed to be at the near-stagnation stage (Van Wychen et al., 2016). Although the above events have been documented, a detailed characterization of Otto Glacier's surge behavior has not yet been undertaken. A detailed analysis would give insight into how and why glaciers surge in the Canadian Arctic and allow for a better characterization of the spectrum of dynamic patterns that exist here.

Fortunately, much more remote sensing data are now available to enable this detailed investigation, which is especially useful since field data are not available for Otto Glacier. For example, European Remote Sensing (ERS) data are openly available for the years 1991-2011, as well as NASA's ITS_LIVE composite data (from Landsat platforms 4,5,7,8) which provide velocity data for Otto Glacier from 1999-2018. RADARSAT-2 (R2), though not openly available, does provide modern data for Otto Glacier from 2009 to the present day. Additionally, openly available glacier surface elevation change data are provided by Hugonnet et al. (2021) and bedrock topography data are openly available from the Centre for Remote Sensing of Ice Sheets (CReSIS) Multichannel Coherent Data Depth Sounder (MCoRDS). While some regional studies have used some of the above data to investigate Otto Glacier (Copland et al., 2003; Van Wychen et al., 2016; Van Wychen et al., 2020), there have been no studies that use all the above data for a detailed, multi-decadal analysis of Otto Glacier's surge evolution. The goal of this thesis is to provide this analysis for Otto Glacier.

1.1.1 Research Objectives

The study has five objectives:

1) characterize Otto Glacier's velocity changes,
2) determine changes in the terminus position,
3) report and compare changes in glacier height over time,
4) map bedrock features under Otto Glacier and determine if/how bedrock features control velocity changes,
5) use the above information to provide a detailed analysis of Otto Glacier's surge event from 1992-2020 in the context of the Canadian Arctic.

1.2 Thesis Structure

This thesis is presented in a traditional thesis format and is comprised of six chapters. The introduction (Chapter 1) provided an overview of the research topic and thesis objectives. Chapter 2 provides a literature review with a more detailed overview of the study site. Following this, the Methodology chapter (Chapter 3) provides a detailed description of the methods and datasets used in the study. Next, Chapter 4 presents the results and Chapter 5 provides the discussion and interpretation of the results. Finally, Chapter 6 provides the thesis conclusion, summarizes the outcomes of each objective, and offers future directions for research.

Chapter 2 - Study Site and Literature Review

This chapter begins with a study site description which reviews the glaciological characteristics of Northern Ellesmere Island and Otto Glacier. This is followed by a literature review that discusses surge processes.

2.1 Study Area

Otto Glacier is situated on Northern Ellesmere Island, Nunavut, Canada (Figure 2-1, inset) on the Northern Ellesmere Island Icefield. Northern Ellesmere Island is the northern-most region of Canada. The icefield holds five large marine terminating glaciers (including Otto Glacier) as well as land-terminating glaciers along the south and east coast that comprise 60% of the ice area (Millan et al., 2017). Other than Otto Glacier, the only other confirmed surge-type glacier on Northern Ellesmere Island is Chapman Glacier, which is adjacent to Otto Glacier (Van Wychen et al., 2016). Milne and McKlintock Glaciers on Northern Ellesmere Island have also been observed to have cyclic velocity variability, however, they have been classified as likely pulse-types, where velocity variability is confined to parts of the glacier below sea level (Van Wychen et al., 2016).

Otto Glacier flows in a southwest direction in a relatively straight valley that is ~35 km long and 4-6 km wide between mountains and nunataks, descending from 1800 m above sea level and reaching sea level where it terminates into a fjord (Hattersley-Smith, 1969; Figure 2-1). The glacier consists of one main branch as well as several tributary branches. A bedrock topography map derived from glacier surface topography suggested that a bedrock ridge exists beneath the glacier terminus (A. Fuzesy in Hattersley-Smith, 1969).

Figure 2-1: Overview of Otto Glacier, glacier extent provided as black outline from the Randolph Glacier Inventory (RGI) Version 6.0. Underlying image obtained from the Sentinel-2 sensor on July 18, 2022, projected in WGS 1984 UTM Zone 17N. Inset shows Otto Glacier's situation on Ellesmere Island.

Several other studies include analyses of Otto Glacier's velocity changes since 1964 and are discussed here. Otto Glacier was first observed to have surged in July 1950 (Hattersley-Smith, 1964), inferred from heavy crevassing in the lowermost 25 km of the glacier, which contrasted neighboring glaciers that had smooth surfaces at the time. Hattersley-Smith (1969) provided further analyses using aerial photos. The photographs from July 1950 to July 1959 showed significant advance of the terminus by 3 km. Prior to the advance, the terminus was grounded below sea level and after the advance, the terminus was seen floating as an ice tongue with surrounding calved icebergs. New crevasses did not appear after this period. In 1964, the lowermost 15 km of the glacier was photographed, and noted another advance of ~3 km. Mapping analysis did not show any volume change in the advanced section of the glacier; rather, the lowermost 15 km of the glacier appeared to have slumped. The mean height change from 1959-1964 ranged from +40.4 m in the 0-50 m zone to -26.1 m in the 200-250 m zone, equivalent to a mean height change below the 250 m zone of -0.79 m/yr. Hattersley-Smith (1964)

suggested that a rise in basal temperature above the melting point may have triggered the surge. “Mrs. A Fuzesy” (in Hattersley-Smith, 1964) constructed a bedrock topography map that revealed a subglacial ridge extending halfway across the glacier and to more than 125 m above sea level. The cross section of the glacier in this region showed an “s-shape” with a relief of about 250 m. Flow lines from the glacier surface conformed with the contours of the bedrock map. Robin (1969) reported that this ridge caused thinning of the part of the glacier that is downstream from the ridge, suggesting that the ridge could cause ice extension as the glacier passes over it.

Copland et al. (2003) analyzed Otto Glacier using optical imagery. Landsat-7 data acquired in 1999 showed that Otto Glacier was still heavily crevassed along the main trunk, and the terminus was digitate and in a similar position to 1964, and this information alone led to the conclusion that Otto Glacier had likely either continued its surge since 1950 or began a new surge around 1999. Velocities during the study period (1999/2000) were not able to be determined since repeat Landsat-7 imagery was not available over Otto Glacier during that period. Millan et al. (2017) used Landsat, ALOS PALSAR, RADARSAT-1, ERS-1, and Sentinal 1-a images from 1991-2016 to analyze Otto Glacier. The investigation showed that glacier slowdown was observed between 1991-2015, with frontal speeds decelerating from >800 m/yr in 1991 to <50 m/yr in 2015.

Van Wychen et al. (2016) studied Otto Glacier using optical and radar imagery and reported speed-up in 2000 from 200 to 400 m/yr in the lowermost 10 km of the glacier, and peak velocities of ~600-700 m/yr in winters 2007 and 2008 in the lowermost 5 km of the glacier. By the winters of 2009 and 2010, velocities in the lowermost ~5 km declined to ~250-300 m/yr and by 2013-2015 this region of the glacier was stagnant. A terminus retreat of ~1.2 km was observed from 2002-2014. Because Otto Glacier was known to also have fast flow with terminus advance in the 1950-1964 period and again in 1991-2012, Van Wychen et al. (2016) hypothesized that Otto Glacier experienced surging. Assuming the surge observed in 1991 was a new surge since 1964, rather than a continued surge, the authors assumed a ~5-10 year

active phase and ~30-35 year quiescent phase for Otto Glacier. The most recent study that included Otto Glacier was completed by Van Wychen et al. (2020) using winter radar imagery. From winter 2015 to winter 2020, Otto Glacier was observed decelerating in the region 10-30 km from the calving front. In this region, velocities decreased from 100-150 m/yr in 2015 to <50 m/yr in 2020, suggesting that Otto Glacier continued to transition to its quiescent phase.

2.2 Literature Review

To provide the appropriate context and background to understand the dynamic behavior of Otto Glacier, the following literature review discusses surge processes and the mechanisms thought to drive surge cycles. First, the general characteristics of all surge-type glaciers are discussed. Next, the two most prominently suggested surge mechanisms are explored (Alaskan-type and Svalbard-type surging), followed by a discussion of glacier dynamics in the Canadian high Arctic. The review concludes with discussion of a general theory for all surge mechanisms and areas necessitating further research.

2.2.1 General Characteristics of Surges

Surge-type glaciers are glaciers that alternate between phases of fast flow and slow flow (Benn and Evans, 2010) and less than 1% of all glaciers are known to surge (Jiskoot et al., 1998). In contrast, normal glaciers typically flow at relatively the same speed each year, with flow speeds changing according to changing mass balance conditions (i.e., smaller glaciers typically flow slower than larger glaciers due to reduced driving stress) (Benn and Evans, 2010). This “normal” type of velocity is termed the glacier’s ‘balance velocity’. Surge-type glaciers, however, do not flow according to expected balance velocities, and instead alternate between phases of high speed (velocities greater than the balance velocity) and slow speed (velocities lower than the balance velocity) for reasons that are not completely understood.

Surge cycle length can vary from months to years between individual surge-type glaciers, but follow a general process described here (Benn and Evans, 2010). During the quiescent phase, where the glacier is slower than the expected balance velocity, ice accumulates in the reservoir area (upper region)

of the glacier because the glacier is moving too slow to discharge newly accumulated ice from snowfall (Benn and Evans, 2010). This results in increased surface elevation in the upper part. Eventually, mass is lost at the lower part of the glacier because the upper part is not flowing fast enough to replenish what is lost due to warmer temperatures at lower elevation and/or ocean driven melting (Benn and Evans, 2010). This results in surface lowering of the lower part of the glacier (Benn and Evans, 2010). Eventually the change in surface gradient between the upper region and lower region becomes so steep that the surge phase is triggered (Benn and Evans, 2010). When this happens, ice from the upper portion is rapidly transferred to the lower part of the glacier (Benn and Evans, 2010). The transfer results in surface lowering of the reservoir area and surface elevation gain in the lower portion (receiving area), and a subsequent advance of the glacier's terminus (Benn and Evans, 2010). At this point, driving stress from the reservoir area is reduced, the glacier returns to flowing at very slow speeds and thus restarts the quiescent phase until the process restarts. This general process is illustrated in Figure 2-2.

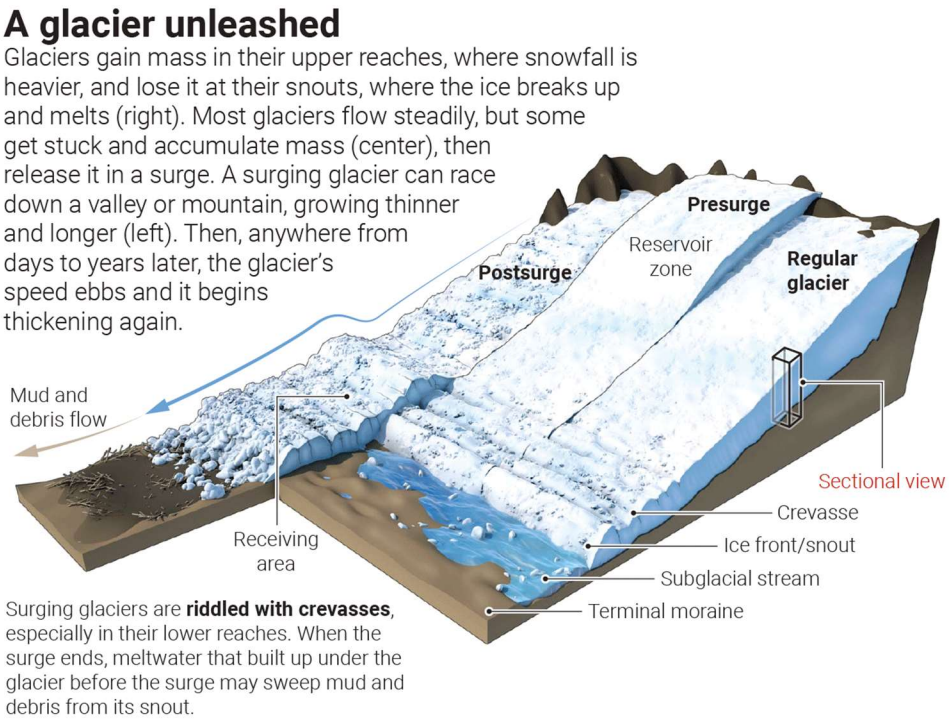

Figure 2-2: An overview of the general process of glacier surging, showing the geometry of a regular non-surge-type glacier (right), the geometry of a 'surge-type' glacier just prior to surge (middle) and the postsurge geometry of a surge-type glacier (left). Figure by C. Bickel, available online at: https://www.science.org/content/article/why-slow-glaciers-can-sometimes-surge-fast-speeding-train-wiping-out-people-their-path (Qiu, 2017).

Although the above description describes the general behavior of all surge-type glaciers, studies that investigate surge processes have generally found wide variability in how surging occurs between glacier basins, and this has led to surge-type glaciers typically being categorized into two distinct classes based on how the surge manifests. These classes are “Alaskan-type” and “Svalbard-type” surging and are named after regions where the surge mechanism was first studied and identified, however it is important to note that surge-type glaciers of each of these classes can occur outside of the regions that they are named after. Svalbard and Alaskan-type surges are most often differentiated from each other based on the duration of active and quiescent phases and the associated surge mechanism. In general, Alaskan-type surge phase lengths typically last months to a few (3-4) years and quiescent phase lengths lasting 35-40 years (Benn and Evans, 2010). The end of the Alaskan-type surge phase is typically associated with outburst floods or proglacial lake filling, suggesting that drainage of subglacial water is a key control on the surge cycle (Kamb et al., 1985). In contrast, Svalbard-type surge cycles are typically longer, with surge phases lasting 7-15 years and quiescent phases lasting 50-100 years (Benn and Evans, 2010), and are not associated with outburst floods or lake filling. These general differences are summarized in Table 2-1, and the following sections discuss the Alaskan and Svalbard-type processes in detail.

Table 2-1: General summary of differences between Alaskan and Svalbard surge-type glaciers

Characteristic	**Alaskan-type surge**	**Svalbard-type surge**
Speed-change controls	Basal hydrology	Bedrock morphology and basal thermal factors
Typical surge phase length	Months - 4 years	7 - 15 years
Typical quiescent phase length	10 - 40 years	50 - 100 years

2.2.2 Alaskan Surge-Type Glaciers: A Hydrologic Mechanism

Alaskan surge-type glaciers are thought to be controlled by subglacial hydrology mechanisms. In this model, the surge occurs in response to an accumulation of liquid water within constricted chambers at the base of the glacier (termed inefficient cavity system, due to the contorted and constricted configuration of the cavities). As surface meltwater trickles down and accumulates at the glacier base, subglacial water pressure increases enough to lift the glacier from the bedrock and allow it to slide at high speeds (Benn and Evans, 2010). Eventually, so much water accumulates that it creates an efficient subglacial network that removes water in massive volumes, reducing the water pressure and allowing the glacier to sink back down (Benn and Evans, 2010). This typically results in a large outburst flood or proglacial lake filling. After this drainage, quiescence ensues again, until subglacial water accumulates again and the process repeats (Benn and Evans, 2010). The theorized process is summarized in Figure 2-3. Two examples of this surge-type are described in detail below.

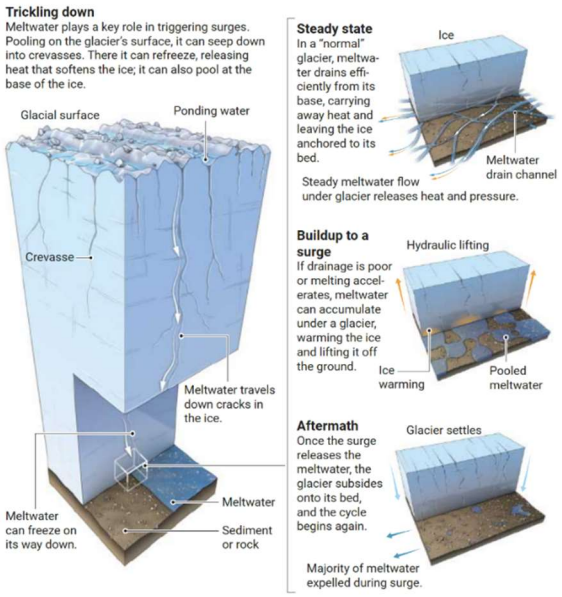

Figure 2-3: Illustration of hydrologic mechanisms that may control Alaskan-type suring. Surface water flows toward the glacier base to an ineffecient cavity system, where water pressure builds as water accumulates. Eventually the pressure is so high that the glacier is uplifted and begins sliding at high speeds. Melt water is later released in large volumes, the glacier sinks down to its bed and the process restarts. Illustration by C. Bickel, available online at: https://www.science.org/content/article/why-slow-glaciers-can-sometimes-surge-fast-speeding-train-wiping-out-people-their-path (Qiu, 2017).

2.2.2.1 Variegated Glacier Surge

One of the most studied 'Alaska-type' surge glaciers is the Variegated Glacier in Alaska (Figure 2-4) (Bindschadler et al., 1977; Kamb, 1987; Kamb et al., 1985). Variegated glacier is a 20 km-long tidewater glacier with a uniform slope of 5 degrees (Bindschadler et al., 1977). It consists of a temperate thermal regime, meaning that most of the glacier's ice is near the melting point (Bindschadler et al., 1976). Surges occurred between the years 1905-1906, 1911-1933, 1942-1948, 1964-1965 (Bindschadler et al., 1977), 1982-1983 (Kamb et al., 1985), and 1995 (Eisen et al., 2005), exhibiting a recurrence period of ~20 years. This review will focus on the 1982 surge, which is the most studied (Kamb, 1987; Kamb et al., 1985).

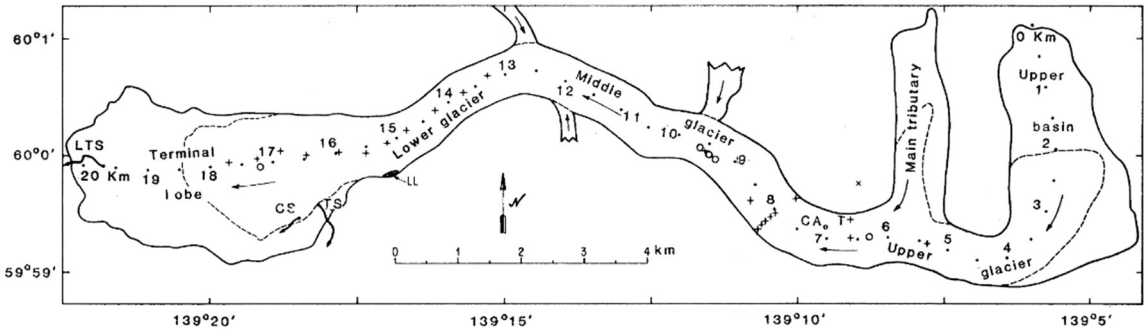

Figure 2-4: Overview map of Variegated Glacier, Alaska from Kamb (1985)

Kamb et al. (1985) observed that the 1982 surge of Variegated Glacier had two phases of acceleration. The first phase began in January 1982 and persisted until June when it reached peak velocity of about 10 m/day. Later in June, the glacier abruptly decelerated to half of its peak velocity over a few hours. The glacier then exhibited five smaller pulses of acceleration but overall decelerated until October, when velocity declined to 1 m/day. This first acceleration occurred only in the upper regions ("upper" meaning away from the ocean-contacting terminus). The second fast flow phase initiated in October, again upglacier, and by June 1983 reached a peak velocity of about 15 m/day. However, by this time, the acceleration had also been activated in the terminus (i.e., the surge had propagated down-glacier), where velocities reached 40-60 m/day. By July 1983, the surge ended abruptly again over a few hours, decreasing to a velocity of 0.2 m/day (below pre-surge velocity). Upon deceleration, a new lake appeared near the

glacier as well as flooding of outlet streams. These new waters had high turbidity, consistent with subglacial water, suggesting that they were sourced by subglacial water that drained during glacier deceleration.

The full surge cycle (including acceleration and deceleration) ended by September 1983, having lasted for ~2 years. The fast flow phase lasted ~18 months. The upper reaches of the glacier thinned by about 50 m due to extension force from the acceleration, while the lower reaches thickened by about 100 m due to compressive forcing from the fast flowing ice upglacier flowing into slower flowing ice downglacier.

2.2.2.2 West Fork Glacier Surge

In 1987, a surge event of West Fork Glacier in Alaska (Figure 2-5) was observed to be similar to that of Variegated Glacier (Harrison et al., 1994). West Fork Glacier is a ~40 km long tidewater glacier and, like Variegated Glacier, it consists of a temperate thermal regime. Its surge only experienced one phase and began in August in 1987 when the glacier accelerated abruptly, similar to the acceleration process of the Variegated Glacier. Surge velocity was measured from March to June 1988 and was determined to be about 21 m/day. The acceleration remained consistent until surge termination in July 1988, which occurred abruptly over a few hours, similar to that of Variegated Glacier. During deceleration, West Fork's outlet streams developed turbidity and a new lake was observed nearby, consistent with observations from Variegated Glacier's deceleration.

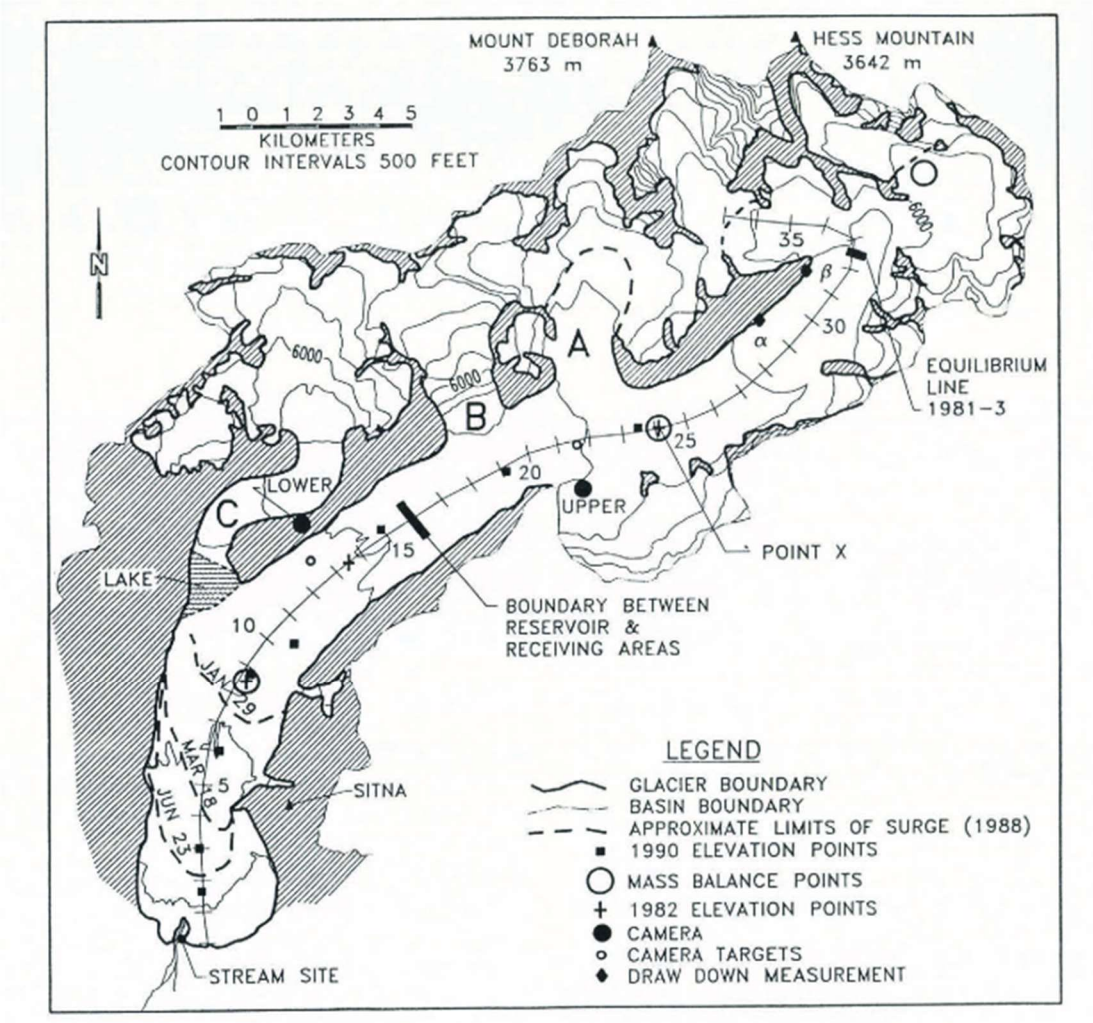

Figure 2-5: Overview of the West Fork Glacier, from Harrison et al. (1994).

2.2.2.3 Hydrologic Controls for Surging

The observations and behavior of the Variegated and West Fork surges exemplify a subglacial hydrologic mechanism of surging. This conceptual model was initially devised during the Variegated Glacier studies and later applied to West Fork Glacier and similar surge-type glaciers in the Alaska region, such as Peters Glacier (Echelmeyer et al., 1987) and Bering Glacier (Herzfeld and Mayer, 1997).

Variegated Glacier's temperate regime allows for the development a complex water conduit system within the glacier (Benn and Evans, 2010). As such, Kamb et al. (1985) proposed that a hydrologic mechanism was involved in the surge. Borehole studies revealed that during accelerations, basal water

pressures were higher than overburden pressure (the weight of the glacier against the bedrock). High basal water pressures were hypothesized to develop as a result of meltwater accumulation in a linked cavity system, where water collects but cannot drain from the glacier (Iken, 1981; Kamb, 1987; Kamb et al., 1985). When basal water pressures exceed overburden pressure, the glacier can float over a film of water at the base and subsequently slide at high speeds, triggering acceleration (Kamb, 1987; Kamb et al., 1985). A winter surge is plausible because colder temperatures can shrink cavity walls, resulting in higher water pressure (Kamb et al., 1985; Rothlisberger, 1972).

Deceleration of a hydrologically-driven surge is thought to be caused by abrupt drainage of the linked cavity system (Kamb et al., 1985). When the Variegated Glacier decelerated in summer of 1983, Kamb et al. (1985) observed the formation of a new lake and the flooding of outlet streams near the glacier. The turbidity of the lake/streams was similar to that of subglacial water, suggesting a connection between the two. Prior to the surge, minimal turbidity was observed in the pre-existing streams. This suggested that the lake/floods formed from an outburst of the subglacial water that occurred only during acceleration in summer. Therefore, it was postulated that during the warmer summer, water from the linked cavity system was able to transition to a more efficient form of subglacial drainage and thus find an exit point, resulting in massive, abrupt outburst floods (Kamb, 1987; Kamb et al., 1985). The outbursts led to a decline in subglacial water pressure and collapse of the cavity roofs, which then caused overburden pressure to exceed basal water pressure. This caused the glacier to cease floatation and begin decelerating in summer. This effectively marked the end of the surge (Kamb, 1987; Kamb et al., 1985).

Similar to Variegated Glacier, the West Fork Glacier demonstrated a short surge duration, abrupt stops, and outburst flooding. These features, combined with the fact that West Fork is a temperate glacier, led to the thinking that the basal water system must have drained during summer deceleration and was likely a key control in the surge cycle (Harrison et al., 1994). However, a key difference between the West Fork and Variegated surge is the seasonal onset of acceleration. While Variegated Glacier accelerated in

winters and decelerated in summers, West Fork Glacier's single acceleration started in late summer and decelerated in early summer (Harrison et al., 1994). This would seem to contradict the theory that surges occur during winter due to the increasing water pressures from cavity shrinkage. However, Harrison et al. (1994) pointed out that in the Alaskan Range where West Fork Glacier is located, glaciers experience very little surface melt in late summer. Therefore, the cavities that formed in early summer were likely already shrinking in late summer due to the reduced melt water input characteristic of the region, resulting in the high basal water pressures that are required to exceed overburden pressure. It was concluded that West Fork's acceleration was driven by a hydrologic cavity mechanism similar to that of Variegated Glacier.

2.2.3 Svalbard Surge-Type Glaciers: A Thermal/Bedrock Mechanism

Although the hydrologic mechanism can explain the Variegated, West Fork, and other Alaskan surge patterns, it does not well explain the more gradual surge decelerations that are not associated with outburst floods, as observed in Svalbard (Fowler et al., 2001; Murray et al., 2003). This led researchers to believe that hydrologic factors were not key drivers for the surges in this region, and rather postulated that a thermal/bedrock mechanism was the important control on surge-activity. Two prominent surge-type glaciers in this category are Bakaninbreen and Monacobreen Glaciers in Svalbard and are described below.

2.2.3.1 Bakaninbreen Glacier Surge

Bakaninbreen Glacier (Figure 2-6) is a tidewater terminating glacier about 17 km long with a slope of 0.8 degrees and underlain by deformable sediment (Murray et al., 1998). It is thought to be a polythermal glacier (Ødegård et al., 1997). Polythermal glaciers have thermal variances within the glacier ice which can occur due to either changes in the pressure melting point (which depends on overlying weight) or due to the release of latent heat from the re-freezing of meltwater within a glacier (Benn and Evans, 2010).

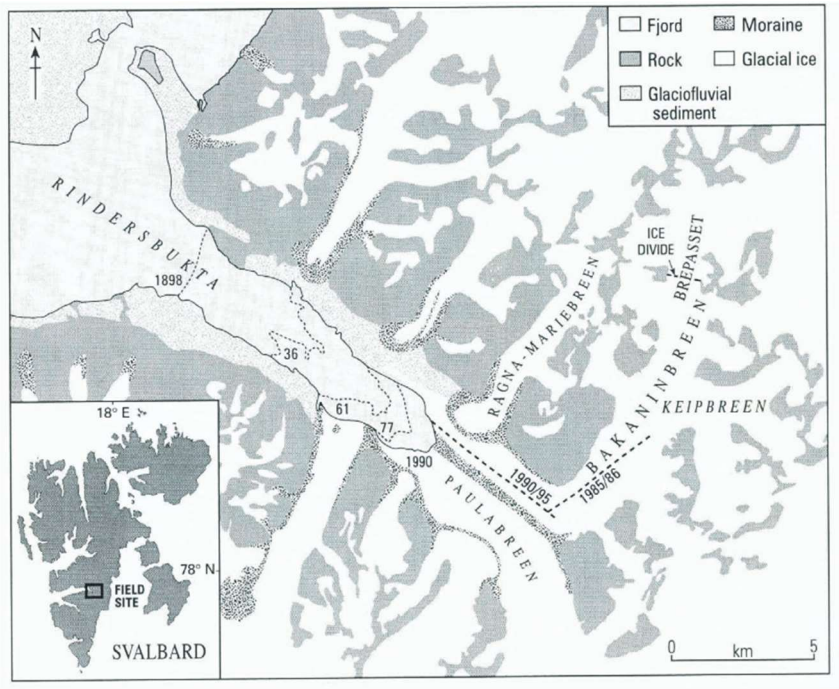

Figure 2-6: Overview map of Bakaninbreen, Svalbard from Murray et al. (1998).

Observations by Murray et al. (1998) began in spring 1985 using several methods. Aerial photography was used to analyze surge front changes. Oblique photographs either from aerial or a terrestrial high point were used to analyze surge front positions as well as glacier slope changes. Additionally, surveyed longitudinal profiles were used to analyze surge front position at specific cross-glacier locations and glacier slope and height changes. In 1985, the glacier was thought to be in an early surge. By August of 1985, glacier velocities peaked at 7.8 m/day. Velocity variability appeared to initiate upglacier and propagate downglacier. This was followed by deceleration which continued until surge termination in 1995, although the exact date of surge termination was uncertain. The deceleration phase of at least 10 years is much longer than the Alaskan-types, where deceleration occurs over a few hours (Harrison et al., 1994; Kamb et al., 1985). The duration of the quiescent phase prior to the surge is unknown, however, it is inferred to be consistent with other surge-type glaciers in Svalbard (Murray et al., 1998). This is also in contrast to Variegated Glacier, where quiescence typically lasts ~20 years (Bindschadler et al., 1977). Because Bakaninbreen Glacier's velocity changed more gradually than the

Alaskan-types and no outburst floods were observed during deceleration, Murray et al. (1998) proposed that the linked-cavity hydrologic mechanism could not have been the main control for the surge. Instead, it was suggested that the gradual surge termination is related to feedbacks between basal heating, melt water production, and seepage of basal water into the underlying deformable till (discussed in detail in 2.2.3.3).

2.2.3.2 Monacobreen Glacier Surge

Monacobreen Glacier in Svalbard (Figure 2-7) is a ~40 km long, polythermal tidewater surge-type glacier with an average surface slope of ~2 degrees (Bamber, 1987; Murray et al., 2003). The glacier overlies two different types of bedrock separated by a fault, where the western bedrock consists of granitic bands, gneiss and schist, and the eastern bedrock consists of course conglomerates and sandstone (Hjelle and Lauritzen, 1982).

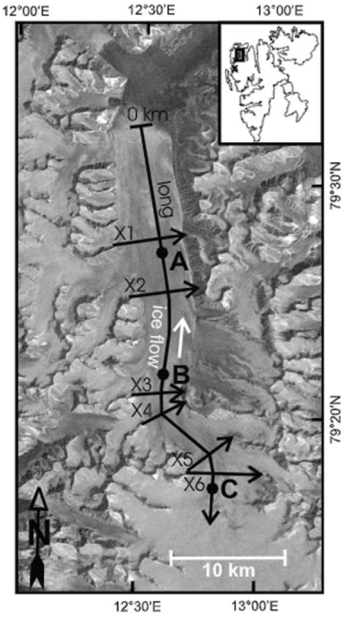

Figure 2-7: Overview map of Monacobreen Glacier, Svalbard from Murray et al. (2003).

For Monacobreen Glacier, Murray et al. (2003) observed that the fast flow phase started in September 1991 and lasted until a velocity peak in January 1994. Velocities peaked at 5 m/day and the spatial distribution of velocity remained constant. The terminus advanced 2 km over the course of the

surge, reaching its maximum extent in April 1996. Between April 1996 and October 1997, the central area of the terminus retreated by 250 m while the western and eastern sections advanced by 100 m. The deceleration phase lasted from January 1994 until October 1997 and was more gradual than the fast flow phase. Between October 1997 and September 1998, the entire margin of the terminus was retreating.

The surge appeared to initiate in the terminus and propagate upglacier throughout the fast flow phase. Data were not available for the transition years between acceleration and deceleration. The study period ended in 1998, however it is thought that the surge had not terminated completely by then since modelled quiescent velocity was much lower than the observed velocity. Extrapolation analyses suggested the surge likely terminated between November 1998 and January 2002 (Murray et al., 2003). These observations suggest a surge cycle duration of 7-11 years which is consistent with other surges on Svalbard (Dowdeswell et al., 1991; Murray et al., 1998). The overall consistency in spatial distribution of velocity variance led to the conclusion that bedrock features, which are typically constant, were key controls on the observed velocity changes (Murray et al., 2003).

2.2.3.3 Thermal-Bed Mechanisms for Surging

The observations of the Bakaninbreen and Monacobreen surges are starkly contrasted with those of the Alaskan-type surges in the following ways: the Svalbard glaciers' accelerations were more gradual than the Alaskan-type surges and had slower speeds and Svalbard decelerations were also more gradual, lasting over years, whereas most Alaskan surge-type glaciers decelerated and stopped within hours (Murray et al., 1998; Murray et al., 2003). The Monacobreen acceleration was relatively uniform in magnitude, unlike Variegated Glacier, which experienced fluctuations of velocity during acceleration and deceleration phases (Murray et al., 2003). Finally, the Bakaninbreen and Monacobreen surges terminations were not associated with outburst floods, whereas the Alaskan surge-type glaciers were commonly associated with floods (Murray et al., 1998; Murray et al., 2003). This information led the

researchers to believe that thermal-bedrock interactions must be involved (Murray et al., 1998; Murray et al., 2003).

A thermal-bed model by Fowler et al. (2001) has been used to explain the surges of Monacobreen and Bakaninbreen Glaciers (Murray et al., 2003) and other Svalbard-type surges, such as Trapridge Glacier in the Yukon (Clarke et al., 1984). The Fowler et al. (2001) model states that prior to acceleration, mass accumulates at the glacier surface (from snowfall) until the pressure melting point is reached at the glacier base. The resulting basal meltwater seeps into bedrock pores, leading to high pore water pressures and bed deformation. This deformation increases sliding friction, which heats the glacier base and produces more meltwater. This becomes a positive feedback cycle, where additional meltwater causes further bed deformation, which results in more friction, heating, and meltwater. The accumulation of meltwater eventually results in basal water pressure that is high enough to exceed overburden pressure and allow the glacier to slide at high speeds. This theory is supported by the fact that Svalbard surge-type glaciers tend to overlie deformable sedimentary bedrock (Hamilton and Dowdeswell, 1996).

The deceleration phase in the Fowler et al. (2001) model is thought to be driven by two mechanisms: the discharge of water blisters and reduced basal temperatures caused by ice thinning. When the basal water pressure exceeds overburden just before acceleration, the water is thought to be stored in “blisters”. When the glacier reaches floatation over the bed, the blisters discharge their water. After the water has been discharged, overburden pressure eventually exceeds basal water pressure again, allowing for termination of the surge. At the same time, ice thinning (caused by acceleration and extension forces) reduces bed temperatures, allowing basal water to freeze with further deceleration of the glacier.

2.2.4 A Unified Surge Theory

Sevestre and Benn (2015) proposed a theory of how climate and glacier geometry can predispose a glacier to surging, regardless of the underlying mechanism. After compiling a global inventory of surge-type glaciers, it was found that surges tend to occur in two types of climate: cold/dry climates (though

surges are rare here), and temperately cold climates, with a mean annual temperature between -10 °C to 0 °C and mean annual precipitation ranging from 30 to 2250 mm/yr (Figure 2-8). The cold/dry climate includes Arctic Canada, and the more temperate climates include the "Arctic Ring" (extending from Alaska to Novaya Zemlya but excluding Arctic Canada) and High Mountain Asia. Within these climate envelopes, surge-type glaciers can co-exist with normal glaciers. Surge-type glaciers are rare or non-existent in warmer, wetter climates. The study additionally found that surge-type glaciers tend to have larger surface areas and longer lengths than normal glaciers, while their slopes tend to be shallower when compared to normal glaciers. Surge-type glaciers also tend to have high "branchiness" (referring to the number of smaller connected tributary glaciers that are ~85% of total glacier length).

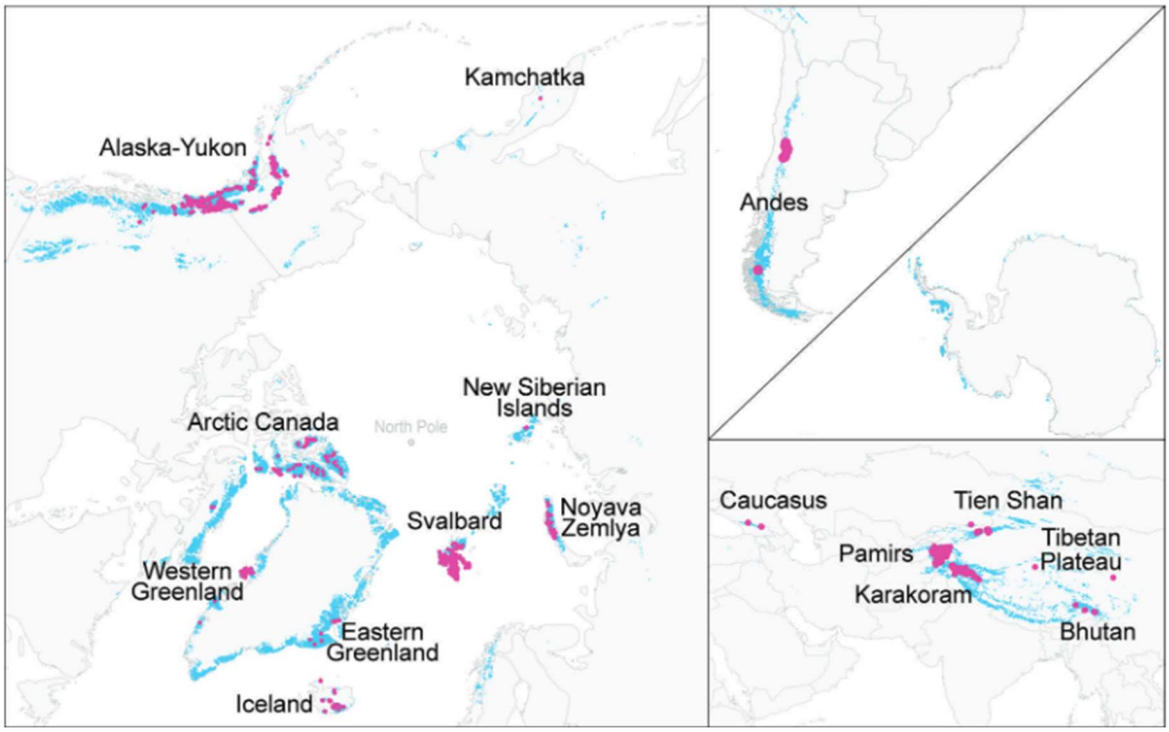

Figure 2-8: Global distribution of surge-type glaciers (pink) and normal glaciers (blue), from Sevestre and Benn (2015)

Using the above inventory, Sevestre and Benn (2015) utilized a Maxent model (a species distribution model) that accurately predicted locations where glaciers are likely to surge. Climate variables contributed ~52% to model prediction and geometry variables ~48%. It was therefore concluded that

climate variables are likely the primary determinant of location of surging, and geometry variables determine which glaciers within those locations surge.

To explain the oscillatory behavior of surge-type glaciers, Sevestre and Benn (2015) proposed a theory of enthalpy (heat) imbalance. This theory suggests that surge acceleration occurs when more heat is gained by the glacier than can be dissipated. Heat can be gained through radiative forcing, meltwater, geothermal heat, or friction, and heat can be dissipated by advection of ice flow, conduction to the surface, or meltwater drainage. When more heat is dissipated than gained, the glacier decelerates. The authors discussed how climate can influence the enthalpy budget. For example, surge-type glaciers are rare in cold/dry climates because heat is dissipated more easily in these environments. In contrast, glaciers in temperate climates are more likely to surge because in these environments, neither heat conduction nor subglacial water drainage have the efficiency to dissipate heat gains. On the warmer, wetter end of the climate spectrum, surges are much less likely because meltwater quantities are high and hydraulic systems are efficient enough to dissipate any heat gained. Geometric variables may also influence enthalpy balance (Sevestre and Benn, 2015). Longer, "branchier" glaciers have higher balance velocities than smaller, simpler glaciers, and therefore high heat production at their bases. Larger, thicker glaciers also have higher velocities and therefore more heat generation, but they are not able to conduct heat away efficiently due to their size.

The enthalpy budget theory has been supported by a mathematical model of enthalpy balance (Benn et al., 2019a) and subsequent application to the Morsnevbreen surge-type glacier in Svalbard (Benn et al., 2019b). After Morsnevbreen's quiescence phase, mass gain in the accumulation zone triggered forward motion. Frictional heating was found to be high and led to basal meltwater accumulation. Furthermore, meltwater led to acceleration and more frictional heating. A cold ice barrier contained the subglacial water until the surge front met the fjord, allowing for the release of subglacial water into the fjord and eventual deceleration. It was suggested that cold ice barriers, which form due to thermal and

geometric factors, could facilitate surge initiation by allowing meltwater (enthalpy) to accumulate, but when they fail, lead to abrupt accelerations with the discharge of the water.

The enthalpy model can be related to the Alaskan and Svalbard-type surge mechanisms. Indeed, Alaska, a temperate region, contains one of the densest concentrations of surge-type glaciers in the world (Sevestre and Benn 2015). The Alaskan-surge mechanism involves the accumulation of melt water at the glacier base to a threshold point that triggers sliding. The melt water adds energy to the base of these glaciers that cannot be easily dissipated, meaning that the energy is stored at the base as liquid water over the quiescent phase. This energy is only dissipated after so much water accumulates that an efficient subglacial drainage network develops that removes the water and thus dissipates the energy (i.e., removing the enthalpy in this model), resulting in deceleration. Enthalpy imbalance can also be inferred for the typical cold-dry climates in which Svalbard-type glaciers exist (Sevestre and Benn, 2015). In the Svalbard mechanism, accumulation of mass in the upper region of the glacier leads to basal temperatures reaching the pressure melting point, which can be interpreted as excess enthalpy. The excess meltwater at the base drains into bedrock pores, deforms bedrock, and up-lifts the glacier leading to sliding at high speeds. The warmer basal temperature (enthalpy) is dissipated when the glacier thins after acceleration or when water drains away, reducing underlying basal pressure, leading to reduced basal temperatures and freezing, and glacier deceleration.

Although the Sevestre and Benn (2015) work offers insights into where surging is more likely to happen, and that it is a result of enthalpy imbalance, the manifestation of surging varies for each world region and can vary even within regions. The following section reviews this variability for the Canadian Arctic.

2.2.5 Velocity Variability in the Canadian Arctic

A wide spectrum of flow patterns exists in the Canadian Arctic, such as normal flow, surging, pulsing, and continuous acceleration (Van Wychen et al., 2016). While some surge-type glaciers in the

Canadian Arctic do follow a typical Svalbard-type surge pattern, other glaciers have shown atypical velocity changes, such as pulsing (Van Wychen et al., 2016), consistent acceleration (Van Wychen et al., 2016; Van Wychen et al., 2020) and slow surging (Van Wychen et al., 2022). Each of these categories will be reviewed here, including a discussion of associated changes in terminus position, which can indicate whether a surge process is causing acceleration as opposed to other processes that cause acceleration. This section will conclude with a discussion of the impact of glacier dynamics on mass loss in the Canadian High Arctic.

2.2.5.1 Surge-Type Glaciers

Surge-type glaciers in the Canadian High Arctic are thought to align more with Svalbard-type surge mechanisms than with Alaska-type surge mechanisms, due to relatively long surge phases that have been previously reported (Copland et al., 2003). Otto Glacier, located on Ellesmere Island (Nunavut) is a good example. Its first observed surge was in 1950 and likely lasted at least until 1964 (~14 year active phase) (Hattersley-Smith, 1964). About 35 years later, in 1999, its velocity was hypothesized to be high due to appearance of crevasses, thought velocity was not measured at this time (Copland et al., 2003). By 2008, the glacier reached peak velocity of 600 m/yr (Van Wychen et al., 2016). Deceleration began in 2013, with velocity dropping to 100-150 m/yr and declining further to <50 m/yr in winter of 2019 (Van Wychen et al., 2020). The Benedict and Middle Glaciers of the Canadian High Arctic follow similar, gradual velocity changes in their surge cycles (Van Wychen et al., 2016; Van Wychen et al., 2020). Most surges in the Canadian Arctic result in terminus advance due to the extension forces of the acceleration and the movement of mass from reservoir areas (upper, accumulation region of the glacier) to receiving areas (the lower region of the glacier that receives mass from the reservoir area as the glacier moves). Mass is not necessarily lost but instead transferred, so there may be no change in mass balance. In contrast, deceleration results in terminus retreat, because the glacier is no longer moving fast enough to replenish the terminus which is depleted due to ocean/atmosphere-induced melting (Van Wychen et al., 2016).

2.2.5.2 Pulse-Type Glaciers

Some glaciers in the Canadian High Arctic that exhibit oscillations in flow speed do not demonstrate the typical surge behavior described above and are instead thought instead to "pulse." A key distinction between pulsing and surging is that in pulsing, velocity variability initiates in the terminal regions which tend to be below sea level, and velocity change does not activate in regions where the bed rises above sea level (Van Wychen et al., 2016). This contrasts with typical surges, which usually exhibit velocity changes along the entire main trunk of the glacier. The Dobbin and Parish Glaciers are pulse-types that exemplify these distinctions. Van Wychen et al. (2016) found that the beds beneath the termini of Dobbin and Parish glaciers are situated below sea level but have prominent sills that rise above sea level just before the beds descend below sea level. After pulse events, the glaciers showed thickening over the sills, thinning down glacier from the sill (which is below sea level), and thickening again at the furthest terminal reaches. This suggested that flowing mass accumulates at the sill and eventually triggers a discharge of mass downglacier from the sill, resulting in the extension and thinning of ice downglacier of the sill. This sequence led to the hypothesis that the point where the bed transitions from the sill (above sea level) to below sea level acts as a hinge point, where velocity changes only occur in the region that is below sea level (Van Wychen et al., 2016). The Milne, McClintock, and Ekblaw Glaciers of Ellesmere Island are also thought to be pulse-type (Van Wychen et al., 2016; Van Wychen et al., 2020). Terminus behavior is similar to surge-type glaciers, where termini advance during acceleration and retreat during deceleration (Van Wychen et al., 2016).

2.2.5.3 Continuously Accelerating Glaciers

2.2.5.3.1 Trinity and Wykeham Glaciers

Trinity Glacier, a tidewater glacier on Ellesmere Island, has shown consistent acceleration since 1999, with surface velocities of at least 800 m/yr in the lower 10 km since 2018 (Van Wychen et al., 2016; Van Wychen et al., 2020). The acceleration has been activating upglacier, reaching 30 km from the

terminus by 2018 (Van Wychen et al., 2020). Wykeham Glacier is adjacent to Trinity Glacier and is also tidewater terminating and has shown similar behavior. Continuous acceleration has been observed in its terminal region since 1999, with velocity reaching ~800 m/yr (Van Wychen et al., 2016; Van Wychen et al., 2020). Acceleration has progressively activated upglacier, reaching ~20 km from the terminus by 2020 (Van Wychen et al., 2020). Most of the length of the beds under the termini of Trinity and Wykeham are situated below sea level, and acceleration has been restricted to this region (Van Wychen et al., 2016). Belcher Glacier of Devon Island may also have been accelerating continuously since 1999 (Van Wychen et al., 2016; Van Wychen et al., 2020).

Although Trinity, Wykeham, and Belcher Glacier have been continuously accelerating over the past two decades, their termini have retreated (Van Wychen et al., 2016). This contrasts with surge and pulse-types, whose termini advance with acceleration. It was proposed that the acceleration of Trinity, Wykeham, and Belcher initially resulted in increased calving (Van Wychen et al., 2020). This is plausible since ocean contact is known to undercut and predispose termini to melting and calving (Motyka et al., 2003). The subsequent retreat may reduce back-stress on the main trunk of the glaciers (i.e., reduced terminal mass available to impede motion of the upper end of the glacier), especially because their beds are below sea level (Van Wychen et al., 2016; Van Wychen et al., 2020). The reduced back-stress is thought to facilitate consistent acceleration toward the ocean (Millan et al., 2017; Van Wychen et al., 2016). Additionally, the termini may be becoming ungrounded and reaching floatation, resulting in further vulnerability to break-up and faster flow (Dalton et al., 2022). Of note, bedrock imaging available for Trinity Glacier showed no presence of a sill, whereas the beds under some pulsing glaciers do have sills. The absence of a sill ridge at Trinity Glacier's terminus, combined with the fact that the terminus is below sea level, may explain why Trinity Glacier's exhibits continuous acceleration as opposed to oscillating acceleration (Van Wychen et al., 2016).

2.2.5.3.2 Split Lake Glacier

Split Lake Glacier, a small glacier on southwest Ellesmere Island, is an example of a glacier that has experienced long-term acceleration. However, unlike Trinity and Wykeham Glaciers, its terminus has remained relatively stable rather than retreated. The midsection of the glacier, which flows through a valley wall constriction, was flowing at elevated speed of 200-300 m/yr in 2000. By 2001, midsection flow increased to 500 m/yr and from 2005-present day, velocities were consistently between 400-550 m/yr. Optical imagery showed the appearance of ogives (a type of crevasse) in ~1970, suggesting that acceleration began around this time. For comparison, nearby geomorphologically similar glaciers have maximum velocities of 100 m/yr (Van Wychen et al., 2016). Split Lake Glacier's terminus was found to be stable/advancing between 1959-2020. In contrast, two adjacent land terminating glaciers showed terminus retreat. From 2000-2014, glacier thinning was observed in the upper region about one order of magnitude higher than adjacent glaciers, while the lower region showed moderate thickening of ~0.25-1 m/yr. This surface elevation gain is contradictory to the expected mass loss modelled by Noël et al. (2018) which indicated that this lower region should show thinning. This discrepancy suggests that glacier flow and transfer of mass must be a key control for the geometry changes of the glacier. The velocity and geometry changes suggested that Split Lake Glacier had been in a 'slow surge' from 1970 to the present day, an unusually long acceleration period for the Canadian Arctic. It was speculated that the valley constriction modulates ice flow in a similar way that bedrock ridges modulate the flow of pulse-type glaciers (Van Wychen et al., 2016).

2.2.5.3.3 Good Friday Bay Glacier

Good Friday Bay Glacier is another glacier which has demonstrated unusually prolonged high speeds. A detailed study by Medrzycka et al. (2019) found that the terminus had advanced 9.3 km over 1948-2018. From 2006-2018, velocity at the main trunk was between 100-250 m/yr. At the terminus, velocity was 350 m/yr, similar to those found in the 1960s by Müller (1969). The bed drops below sea level

at 20 km from terminus, however, this is not consistent over the full width of the channel and most of the ice is grounded above sea level. Ice motion showed greater variability downglacier from the point where the ground dips below sea level, with a velocity peak immediately down glacier of a nunatak located ~9km upglacier of the terminus. Thickening was observed upglacier of the nunatak and thinning observed downglacier of the nunatak. It was concluded that Good Friday Bay Glacier may be in an ongoing surge that initiated in 1950s, which would be the longest active phase ever documented.

2.2.5.4 Ice Discharge and Glacier Dynamics

It is important to understand how glacier dynamics affect ice discharge to the ocean (mass loss due to calving) in the Canadian Arctic. Millan et al. (2017) found that from 1991-2005, ice discharge in the Queen Elizabeth Islands accounted for ~52% of the mass lost to the to the ocean. The remaining ~48% of the mass loss was attributed to glacier surface melt and runoff. However, from 2005-2014, ice discharge represented only ~10% of mass loss whereas surface melt represented ~90% of loss. Although surface melt dominated mass loss in the Canadian Arctic in recent years, ice dynamics (including surges) were the dominant cause of mass loss in a few regional basins during this period (Millan et al., 2017).

Accelerating glaciers can contribute markedly to mass loss, especially from individual glacier basins. For example, the Trinity and Wykeham glaciers, which have both been accelerating since at least 1999, contributed ~62% of the total ice discharge to the ocean from the Ellesmere/Axel Heiberg Island region between 1999-2015 (Van Wychen et al., 2016). These glaciers were found to contribute to 37% of ice discharge from the Queen Elizabeth Islands as a whole from 2010-2015 (Millan et al., 2017). More broadly, only 10 glaciers from Ellesmere/Axel Heiberg Islands contributed ~70% of the total dynamic discharge between 1999-2015 (Van Wychen et al., 2016). The variation in dynamic discharge between glaciers implies a need for further study of how mass loss evolves with changing dynamics in the Canadian Arctic (Van Wychen et al., 2020).

2.2.5.5 Velocity Variability in the Canadian Arctic

The classical surge-type glacier in the Canadian Arctic tends to align with the Svalbard surge cycle timing and is therefore likely regulated by similar mechanisms (Copland et al., 2003). However, striking variability in flow patterns occurs in the region, as demonstrated by the pulse-types and consistently accelerating glaciers discussed above. This led Van Wychen et al. (2020) to suggest that glacier flow patterns follow a spectrum of behavior, rather than discrete classes of "surge" or "normal" flow. Furthermore, surge behavior itself may be a spectrum, where patterns exist that do not align with the traditional classification structure of Alaskan and Svalbard types, such as the pulse-types and continually accelerating glaciers. The causes for this variability remain elusive. This uncertainty can be attributed to the fact that many of the Canada-focused studies are region wide and only offer brief analysis of when and how individual glaciers surge. Studies dedicated to individual surge-type glaciers are needed to investigate the causes of dynamic variability and to fully catalogue the wide variability in surge characteristics within the region. Critically, more information is needed on the relationships between bedrock topography, subglacial hydrology, and velocity changes at the individual glacier basin level.

2.2.6 Summary

The enthalpy balance theory by Sevestre and Benn (2015) suggests that climate and glacier geometry are likely implicated in all surge mechanisms. Based on this premise, the global distribution of surge-type glaciers could change with ongoing climate change (Sevestre and Benn 2015). Studies of surge behavior remain essential for quantifying how glacier dynamics may evolve in a warming climate and continue to contribute to sea level rise. Though the Alaskan-type and Svalbard-type studies offer explanation as to why some glaciers surge, these categories cannot explain the observations for all oscillatory dynamic behavior. The dynamic variability seen in the Canadian Arctic points to the possibility that a spectrum of dynamic patterns and surge mechanisms likely exists. Studies of individual surge-type glaciers in the Canadian Arctic are needed to further characterize and quantify the causes of flow pattern

variability, and the study of Otto Glacier in this thesis was undertaken to help fill this gap. This knowledge can be used to complete a catalogue of dynamic behavior in the Canadian Arctic, as well as aid in the interpretation of other types of dynamic behavior in Canada and other remote parts of the world.

Chapter 3 - Methodology

The datasets and processing methods used to determine glacier velocity changes, terminus extent changes, surface elevation changes, and bedrock topography change of Otto Glacier are presented here. Since field data were not available for Otto Glacier, the following remotely sensed datasets were used in this study:

- Velocity changes for Otto Glacier:
    - European Remote Sensing (ERS) data for the years 1992-1994 (synthetic aperture radar)
    - NASA's ITS_LIVE optical data for the years 1999-2012
    - RADARSAT2 (R2) for the years 2009-2020 (synthetic aperture radar)
- Glacier terminus extent changes: ERS, Landsat (optical), and R2 data
- Glacier surface elevation changes: pre-generated elevation change products from Hugonnet et al. (2021)
- Bedrock topography: Centre for Remote Sensing of Ice Sheets (CReSIS) Multichannel Coherent Data Depth Sounder (MCoRDS)

3.1 Glacier Velocity Datasets

Satellite imagery can be used to derive glacier velocity by calculating the displacement of the glacier between a reference image and a repeat image acquired later in time. For this study, velocity measurements were derived from both optical imagery and SAR data. SAR imagery has the advantage of the ability to image during the polar night and through clouds, however optical imagery is available for a longer period of time. Therefore, the combined use of RADAR and optical imagery allows for a time-dense record of Otto Glacier's velocity changes to be created. Optical data have been known to produce slightly higher velocities than RADAR data because optical data can only be captured during the polar summer, when velocities are typically higher due to increased basal melt water and subsequent sliding (Van

Wychen et al., 2016). However, the difference has been found to be small (optical summer velocities ~14% higher than winder RADAR) in the context of the high speeds of surging glaciers (Van Wychen et al., 2016). In this section, the methodologies used to derive glacier velocity from each sensor are reviewed. Differences of resolution between optical and radar products are summarized in Table 3-4. Error sources for each sensor are discussed at the end of each sub-section.

3.1.1 Optical-Derived Velocities

Optical remote sensing is a form of passive remote sensing, which acquires images by capturing solar radiation that is reflected by objects. Because of this, optical sensors are not able to collect images of earth surface when the view is obstructed by clouds and are unable to acquire imagery at night. Optical imagery can be used to determine glacier velocity through feature tracking. Feature tracking measures the displacement of a group of pixels from a reference image and a repeat image over the same area acquired at a later time. The output is a raster image showing velocity values for each pixel. This method is commonly used to measure optical-derived velocity data in the Canadian Arctic, including the velocities of fast flowing glaciers (Copland et al., 2003; Medrzycka et al., 2019; Van Wychen et al., 2016).

Pre-generated glacier velocity products derived from optical imagery were obtained from the ITS_LIVE Project by NASA Jet Propulsion Laboratory (Gardner et al., 2019, https://its-live.jpl.nasa.gov/). The ITS_LIVE Project provides a global set of glacier and ice sheet velocity products compiled from Landsat 4,5,7, and 8 platforms. Data covering Otto Glacier is available for the years 1999-2018 and products are available as either annual velocity composites or individual image pairs that can be selected by the user. In this thesis the pre-derived annual velocity composites are used which have the advantage of capturing velocity changes across all seasons.

These velocity products were created using the Jet Propulsions Laboratory's autonomous repeat image feature tracking (auto-RIFT) algorithm, as described in Gardner et al. (2018). The secondary image can either be from the same satellite position as the reference image (same-path-row) or a different

satellite position in either adjacent or near-adjacent orbit swaths (cross-path row). Same-path-row image pairs are processed if they were acquired less than 546 days apart. Cross-path image pairs are processed if they are acquired 10-96 days apart. The reason for this difference in time between images is that the appearance of glacier surface features differs between images acquired from different flight paths due to differences in imaging geometry. Cross-path images must therefore be processed with a shorter period of time separation, since the images are acquired from slightly different perspectives and therefore the appearance of the features will change more quickly between images. Cross-path row images were included to increase data density prior to the launch of Landsat 8, the most recent platform for the data. Additionally, the cross-path rows produce lower signal-to-noise ratios due to residual parallax from imperfect terrain correction (Gardner et al., 2018).

The methods for processing the already made velocity products are described by Gardner et al. (2018). For the auto-RIFT feature tracking, same-path-row and cross-path-row reference and repeat images are searched for matching features using a normalized cross correlation (NCC) algorithm. The NCC algorithm finds a local NCC maxima within a specified search distance. A sparse search is used initially to find areas of coherent correlation between images. The sparse search results then guide a dense search, where search centers are spaced so that there is no overlap between adjacent template search chips. Successful matches (good correlation between features) are found using a novel normalized displacement coherence (NDC) filter (filtering is applied to search-normalized displacements). Normalized displacements were accepted if at least 7 of the values in a 5 by 5 pixel-centered window are within one quarter of a search distance for both the horizontal and vertical displacement. This process iterates three times. Lastly, a two-times iterative filter is applied to remove any displacements that were accepted due to random agreement with neighbors. For this second filter, only displacements that agree within 4 times the centered 5 by 5 window mean absolute deviation are retained. The final resolution is 240 m x 240 m. Velocity uncertainty in these products can be as high as 15 m in x and y directions due to geolocation

errors. This can result in velocity errors of up to 30 m/yr. However, this error is negligible for the study of Otto Glacier, since this glacier has been found to surge at >1000 m/yr (Van Wychen et al., 2020).

3.1.1.1 ArcPro 2.9.0 and Post-Processing

For this thesis, the ITS_LIVE velocity products were visualized as raster images in ArcPro 2.9.0 and arranged in chronological order. A centerline was drawn manually along the glacier (Figure 3-1), from which velocity data were extracted, and is a common method for measuring glacier velocity (Dalton et al., 2022; Millan et al., 2017; Van Wychen et al., 2020). These "centerline" velocities were used because the center is typically the fastest moving section of a glacier, as it is furthest away from adjacent constrictions such as valley walls or neighboring glaciers. The centerline was drawn manually to capture the maximum velocity variability along the raster image. The line was then divided into points that are 100 m apart. The interval of 100 m was chosen, as this is usually the minimum distance where appreciable velocity changes can be detected but is also large enough to reduce sample points and processing time. Velocity data from each of these points were then extracted into an excel file using the "Extact Multi Values to Points" tool, where the quantitative data were further analyzed. Due to the high volume of data points, velocities were averaged every 400 m and then plotted on line graphs. The graphs include black vertical lines that delineate important changes in velocity trends based on qualitative assessment of the data.

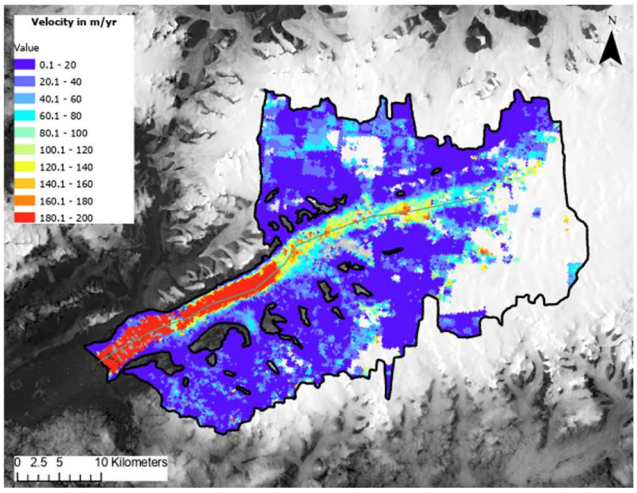

Figure 3-1: Example of centerline over ITS_LIVE annual velocity composite (from 2004) over Landsat 8 imagery (acquired August 16, 2021), clipped to the RGI 6.0 outline for Otto Glacier. The green line represents the manually digitized centerline used to extract velocity. The centerline was manually drawn to capture the most velocity activity.

3.1.2 SAR-Derived Velocities

In the simplest terms, SAR sensors emit radar energy to the earth surface and measure how much of energy is returned to the sensor (NASA, 2021). For radar sensors, longer antennas typically produce higher spatial resolutions. SAR antennas are made shorter to reduce payload, however, multiple images are combined to produce high spatial resolutions, thus simulating a large antenna, and lending the term "synthetic" (NASA, 2021). An additional advantage is that SAR sensors emit radiation from the microwave portion of the electromagnetic spectrum (wavelength 1 cm - 1 m, frequency ~0.3-40 GHz), and these longer wavelengths allow signal to penetrate cloud and rain (Government of Canada, 2015). As such, because SAR does not rely on solar light, it is able to image during the polar winter. Individual SAR sensors can only emit one wavelength/frequency, and the wavelength is referred to as a band (Government of Canada, 2015). Bands are named with code letters that were assigned during World War II (e.g. C-band, X-band) and are still used today (Table 3-1) (Government of Canada, 2015). Each band interacts uniquely with different types of targets, and therefore has unique purposes as shown in Table 3-1.

Table 3-1: SAR bands and associated frequency, wavelengths, and applications. From https://www.earthdata.nasa.gov/learn/backgrounders/what-is-sar

Band	**Frequency**	**Wavelength**	**Typical Application**
Ka	27–40 GHz	1.1–0.8 cm	Rarely used for SAR (airport surveillance)
K	18–27 GHz	1.7–1.1 cm	Rarely used (H_2O absorption)
Ku	12–18 GHz	2.4–1.7 cm	Rarely used for SAR (satellite altimetry)
X	8–12 GHz	3.8–2.4 cm	High resolution SAR (urban monitoring, ice and snow, little penetration into vegetation cover; fast coherence decay in vegetated areas)

C	4–8 GHz	7.5–3.8 cm	SAR Workhorse (global mapping; change detection; monitoring of areas with low to moderate penetration; higher coherence); ice, ocean maritime navigation
S	2–4 GHz	15–7.5 cm	Little but increasing use for SAR-based Earth observation; agriculture monitoring (NISAR will carry an S-band channel; expends C-band applications to higher vegetation density)
L	1–2 GHz	30–15 cm	Medium resolution SAR (geophysical monitoring; biomass and vegetation mapping; high penetration, InSAR)
P	0.3–1 GHz	100–30 cm	Biomass. First p-band spaceborne SAR will be launched ~2020; vegetation mapping and assessment. Experimental SAR.

Radar sensors can emit and measure backscatter in different polarizations, which refers to the orientation of the electromagnetic wave relative to the flight path and affects how the wave interacts with the target object (Government of Canada, 2015). Polarization may be either horizontal, vertical, or circular positioned, but radar sensors typically transmit and receive either horizontally or vertically polarized microwaves. These polarizations are designated by H and V, respectively (Government of Canada, 2015). Therefore, there can be four combinations of transmission/reception polarization: HH for horizontal transmit and horizontal receive, VV for vertical transmit and vertical receive, HV horizontal transmit and vertical receive, and VH for vertical transmit and horizontal receive. (Government of Canada, 2015).

Radar systems consist of a transmitter, receiver, antenna, and an electronics system that records the data (Government of Canada, 2015). The transmitter emits regularly-timed timed pulses (A in Figure 3-2) which are focused into a beam by the antenna (B in Figure 3-2). The beam is then emitted obliquely,

typically at a right angle to the flight path, and interacts with the earth surface. Energy that is reflected by the surface and detected by the sensor is called backscatter (C in Figure 3-2). The sensor then records the intensity and the phase of the backscatter. The sensor also records the time duration between transmission and reception of signal, which allows the object's location to be determined. The amount of backscatter received depends on the properties of the object reflecting it, such as roughness, impurities, and moisture content. The strength of the backscatter produces raw images that appear as a salt and pepper pattern with no recognizable object. The raw images must be processed to produce an image with recognizable objects.

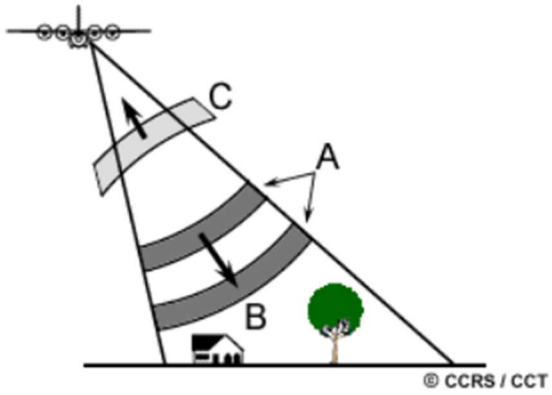

Figure 3-2: Radar transmission and reception (Government of Canada, 2015) https://natural-resources.canada.ca/maps-tools-and-publications/satellite-imagery-and-air-photos/tutorial-fundamentals-remote-sensing/microwave-remote-sensing/radar-basics/9355

Imaging geometry is an important consideration when comparing satellite imagery (Figure 3-3). Geometric distortion can occur when comparing images from different satellites (and therefore different imaging geometry), or from the same satellites but different flight paths (also different image geometry). In radar systems, the flight path is the direction of flight (A in Figure 3-3) and nadir is directly beneath the platform (B in Figure 3-3). The beam is transmitted obliquely at right angles to the flight path, illuminating a swath (C in Figure 3-3), creating a side-looking viewing geometry. "Range" refers to the dimension that

is perpendicular to flight path (D in Figure 3-3), and “azimuth” refers to the dimension that is parallel to flight path (E in Figure 3-3).

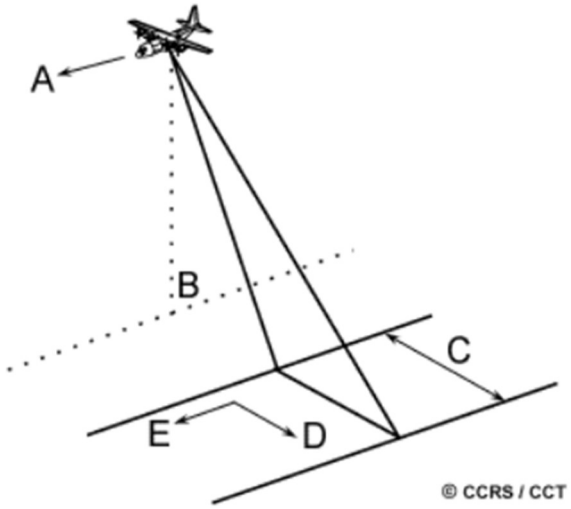

Figure 3-3: Imaging Geometry of a typical radar platform (Government of Canada, 2016: https://natural-resources.canada.ca/maps-tools-and-publications/satellite-imagery-and-air-photos/tutorial-fundamentals-remote-sensing/microwave-remote-sensing/viewing-geometry-and-spatial-resolution/9341).

To determine glacier velocity from SAR data, an offset tracking code is used to calculate displacement between the reference image to a repeat image later in time. Offset tracking is similar to feature tracking, however the offset tracking in the context of this thesis specifically handles SAR data. Offset tracking requires coherence between images, meaning that backscatter values must be similar (Strozzi et al., 2002). Incoherence results in errors in displacement calculation (Strozzi et al., 2002). To maintain coherence, images must have the same look-geometry (i.e., they must come from the same sensor and same flight path), as geometric distortion between images will change backscatter values. Images must also have surface features that are preserved between acquisitions, so changes in snow accumulation or melt water on the glacier surface, which can alter backscatter values between images, need to be minimized (Strozzi et al., 2002).

For this study, data from two SAR missions were used: ERS-1 data and R2 data. Reference and repeat images were manually arranged into pairs that allow for good coherence. Each dataset is described below, followed by a section that describes the offset tracking procedure.

3.1.2.1 ERS Data

ERS consisted of two satellites operating in tandem, ERS-1 (launched in 1991, discontinued in 2000) and ERS-2 (launched in 1995, discontinued in 2011) (European Space Agency, n.d.). The tandem system consisted of a set of four radar antennae: three for a scatterometer and one for the SAR. Backscatter from the earth surface provided data on wind fields and wave spectra. For the purposes of this study, ERS-1 data spanning the years 1992-1994 were utilized, since this was the only period that offered images covering Otto Glacier. Therefore, only ERS-1 is discussed here.

ERS-1 consisted of an active microwave instrument (AMI), radar altimeter, along-track scanning radiometer and microwave sounder, laser retro reflector (ensures accuracy of satellite tracking from the ground), and perceive range and range-rate equipment (European Space Agency, 2012). The AMI collected the images used in this thesis. ERS-1 could collect data in three modes: imaging mode (for earth surface analysis), wave mode (ocean wave analysis) and wind scatterometer mode (for wind analysis). Glacier images were collected in the imaging mode in C-band (frequency 5.3 GHz, wavelength 5.66 cm) at a spatial resolution of <=30 m in azimuth and <=26 m in range, swath width 100 km, and incidence angle 23 degrees, altitude 782-785 km, and a polarization of VV (European Space Agency, 2012). The repeat cycle (orbital period) at the time of data acquisition for this study was 3 days, which allows glacier displacement to be calculated over any time duration that is a multiple of three. The high spatial and temporal resolution of ERS-1, as well as the historic operational dates, make ERS-1 an ideal instrument for acquiring multi-decadal velocity data in glaciers in fine detail.

Images from ERS-1 that covered Otto Glacier were downloaded from the Alaskan Satellite Facility data portal (https://search.asf.alaska.edu/#/?zoom=3.000andcenter=-97.494,39.673). Images were manually arranged into pairs that could be used in the offset tracking code. For the purposes of this study, images acquired at 6 or 12 days apart were used. Image pairs of shorter time separation are less likely to reveal appreciable changes in Otto Glacier's velocity structure and so were not included. Image pairs of

longer time separation are more likely to show significant change in the glacier surface, resulting in loss of coherence and subsequent inaccuracy of displacement calculation during offset tracking, and so images over 12 days apart were not included. Image pairs must be from the same look direction to allow for the same imaging geometry and thus sufficient overlap of the glacier between images. This allows for geometric coherence and better accuracy in calculating glacier displacement. The following image pairs were used (Table 3-2):

Table 3-2: Summary of ERS-1 image pairs used to determine glacier flow used in this thesis.

Reference image (yyyy/mm/dd)	**Repeat image (yyyy/mm/dd)**	**Polarization**
1992/02/11	1992/02/23	VV
1992/02/20	1992/03/03	VV
1992/03/03	1992/03/15	VV
1992/03/18	1992/03/30	VV
1992/03/21	1992/03/27	VV
1993/12/29	1994/01/10	VV

3.1.2.2 R2 Data

The R2 mission is a Canadian SAR sensor that was launched in 2007 and is still operational today (Government of Canada, 2021). R2 emits radar waves in C-band (frequency 5.4 GHz) and operates at an altitude of 798 km with an orbital period of 24 days. R2 can operate in various beam modes (Fine, Wide Fine, Standard, ScanSAR Narrow, ScanSAR Wide, Ocean Surveillance), each of which have different spatial resolutions. This study used data from fine beam mode, which provide the highest spatial resolution at 8 m and swath width of 50 km. R2 polarization is available in HH, VV, HV, and VH, however the data obtained for this study were acquired in HH polarization. Images were obtained from Environment and Climate Change Canada and were manually arranged into pairs so that the offset tracking code can track glacier

displacement. Images that were 24 days apart could be paired and in total 85 image pairs were usable for analysis (Table 3-3).

Table 3-3: Summary of R2 image pairs used for analysis, including reference/repeat image date, beam mode, polarization.

Reference image date (yyyy/mm/dd)	Repeat image (yyyy/mm/dd)	Beam Mode	Polarization
2009/01/07	2009/01/31	F2	HH
2009/01/31	2009/02/24	F2	HH
2009/02/14	2009/03/10	F6	HH
2009/02/20	2009/03/16	F22	HH
2009/02/22	2009/03/18	F6	HH
2009/02/24	2009/03/20	F2	HH
2009/02/26	2009/03/22	F23	HH
2009/03/10	2009/04/03	F6F	HH
2009/03/16	2009/04/09	F22	HH
2009/03/18	2009/04/11	F6	HH
2009/03/20	2009/04/13	F2	HH
2009/04/13	2009/05/07	F2	HH
2009/08/24	2009/09/17	F21N	HH
2009/09/17	2009/10/11	F21N	HH
2009/10/11	2009/11/04	F21N	HH
2009/11/04	2009/11/28	F21N	HH
2010/02/20	2010/03/16	F4	HH
2011/01/26	2011/02/19	F2F	HH
2012/01/03	2012/01/27	F0W1	HH
2012/01/04	2012/01/28	F0W1	HH
2012/01/28	2012/02/21	F0W1	HH
2012/02/20	2012/03/15	F0W1	HH
2012/02/21	2012/03/16	F0W1	HH
2013/03/11	2013/04/04	F0W1	HH
2013/11/05	2013/11/29	F0W1	HH
2013/11/06	2013/11/30	F0W1	HH
2013/12/23	2014/01/16	F0W1	HH
2014/01/16	2014/02/09	F0W1	HH
2014/01/17	2014/02/10	F0W1	HH
2014/02/09	2014/03/05	F0W1	HH
2014/02/10	2014/03/06	F0W1	HH
2014/03/05	2014/03/29	F0W1	HH
2014/03/06	2014/03/30	F0W1	HH
2014/03/30	2014/04/23	F0W1	HH
2014/12/18	2015/01/11	F0W1	HH
2014/12/19	2015/01/12	F0W1	HH
2015/01/11	2015/02/04	F0W1	HH
2015/01/12	2015/02/05	F0W1	HH
2015/02/04	2015/02/28	F0W1	HH
2015/03/01	2015/03/25	F0W1	HH
2015/12/13	2016/01/06	F0W1	HH
2015/12/14	2016/01/07	F0W1	HH
2016/01/07	2016/02/23	F0W1	HH

2016/03/18	2016/04/11	F0W1	HH
2016/03/19	2016/04/12	F0W1	HH
2016/11/13	2016/12/07	F0W1	HH
2016/11/14	2016/12/08	F0W1	HH
2016/12/07	2016/12/31	F0W1	HH
2016/12/31	2017/01/24	F0W1	HH
2017/01/24	2017/02/17	F0W1	HH
2017/01/25	2017/02/18	F0W1	HH
2017/02/17	2017/03/13	F0W1	HH
2017/02/18	2017/03/14	F0W1	HH
2017/03/13	2017/04/06	F0W1	HH
2017/03/14	2017/04/07	F0W1	HH
2017/04/06	2017/04/30	F0W1	HH
2017/11/08	2017/12/02	F0W1	HH
2017/11/09	2017/12/03	F0W1	HH
2017/12/02	2017/12/26	F0W1	HH
2017/12/03	2017/12/27	F0W1	HH
2017/12/26	2018/01/19	F0W1	HH
2017/12/27	2018/01/20	F0W1	HH
2018/01/19	2018/02/12	F0W1	HH
2018/01/20	2018/02/13	F0W1	HH
2018/02/12	2018/03/08	F0W1	HH
2018/02/13	2018/03/09	F0W1	HH
2018/03/08	2018/04/01	F0W1	HH
2018/04/01	2018/04/25	F0W1	HH
2018/04/02	2018/04/26	F0W1	HH
2018/11/03	2018/11/27	F0W1	HH
2018/11/04	2018/11/28	F0W1	HH
2018/11/27	2018/12/21	F0W1	HH
2018/11/28	2018/12/22	F0W1	HH
2018/12/21	2019/01/14	F0W1	HH
2018/12/22	2019/01/15	F0W1	HH
2019/01/14	2019/02/07	F0W1	HH
2019/02/08	2019/03/04	F0W1	HH
2019/03/03	2019/03/27	F0W1	HH
2019/03/04	2019/03/28	F0W1	HH
2020/01/10	2020/02/03	F0W1	HH
2020/02/02	2020/02/26	F0W1	HH
2020//02/03	2020/02/27	F0W1	HH
2020/02/26	2020/03/21	F0W1	HH

3.1.2.3 Offset Tracking of RADAR Data

The R2 and ERS-1 data were processed using an offset tracking algorithm which determines the glacier's velocity by calculating glacier displacement between the reference image and a repeat image over the orbital period (Short and Gray, 2005; Strozzi et al., 2002). The output is again a raster image

containing velocity data for each pixel. Offset tracking has proven to be an effective method for deriving glacier velocity from SAR images (Short and Gray, 2005; Van Wychen et al., 2016). The code was run in the GAMMA-Remote Sensing InSAR software and the following sections provide a detailed overview of the offset tracking procedure.

SAR Image pairs were manually arranged for each sensor, with each pair containing a reference image and a repeat image after completion of the orbital period, as described in the preceding sections. ERS-1 images were paired at 6 and 12 days apart and R2 images at 24 days apart. To maintain coherence between images, both images must have been taken from the same orbital path so that look-geometry is maintained. Using images that have the same look-geometry preserves the backscatter values that are received by the sensor in both images, whereas a different look geometry can produce different backscatter between images and make offset tracking impossible. The images were obtained in a proprietary single-look complex (SLC) format. Therefore, before the offset tracking code can begin, the SLC SAR images are converted into a more generic SLC format that the GAMMA InSAR software can use along with an accompanying parameter file. These new SLC files are then used to create multi-look files that allow the user to interpret the image visually (no phase information, only intensity information). The parameter file contains parameter information such as beam mode, pixel size, date of image acquisition, and other important details. The new image files were then coregistered prior to offset tracking. Digital elevation models (DEMs) are used to remove the topographic portion of slant range displacement and geolocate the results. For this project, DEMs were obtained from the Copernicus collection using the GLO-30 dataset from the TanDEM-X data, from https://spacedata.copernicus.eu/collections/copernicus-digital-elevation-model.

To measure the displacement of a group of pixels between the reference and repeat image, the offset tracking code must first search for a group of pixels in the reference image that correlates to a group of pixels in the repeat image. The group of pixels with the highest correlation is then used to calculate

displacement. To search pixels, a search window size must be decided by the user and entered into the code. The search window is the number of pixels that are searched at a time (in x and y directions). Step size must also be determined by the user and entered into the code, which is the distance moved by the search window with each search. Window and step size can affect the noise and error in the final velocity raster image output, and sometimes requires experimentation with different values to determine appropriate sizes. For R2 data in the Canadian Arctic, window sizes of 200 x 200 and step sizes of 20 x 20 pixels have proven effective for deriving glacier velocity (Short and Gray, 2005; Van Wychen et al., 2020). These parameters produced good results for Otto Glacier and did not require further experimentation. For ERS-1 data, a window sizes of 200 x 200 pixels and step size of 20 x 20 produced large errors (Figure 3-4A) where streaking appeared over the glacier and over the ground which should not have any velocity. A new window size of 256 pixels in range and 512 pixels azimuth, and a new step size of 32 pixels in range and 64 pixels in azimuth was next attempted, since this produced good results for ERS-1 data in other surge-type glaciers in the Canadian Arctic (Lauzon, 2022). These produced the relatively clean and consistent results for the ERS-1 data and thus were used for the remainder of ERS-1 processing (Figure 3-4B).

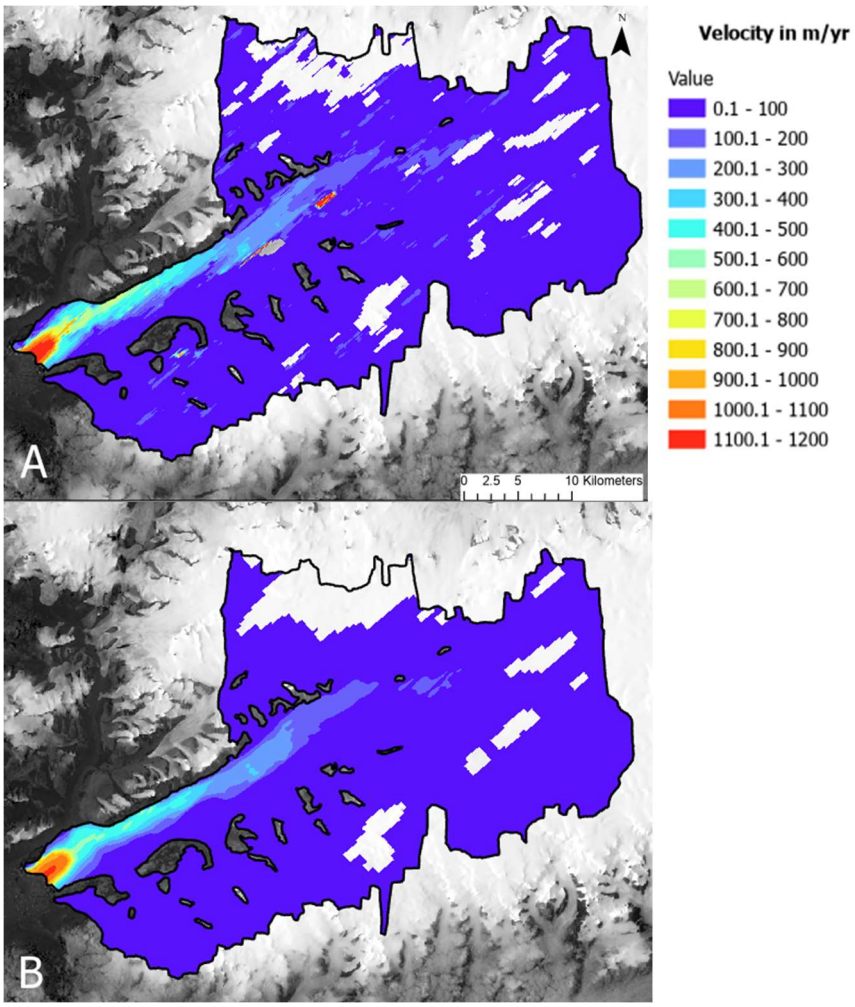

Figure 3-4: Comparison of ERS-1 velocity data processed with different window and step sizes (raster images derived from velocity data for 1992/01/18-1992/01/30. (A) was produced using a window size of 200 x 200 pixels and step size of 20 x 20 pixels and resulted in streaking over the glacier. (B) was produced with a window size of 256 pixels in range and 512 pixels in azimuth and a step size of 32 pixels in range and 64 pixels in azimuth and resulted in less noise in the final raster image. Glacier extent provided as black outline from the RGI 6.0. Underlying image obtained from Landsat 8 (acquired August 16, 2021).

Offset tracking applies a cross correlation algorithm to locate a group of matching pixels between each the reference and repeat, and the calculated displacement of this correlated group of pixels in x and y directions is used to infer glacier velocity (Figure 3-5). Total displacement is calculated by the code using Equation 3-1:

Equation 3-1: Displacement calculation in offset tracking.

Total displacement = SQRT((azimuth displacement^2) + (range displacement^2))

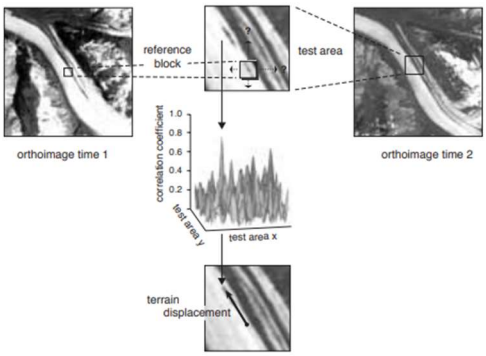

Figure 3-5: Process of measuring horizontal displacement during offset tracking, from Kääb (2005).

After offset tracking is complete, the code outputs a GeoTIFF raster image containing displacements along the glacier that can be visualized in GIS software, in this case ArcPro 2.9.0. Figure 3-6 shows a simplified workflow of the offset tracking procedure.

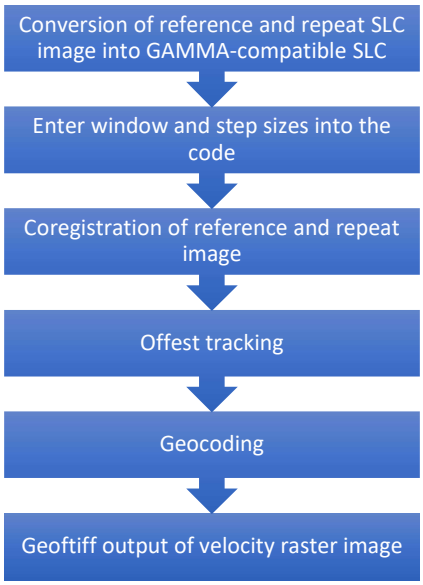

Figure 3-6: Simplified workflow of offset tracking procedure. The process begins with converting the reference and repeat image into a GAMMA-compatible format, entry of window and step sizes, and coregistration of the images. Offset tracking then proceeds with geocoding of the results and the output is a GeoTIFF velocity raster image that can be viewed in ArcPro 2.9.0.

3.1.2.4 ArcPro 2.9.0 and Post-Processing

ArcPro 2.9.0 was used for post-processing of the output GeoTIFF files produced by the GAMMA offset tracking function. Specifically, the "Raster Calculator" tool was used to convert the GAMMA velocity GeoTIFFs into a standardized m/yr product. This must be done because the GAMMA GeoTIFFs are produced in displacement per days in a repeat pass, e.g. meters per 24 days in the case of R2 imagery and

meters per 6 or 12 days for the ERS-1 imagery, and velocity values cannot be compared when they are in different unit formats. Thus, in raster calculator, the output displacement tiff is divided by 24 for R2 data and either 6 or 12 for ERS-1 data, and multiplied by 365.25 (0.25 days was added to account for leap years) which gives a result in m/yr. A glacier outline polygon from the Randolf Glacier Inventory (RGI) (version 6.0: GLIMS: Global Land Ice Measurements from Space) was used to clip the velocity data to the Otto Glacier area. Velocities were then binned at 50-200 m/yr intervals (10-12 groups) to more easily visualize flow along the glacier.

Next, velocity data from the center of the glacier were collected. The centerline was drawn manually in ArcPro 2.9.0. A new line was drawn for each sensor to ensure the line followed the path of maximum velocity variability (Figure 3-7 for ERS-1, Figure 3-8 for R2). The centerline was then divided into points that are 100 m apart, as with the optical data. Velocity data from each of these points were then extracted (using the "Extract Multi Values to Points" tool) into an MS Excel file for further quantitative analysis, including visualization with line graphs, where black vertical lines were again used to indicate important changes in velocity trends based on qualitative assessment. Figure 3-9 shows a simplified workflow for post processing in ArcPro 2.9.0.

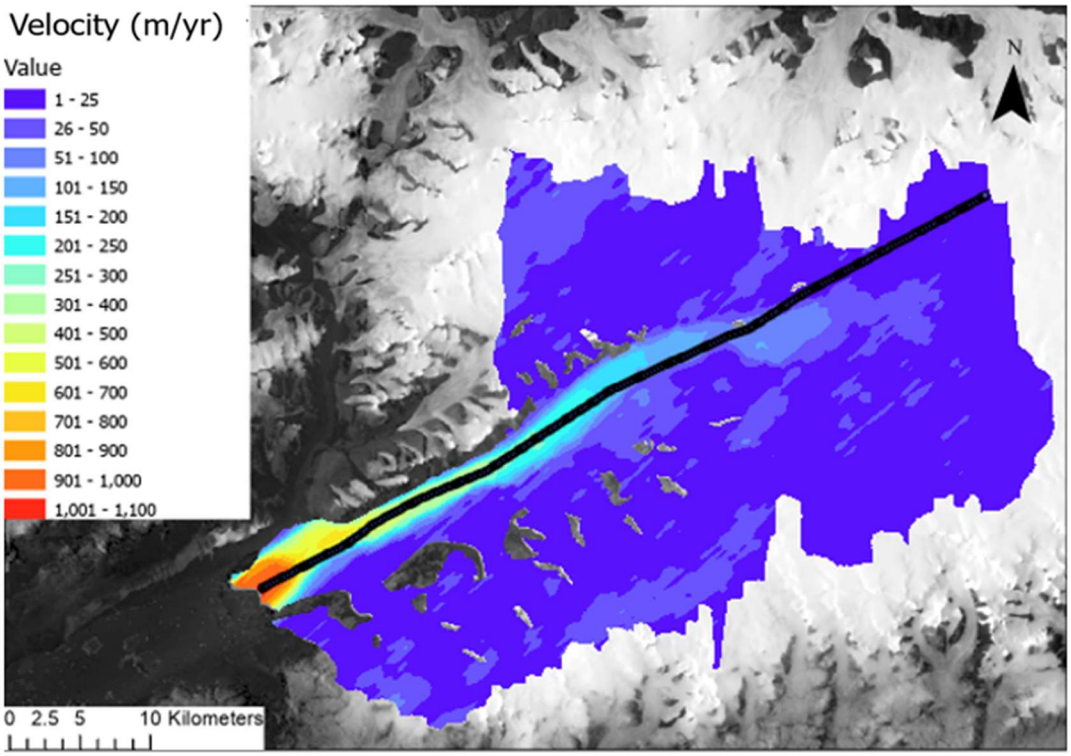

Figure 3-7: Example of centerline points used for extraction for ERS-1 raster with velocity from 1992/02/11-1992/02/23 (overlaid on Landsat 8 imagery acquired on August 16, 2021).

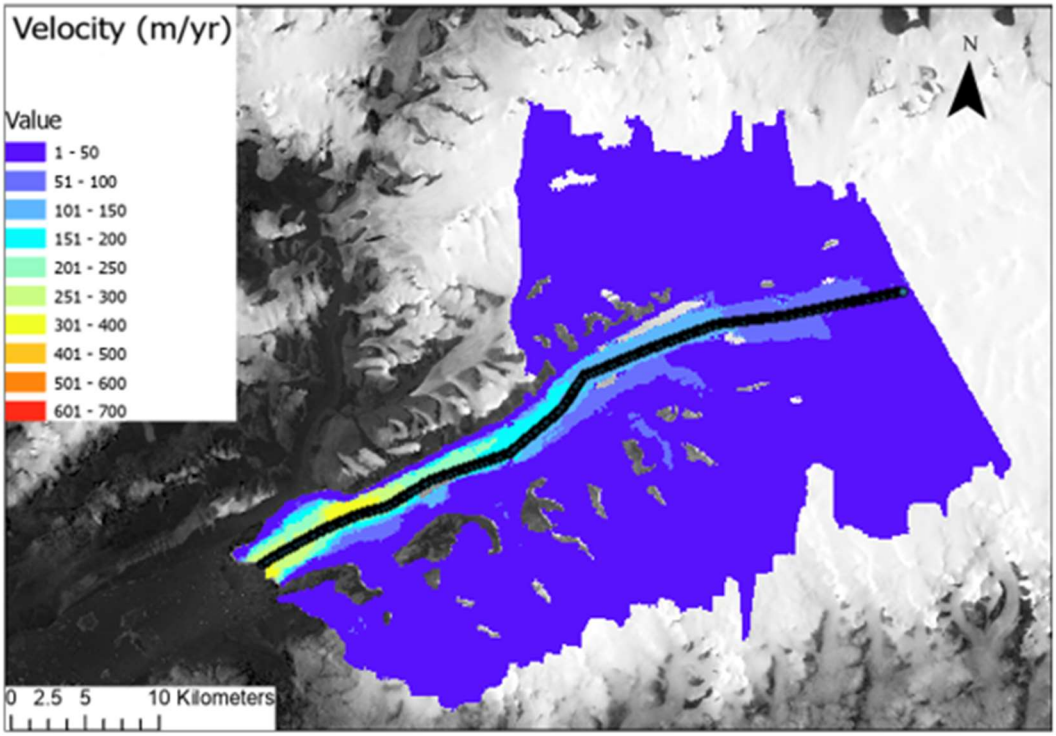

Figure 3-8: Example of centerline points used for extraction of R2 raster with velocity from 2009/02/20-2009/03/16 (overlaid on Landsat 8 imagery acquired on August 16, 2021).

Figure 3-9: Post-processing workflow in ArcPro 2.9.0. The GeoTIFFs produced by GAMMA were opened in ArcPro 2.9.0 and converted to m/yr with raster calculator, then clipped to the RGI 6.0 glacier extent. The rasters were then classified into 10-12 groups for easier visualization.

3.1.2.5 Error Analysis for SAR Velocity

Errors in the SAR offset tracking can emerge from ionospheric interference, glacier crevassing, surface meltwater, mis-registration of input images, or tidal rising and falling of a glacial terminus (Short and Gray, 2004). Error values from offset tracking can be determined by calculating the apparent velocity of non-moving or bedrock regions (Short and Gray, 2004; Van Wychen et al., 2014). As ground is not expected to move, the apparent mean ground velocity values were considered to represent the error range for glacier velocity. In the Canadian High Arctic, velocity errors caused by these issues typically range ~2-10 m/yr (Short and Gray, 2005). Higher errors can result from loss of coherence between images, such as from crevassing or melt water, and can be as high as 20 m/yr (Short and Gray, 2005; Van Wychen et al., 2016). Crevassing typically occurs on glacier surfaces during a surge, so for this study, errors between 2-20 m/yr were expected.

Error analysis for this study was done in ArcPro 2.9.0 first by drawing a polygon that covered the full extent of the raster images. A new polygon was drawn for each sensor. For R2, two different polygons were used, one that covered smaller raster images and one that covered larger raster images. The polygon was drawn to exclude water bodies since velocities cannot be derived in these areas. Glaciated areas (from the RGI) were erased from the polygon using the Erase tool, which resulted in a shapefile that only contained parts of the polygon that covered bedrock (Figure 3-10). A buffer was used to ensure water/glaciated terrain were excluded from the polygon. The buffer size was determined for each sensor

by multiplying the maximum dimension of the window size used for offset tracking by the maximum pixel size. For ERS-1 data, a buffer of 2022 m was used and for R2, a buffer of 1030 m.

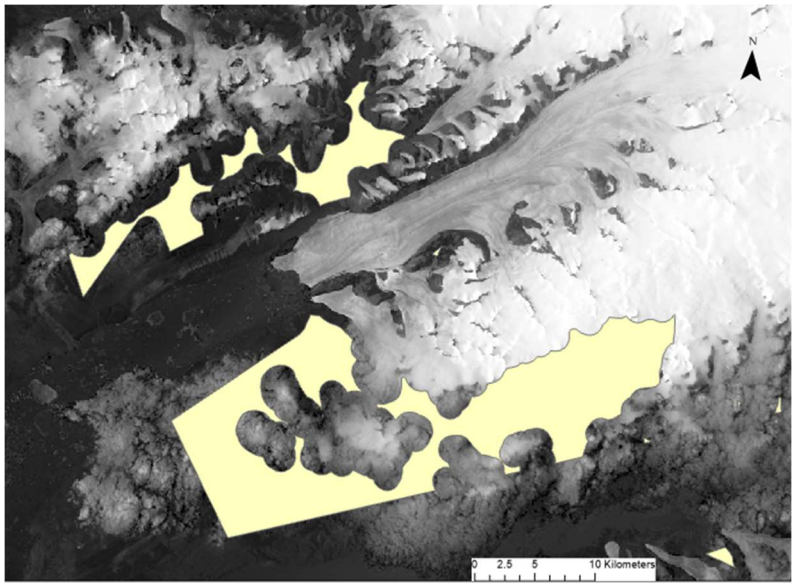

Figure 3-10: Example of R2 polygon used for bedrock velocity extraction error analyses, overlying Landsat imagery (acquired August 16, 2021).

The bedrock shapefile was used to extract the apparent bedrock velocities from each raster image using the 'Extract by Mask' Tool. The resultant extracted raster images were then converted to point files, where each point represented the value of each pixel. The attribute table for each point file was then opened, which showed the velocity value at each point. Statistics, including mean and standard deviation, were derived by right clicking on the "grid code" column within the attribute table for each shapefile and selecting "statistics". This provided the mean bedrock velocity and standard deviation for each velocity product. Finally, the average mean bedrock velocity and the average standard deviation were calculated for each sensor using Excel. For ERS-1, average mean bedrock velocity was 12.4 m/yr with a standard deviation of 7.5 m/yr. For R2, the mean bedrock velocity was 5.8 m/yr with a standard deviation of 5.3 m/yr. The higher error for ERS-1 data is expected, since peak surge velocities occur in this data set, which likely resulted in glacier crevassing and distorted coherence between reference and repeat images. The

average mean error for each sensor is consistent with typical error values for offset tracking in the Canadian Arctic, ~2-10 m/yr (Short and Gray, 2004; Van Wychen et al., 2014).

Table 3-4: Comparison of error analyses for ERS-1 and R2 data, including the average mean error and average standard deviation.

Sensor	Average mean error (m/yr)	Average standard deviation (m/yr)	Number of image pairs
ERS-1	12.4	7.5	6
R2	5.8	5.3	85

3.1.3 Terminus Extent Changes

Changes in glacier terminus extent also aid in determining whether/when a surge has occurred. For example, terminus advance that is coincident with acceleration can indicate a surge. In contrast, terminus retreat that is coincident with deceleration can indicate that atmospheric or ocean-induced melting is causing terminal retreat and subsequent acceleration due to reduced back stress on the glacier (Van Wychen et al., 2016). For this thesis, terminus extent changes were digitized manually in ArcPro 2.9.0 using imagery for each year from ERS-1 (1992-1994), Landsat 7 (1999-2008), 2009-2019 (R2), and 2020 (Landsat 8) (Figure 3-11). ERS-1, Landsat, and R2 imagery covering Otto Glacier was not available for the years 1994-1998. Specifically, the multilooked images from the SAR data were used, which provide a clear image of terminus extents. An image from January of each year was displayed in ArcPro 2.9.0, and the draw tool was used to manually trace the terminus extent from year to year. Extent changes were measured using the ruler tool by starting measurement at the centerline of the earlier terminus and measuring the distance to the centerline intersection at that subsequent terminus.

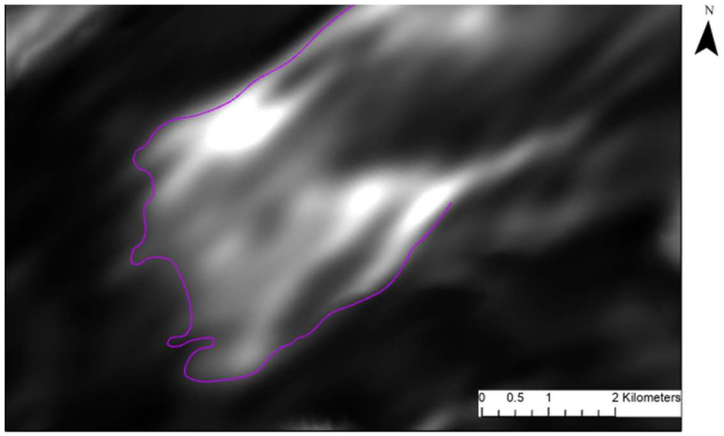

Figure 3-11: Example of digitized terminus extent overlaid on ERS-1 multi-look image acquired on February 11, 1992.

3.1.3.1 Error Analysis for Terminus Extents

The manual digitization of terminus extents was expected to be a source of error in this analysis. An additional source of error is likely different imaging geometries between different sensors. To quantify error, each terminus digitization was re-drawn five times for the same scene in ArcPro 2.9.0. The maximum difference between the re-drawn scenes was measured with the ruler tool, and this maximum value was considered the error for this method. The largest difference in the extents was ~193 m. This is negligible when there are large changes in terminus position (i.e., ~ 1000 m), however, any change within 193 m may be a result of error.

3.1.4 Glacier Surface Elevation Changes

Glacier surface elevation change can also offer clues as to whether a surge has occurred and is therefore important in an analysis of surge behavior. Surface elevation lowering coincident with acceleration typically indicates a surge, where the glacier undergoes structural extension due to extreme high speeds (Millan et al., 2017; Van Wychen et al., 2016). In contrast, surface elevation gains that are coincident with slow down typically indicate that one part of the glacier is slowing more quickly than the region behind it, suggesting progression into the quiescent phase of surging (Millan et al., 2017; Mortimer et al., 2018; Van Wychen et al., 2016). In this thesis, pre-determined geometry change products, derived from the differencing of DEMs, were obtained from openly available elevation change data provided by

Hugonnet et al. (2021), obtained from https://doi.org/10.6096/13. DEM change products are available for the years 2000-2019 over glaciers and ice sheets worldwide. The authors created differenced products using DEMs from ASTER, ArcticDEM, and Reference Elevation Model of Antarctica (REMA), and TanDEM-X. The TanDEM-X data was used for coregistration and bias correction over ice-free ground. After co-registration, DEMs were excluded if the root-mean-square error of the differenced elevation with TanDEM-X on ice-free ground was larger than 20 m. Differenced DEM products were then validated using ICESat and IceBridge laser and optical DEMs from the National Snow and Ice Data Centre. Regional and seasonal vertical shifts of less than 2 m of surface elevation were found and attributed to snow cover in the TanDEM-X global DEM and seasonal variability of snow cover in ASTER, ArcticDEM and REMA DEMs. Final uncertainty estimates in elevation change for each glacier were found to be 0.5 m/yr at a 95% confidence interval. The DEM change products in this study were compared spatially and temporally to velocity changes along Otto Glacier between for four epochs: 2000-2004, 2005-2009, 2010-2014, 2015-2019.

3.1.5 Bedrock Topography

Bedrock ridges have been hypothesized to influence cyclic surging behavior as described in detail by Van Wychen et al. (2016). Bed topography data from CReSIS MCoRDS are therefore used to map the bedrock elevation profile under Otto Glacier (Figure 3-12). The data covering Otto Glacier were obtained from the National Snow and Ice Data Centre and were captured in 2014. The topography datasets were created from a compilation of radar depth sounding, airborne lidar data for ice surface, optical data for ice boundaries, and DEMs for when lidar data were not available (Paden et al., 2013). The MCoRDS sensor operated at a frequency of 180-220 MHz and data were gridded with radar tomography processing into a ~3 km swath width. Along-track sample spacing is ~16 m and cross track spacing is ~30 m at nadir and 100 m at the swath edge. Spatial resolution varies with the year and platform. Error sources for penetrating radar data include electronic noise, multiple reflectors, and off-nadir reflections (Paden et al., 2013).

Multiple reflections occur when multiple surfaces are present with high impedance, such as air-ground or basal ice-water interfaces, and the sensor body. Off-nadir reflections can be caused by crevasses, melt water, rocks, or metal (Paden et al., 2013). Uncertainties in ice thickness have been found to range 10-20 m (Wu et al., 2011). Data were obtained in the form of GeoTIFFs that were visualized in ArcPro 2.9.0 using classification symbology.

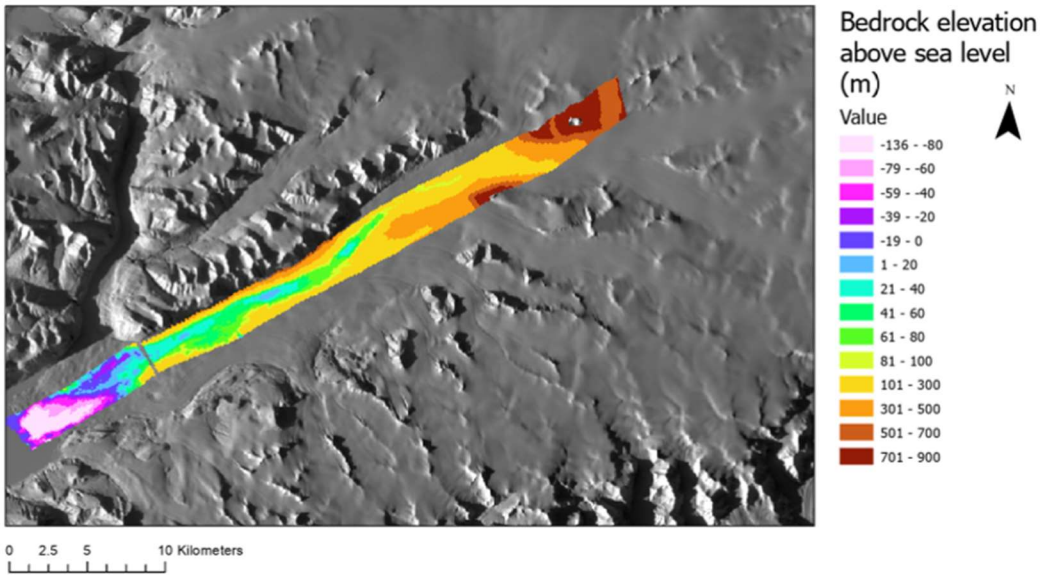

Figure 3-12: Bedrock elevation profile under Otto Glacier, from the CReSIS MCoRDS sensor data acquired in 2014, overlying Landsat imagery (acquired in April 2020). A data gap occurs at ~10 km from the terminus.

External data used in compilation of bedrock topography profiles:

NASA ATM LIDAR: IceBridge ATM L2 Icessn Elevation, Slope, and Roughness (http://nsidc.org/data/ilatm2.html).

ICESAT 1 KM DEM: GLAS/ICESat 1 km Laser Altimetry Digital Elevation Model of Greenland (http://nsidc.org/data/nsidc-0305.html).

IceFree Mask: Howat I.M and A. Negrete, in prep, A High-resolution Ice Mask for the Greenland Ice Sheet and Peripheral Glaciers and Icecaps, (http://www.bpcrc.osu.edu/gdg/data/icemask).

ICESat 500 m DEM: GLAS/ICESat 500 m Laser Altimetry Digital Elevation Model of Antarctica (http://nsidc.org/data/nsidc-0304.html).

IceFree Mask The Antarctic Digital Database, Scientific Committee on Antarctic Research 1993 - 2006. E00 Rock Outcrop, Lines and Polygons, (http://www.add.scar.org/home/add7)

3.1.6 Comparison of Velocity Changes to Bedrock Topography

To compare velocity changes to bedrock topography, the velocity variance for every velocity product was plotted along with the bedrock elevation profile. Velocity variance was calculated as the difference between the minimum and maximum centerline velocity value of a given pixel over the glacier for every raster image used in the study. For this comparison, the terminus extent from 1992 is used to clip both the velocity and bedrock data since the 1992 terminus extent is common to all velocity products and thus provides a common reference location to all velocity products. Areas of high velocity variance indicate areas of large velocity differences over the course of the study.

3.1.7 Summary of Remote Sensing Data

Velocity data used in this thesis include: pre-generated velocity products from NASA's ITS_LIVE project (1999-2018) and velocity raster products derived for this thesis using offset tracking (ERS-1 for 1992-1994, R2 for 2009-2020). Glacier surface elevation change products were obtained as pre-generated DEM change products from Hugonnet et al. (2021). The bedrock topography profile was obtained from CReSIS MCoRDS data, available from the National Snow and Ice Data Center. Table 3-5 provides a summary of the remote sensing data used in this thesis.

Table 3-5: Summary of remote sensing data used in this thesis.

Data source	Utility in thesis	Frequency	Resolution	Estimated Error	Number of scenes used	Dates covered
ITS_LIVE Project	Velocity	Composite	240 m	30 m/yr	20	1999-2018
ERS-1	Velocity and terminus extent changes	5.4 GHz	30 x 26 m	12.4 m/yr	6	1992-1994
R2	Velocity and terminus extent changes	5.3 GHz	8 m	5.8 m/yr	85	2009-2020
Hugonnet et al. (2021)	DEM changes	Composite	100 m	0.5 m/yr	4	2000-2019
CReSIS MCoRDS	Bedrock topography	180-220 MHz	Varies with platform	Varies with platform	1	2014

Chapter 4 - Results

The results chapter provides the findings for objectives 1-4. First, velocity data for Otto Glacier are reported using ERS-1, ITS_LIVE, and R2 data. This is followed by a report of terminus extent changes over time and then glacier surface elevation changes over time. Next, the bedrock profile for Otto Glacier is reviewed, and this is then compared to velocity variability along the glacier.

4.1 Otto Glacier Velocity Structure

The velocity data sets below are organized according to sensor and are presented in chronological order of image acquisition date.

4.1.1 1992-1994: ERS-1 Dataset

This section will review the velocity structure of Otto Glacier for the earliest period of the study in detail. Glacier velocities here were determined from the ERS-1 data and consisted of six image pairs, collected between February 1992 and January 1994. These images were acquired between the months January to March and images within pairs separated by 6 or 12 days, offering good temporal resolution.

Figure 4-1 provides the ERS-1 velocity data overlaid on the glacier, demonstrating how velocity changes along the glacier for each time period. For all image pairs, the velocities are highest within the lowermost ~6 km of the glacier and gradually decline upglacier from this point. Azimuth streaking due to ionospheric interference is present in some of the velocity maps (instances are annotated in Figure 4-1a, b, c, d, e). This causes phase shifts in the radar pulse and causes unreliable velocity results and can contribute an error of 10-20 m/yr in derived velocity products (Short and Gray, 2005). However, since velocities reach >1000 m/yr during this period, the overall error is likely negligible for the purposes of this analysis.

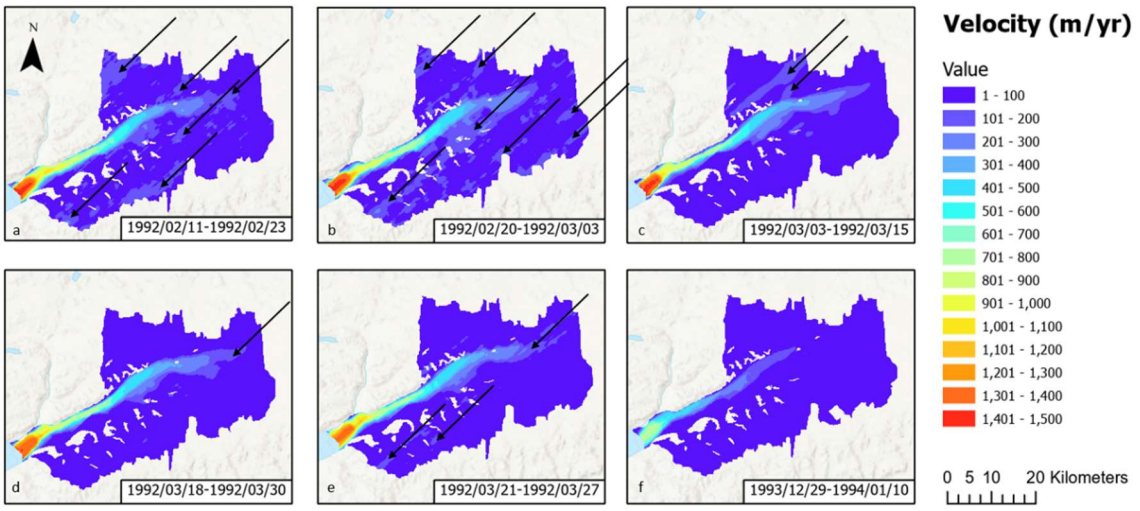

Figure 4-1: Otto Glacier velocities derived from ERS-1 data collected in 1992-1994, clipped to the RGI 6.0 outline for Otto Glacier. The black arrows indicate instances of streaking from ionospheric interference, which contributes an estimated error of 10-20 m/yr.

For the earliest image pair showing velocity over the February 11 -23, 1992 period (Figure 4-1a, Figure 4-2), velocities are highest within the lowermost ~6 km and range 800-1000 m/yr. From the ~6 km location to the ~14 km location upglacier, velocities are slightly lower at 500-700 m/yr but still higher than the uppermost sections of the glacier. From this location to ~22 km upglacier, velocities slow again to 300-500 m/yr. From ~22-40 km upglacier, velocities slow to 100-300 m /yr. From ~40 km to the uppermost point of the glacier, velocities are <100 m/yr. In the next time period, from February 20 to March 3, 1992 (Figure 4-1b, Figure 4-2), velocities are highest in the lowermost ~6.4 km at >1000 m/yr. From this point to ~10 km upglacier, velocities vary from 500-800 m/yr and from the ~10 km location to ~24 km upglacier, velocities vary between 300-500 m/yr. From ~24-39 km velocities decrease again to 100-300 m/yr and upglacier of ~39 km, velocities are <100 m/yr. The velocity structure for March 3-15, 1992 (Figure 4-1c, Figure 4-2) is similar to the February velocities. Velocities are highest within the lowermost ~6 km ranging from 800-1200 m/yr. Velocities from this point to ~10 km from the terminus range 500-700 m/yr. Between ~10-23 km, velocities decline to 300-500 m/yr and from ~23-40 km upglacier, velocities range 100-300 m/yr, and upward of 40 km are <100 m/yr. Later in the month, from March 18-30 (Figure 4-1d, Figure 4-2), velocities in the lowermost ~6 km remain at 800-1000 m/yr. From ~6-11 km upglacier, velocities decline

to 500-700 m/yr. From this point to ~23 km upglacier, velocities decline to 300-500 m/yr and from ~23 km upglacier to ~42 km up glacier, velocities are 100-300 m/yr, and beyond this point are <100 m /yr. Velocities were also derived for the March 21-27, 1992 period (Figure 4-1e, Figure 4-2), a subset of March 18-30 but a finer temporal resolution, and follow a similar trend. The final glacier velocity map, derived from the ERS image pair from December 29, 1993 to January 10, 1994 (Figure 4-1f, Figure 4-2), is significantly different from the preceding velocity products. At this time, in the lower most ~6 km of the glacier, velocities are 600-700 m/yr whereas in the preceding velocity maps, velocities were consistently higher than that. From the ~6 km point to the ~16 km point on the glacier, velocities are 400-600 m/yr and from ~16-29 km upglacier velocities range 200-400 m/yr and from ~29-42 km velocities decrease to 100-200 m/yr. Upward of ~42 km, velocities are <100 m/yr.

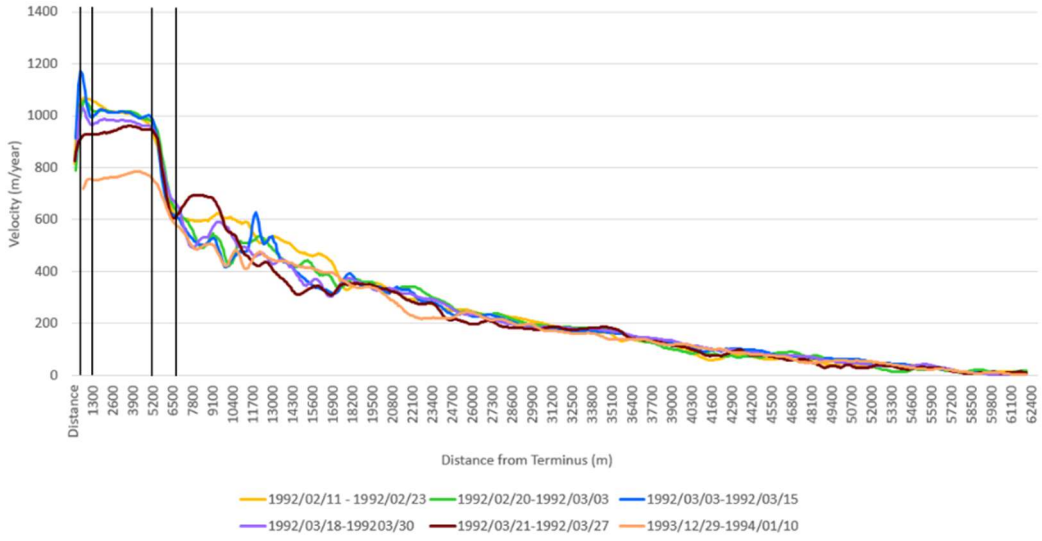

Figure 4-2: ERS-1-derived velocities for Otto Glacier in relation to distance from the terminus, from 1992-1994. Black vertical lines delineate locations of important velocity trends based on a qualitative assessment of the data.

Figure 4-2 provides the extracted centerline ERS-1 velocity data for Otto Glacier, which more precisely characterize how velocities vary in relation to distance from the terminus. In this dataset, the highest velocities consistently occur in the lowermost ~5 km of the glacier. Of note, a sudden slowing of velocities occurs in the region located ~5-6.5 km from the terminus (Figure 4-2). Some variability occurs

between ~6.5-18.9 km from the terminus but an overall slowing with progression upglacier is observed, and upglacier of ~20 km velocities consistently decline with minimal to no variability.

4.1.2 1999-2018: ITS_LIVE Annual Velocities

The ITS_LIVE velocity data include annual velocity averages from 1999-2018 derived from optical imagery. The description of the velocities for Otto Glacier from this dataset are divided into two time periods: the 1999-2010 period which presents generally higher velocities (section 4.1.2.1) and the 2011-2018 period which presents generally lower velocities (section 4.1.2.2).

4.1.2.1 ITS_LIVE Velocities for 1999-2010

Figure 4-3 presents the velocity structure of Otto Glacier from 1999-2010. In general, maximum velocities occur within the lowermost ~2 km of the glacier and gradually decline with increasing distance from the terminus. The greatest variability occurs within the lowermost ~6 km, and peak velocities occur in 2005 and 2007. The velocity structures for each year in this period is discussed in detail below.

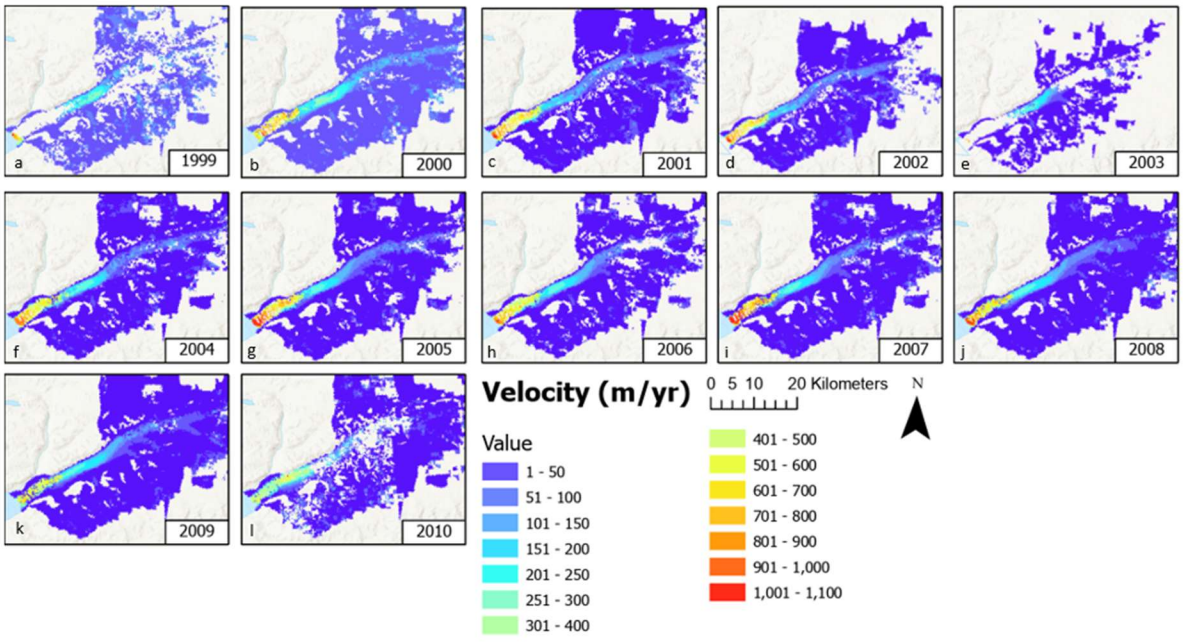

Figure 4-3: ITS_LIVE composite velocity products by NASA Jet Propulsion Laboratory (Gardner et al., 2019, https://its-live.jpl.nasa.gov/), covering Otto Glacier from 1999-2010, derived from optical imagery. Each image shows velocities averaged over one year and are clipped to the RGI 6.0 outline for Otto Glacier. Note the change in scale from Figure 4-5.

In 1999 (Figure 4-3a, Figure 4-4), velocities in the lower most ~1 km range 700-900 m/yr, however, there is a large data gap from here to ~12 km upglacier. From ~12-25 km upglacier, velocities are much lower ranging between 100 and 300 m/yr. At ~25-30 km upglacier, velocities are 100-200 m/yr and beyond ~30 km are <100 m/yr, however much of the data are missing. The year 2000 (Figure 4-3b, Figure 4-4) has more data in the terminus region, with velocities in the lowermost ~4 km ranging 700-900 m/yr. From ~4-11 km along the glacier trunk, velocities slow and range from 500-700 m/yr. Continuing along the main trunk further, velocities continue to decline between ~11-14 km from the terminus and vary between 200-400 m/yr. From ~14-28 km upglacier of the terminus, velocities decline again to 100-200 m/yr and beyond 28 km, velocities are ~100 m/yr or less. In 2001 (Figure 4-3c, Figure 4-4), velocities are slightly lower than in 2000. In the lowermost ~2 km, velocities range 500-700 m/yr. Moving upglacier to the region ~2-10 km from the terminus, velocities decline to 300-500 m/yr and in the region ~10-27 km from the terminus, velocities slow again to 100-300 m/yr. Upglacier of ~27 km, velocities are less than 200 m/yr. In 2002 (Figure 4-3d, Figure 4-4)**,** velocities in the lowermost ~2 km of the glacier are 800-1000 m/yr, which is an increase from the previous year. From ~2-10 km upglacier, velocities are lower at 600-800 m/yr while from ~10-13 km upglacier, velocities decline to 400-600 m/yr. From ~13-28 km velocities drop markedly lower to 100-200 m/yr and beyond ~28 km velocities vary around 100 m/yr, however, no data are available upglacier of 49 km. In 2003 (Figure 4-3e, Figure 4-4), significant gaps occur in the glacier velocities and data are generally unavailable from the terminus to 13 km upglacier. Along the ~13-28 km section of the trunk of the glacier, velocities range 100-300 m/yr. Upglacier of ~28 km, a significant amount of data are again missing. In 2004 (Figure 4-3f, Figure 4-4)**,** terminus velocities remain high, ranging 700-900 m/yr in the lowermost ~5 km of the glacier. Upglacier to the section ~5-9 km from the terminus, velocities decline to 500-700 m/yr and in the ~10-23 km section of the glacier, velocities range 200-400 m/yr. From ~23-29 km up glacier, velocities are slightly lower at 100-200 m/yr. Beyond ~29 km from the terminus, velocities are generally less than 100 m/yr.

The year 2005 (Figure 4-3g, Figure 4-4) has some of the highest velocities of the ITS_LIVE dataset. For example, in the lowermost ~5 km, velocities are between 800 and 1300 m/yr. Moving upglacier to the section ~5-13 km from the terminus, velocities range 500-700 m/yr while in the section ~13-28 km upglacier, velocities range 100-300 m/yr. Beyond ~28 km, velocities once again vary around 100 m/yr and gradually decline toward the uppermost regions. In 2006 (Figure 4-3h, Figure 4-4), velocities are overall slightly decreased compared to 2005. Here, the lowermost ~1 km of the glacier is flowing between 800 and 1000 m/yr. The section upglacier located ~1-10 km from the terminus ranges in flow speeds from 500-700 m/yr and upglacier to the location ~10-22 km from the terminus, velocities range 200-400 m/yr. In the section upglacier located ~22-33 km from the terminus, velocities are lower again at 100-200 m/yr. Upglacier of 33 km from the terminus, most of the data are missing. The year 2007 (Figure 4-3i, Figure 4-4), like 2005, shows some of the highest velocities in the entire ITS_LIVE dataset, with velocities of 800-1300 m/yr measured in the lowermost ~5 km of the glacier. From ~5-7 km upglacier of the terminus, velocities are 700-800 m/yr, however upglacier the ~7 km location, velocities decrease markedly to 300-500 m/yr. In the region between ~7-23 km from the terminus, velocities are consistent around 100-300 m/yr. Upglacier of ~23 km from the terminus, velocities again vary around 100 m/yr and gradually slow upglacier.

In 2008 (Figure 4-3j, Figure 4-4), velocities along the glacier decline relative to 2007. In the lowermost region of the glacier (from the terminus to ~2 km upglacier) velocities range from 800-1000 m/yr. Moving upglacier, in the section ~2-4 km from the terminus, velocities are slightly lower at 500-700 m/yr and in the section ~4-10 km, velocities are 400-600 m/yr. Continuing further upglacier, in the section ~10-27 km from the terminus, velocities are 100-300 m/yr and decline with progression upglacier. Upglacier of ~27 km, velocities again vary around 100 m/yr with an overall decline toward the upper regions. The year 2009 (Figure 4-3k, Figure 4-4) represents a significant change in the velocity structure of Otto Glacier compared to all other years in the ITS_LIVE dataset (where data are available), where a

decline in velocities along the entire glacier are observed compared to 2008. In 2009, velocities range 600-700 m/yr in the lowermost ~3 km. Data are missing for ~2-5 km, but in the section of the glacier located ~5-12 km from the terminus, velocities range 300-500 m/yr. Moving further upglacier, in the section located ~12-37 km from the terminus, velocities range 100-300 m/yr with gradual decline upglacier. Upglacier of ~37 km, velocities vary around 100 m/yr but are mostly <100 m/yr. The year 2010 (Figure 4-3l, Figure 4-4) shows a sharp slowing of velocities along the glacier compared to previous years and shows less variability in velocities along the main trunk. Velocities in the lowermost ~15 km of the glacier are 300-500 m/yr (with faster velocities closer to the terminus). From ~15-28 km upglacier, velocities decline to 100-200 m/yr. Upward of ~28 km, velocities are <100 m/yr and are overall lower than the previous years.

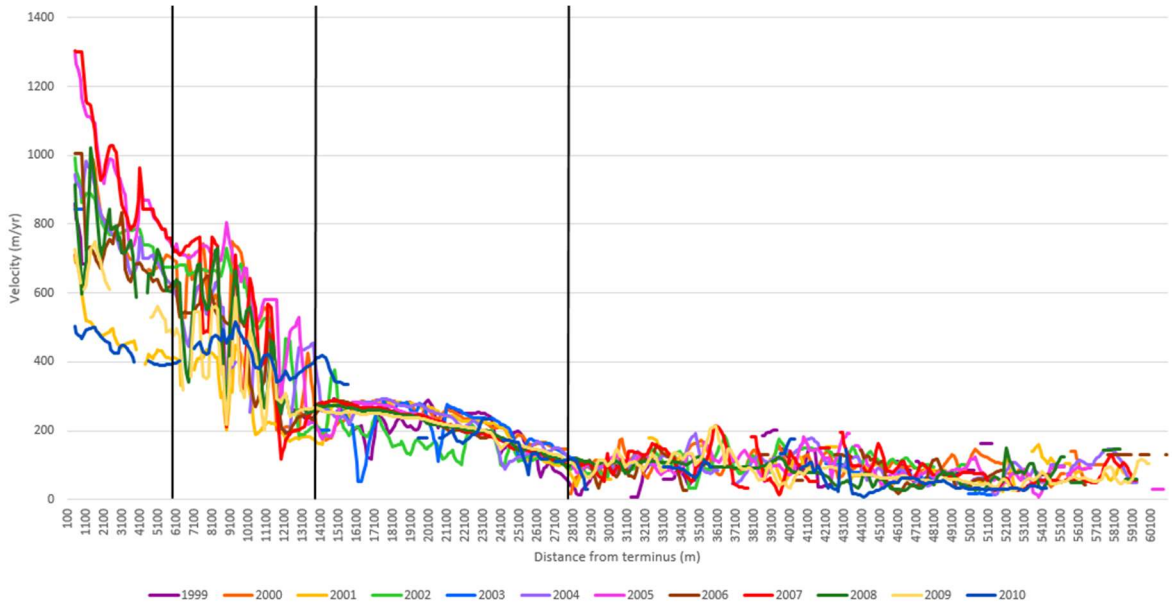

Figure 4-4: Average annual velocities for Otto Glacier from 1999-2010, derived from ITS_LIVE composite velocity products by NASA Jet Propulsion Laboratory (Gardner et al., 2019, https://its-live.jpl.nasa.gov/). Black vertical lines denote important velocity trends based on a qualitative assessment of the data. Velocities are averaged over every 400 m.

Figure 4-4 presents the extracted centerline velocities from all ITS_LIVE datasets from the 1999-2010, which allows for a detailed comparison of the year-to-year velocity structure of Otto Glacier over this time period. The greatest variability is seen in the lowermost ~6 km section of the glacier, where the

highest measured flow speeds are observed in 2005 and 2007 and lowest in 2010. The region located ~6-14 km from the terminus is another unique area in terms of the velocity structure of Otto Glacier. In this area there is still variability, but less so than the lowermost terminus region. This section of the glacier marks an area of slowdown, where velocities slow as one moves upglacier and is a pattern observed in all years. The third interesting section of the glacier is located ~14 to 28 km from the terminus. This region shows even less variability than the areas located downglacier, with velocities slowing as one moves further upglacier within this section. In this region, there is relatively little variation in year-to-year flow speeds over the time period. The region ~28 km upglacier of the terminus shows some variability although glacier velocities are generally low.

4.1.2.2 ITS_LIVE Velocities for 2011-2018

Figure 4-5 provides the surface centerline velocities of Otto Glacier for the years 2011-2018 from the ITS_LIVE dataset (note the change in scale from Figure 4-3). These years are separated from the earlier period because the flow speeds here are lower than in the 1999-2010 period. Most notably, from 2013-2018, the lowermost terminus region is flowing at much slower speeds (near stagnation at <40 m/yr) compared to the ERS-1 data from 1992-1994 and the earlier ITS_LIVE dataset from 1999-2010, where this region was consistently the fastest flowing compared to any other location on the glacier (Figure 4-1, Figure 4-2, Figure 4-3, Figure 4-4). In all years from 2011-2018, the fastest ice motion is found in the region of the glacier located from ~6-40 km from the glacier terminus, although general slowing of ice motion does occur from year to year. The section below provides a year-by-year description of the velocity structure of Otto Glacier for this time period.

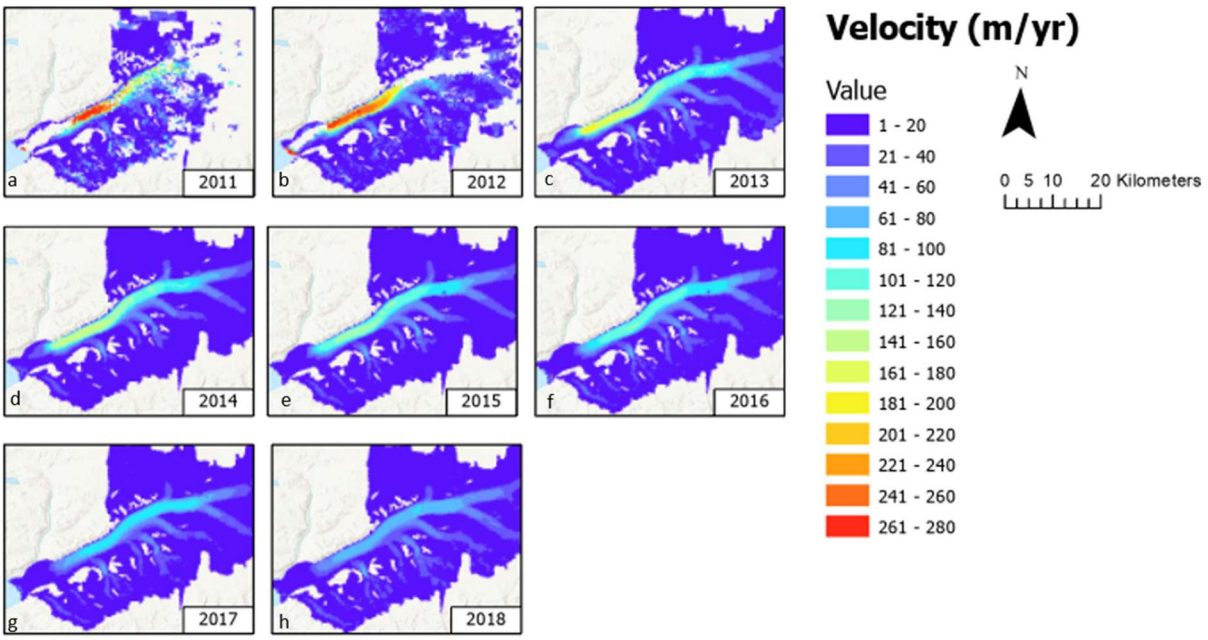

Figure 4-5: ITS_LIVE composite velocity products by NASA Jet Propulsion Laboratory (Gardner et al., 2019, https://its-live.jpl.nasa.gov/), covering Otto Glacier from 2011-2018, derived from optical imagery. Each image shows velocities averaged over one year. Note the change in scale from Figure 4-3.

In the 2011 velocity data (Figure 4-5a, Figure 4-6) there is a significant gap in results, with data missing for the lowermost ~9 km of the glacier. However, data are available beginning ~9 km from the terminus and velocities are 100 m/yr in the area from ~9-12 km from the terminus. In the section of the glacier ~12-21 km from the terminus, velocities are slightly higher than the lower region, ranging between 200-280 m/yr. Upglacier of ~22 km from the terminus, velocities vary around 100 m/yr but with some data missing. In 2012 (Figure 4-5b, Figure 4-6), data are again missing for the lowermost portion of the glacier. Measured velocities in the section of the glacier ~6-10 km from the terminus are 100-200 m/yr while in the region located ~10-24 km upglacier from the terminus, velocities increase to 200-250 m/yr. In the region located ~24-28 km upglacier of the terminus, velocities decrease to 100-200 m/yr. Moving further upglacier, velocities are 40-60 m/yr at the location ~28-50 km from the terminus and upglacier of ~50 km velocities are ~20 m/yr albeit with significant data gaps due to missing results. In 2013 (Figure 4-5c, Figure 4-6) velocities slow along the entire glacier. In the lowermost ~6 km, velocities are 20-40 m/yr and gradually increase to 50-100 m/yr in the section of the glacier ~6-8 km from the terminus. At ~8-9 km

from the terminus, velocities of 100-150 m/yr are determined. Velocities increase again in the ~9-12 km region to ~170 m/yr and in section ~12-27 km from the terminus, velocities gradually slow and range 100-160 m/yr. Upglacier from ~27 km, velocities vary around 100 m/yr and decrease toward the uppermost regions. The year 2014 (Figure 4-5d, Figure 4-6) shows a similar velocity structure to 2013 although again slightly slower. Velocities are slowest in the region ~6 km from the terminus at 10-30 m/yr. From there, velocities gradually increase with progression away from the terminus. By ~9 km upglacier from the terminus, velocities reach 100 m/yr and velocities continue to increase upglacier, reaching 120-140 m/yr in the section ~9-14 km upglacier from the terminus. Velocities increase to 140-150 m/yr at ~14-18 km upglacier from the terminus. Upglacier of this point, velocities decelerate. From ~18-24 km upglacier from the terminus, velocities decline from ~150 to 130 m/yr. Upglacier to ~24-28 km from the terminus, velocities decelerate further from 120 to 100 m/yr and from ~28-44 km upglacier of the terminus, velocities vary around 100 m/yr before gradually declining to <10 m/yr upglacier of 59 km.

By 2015 (Figure 4-5e, Figure 4-6), velocities along the entire glacier are lower than in previous years, continuing a pattern of progressive slowing of Otto Glacier. In the lowermost ~6 km of the glacier, velocities are near stagnation and range 1-20 m/yr. Velocities then gradually increase to ~100 m/yr between ~6-11 km from the terminus and increase to a maximum value of 110-130 m/yr in the section of the glacier ~11-18 km from the terminus. After this point, velocities decrease to 100 m/yr by ~28 km from the terminus. Velocities between ~28-43 km decrease to 80-100 m/yr and then further decrease gradually upglacier of ~43 km to <10 m/yr in the upper most regions. Velocities in 2016 (Figure 4-5f, Figure 4-6) follow a similar pattern, with velocities of less than 20 m/yr in the lowermost 6 km, and gradual speed up to 120 m/yr between ~13-20 km from the terminus. In the section of the glacier located ~20-28 km from the terminus, velocities decline to 100 m/yr and from ~28-43 km from the terminus, velocities vary between 80-100 m/yr. Upglacier of ~43 km, velocities gradually slow, reaching <10 m/yr beyond ~59 km from the terminus. In 2017 (Figure 4-5g, Figure 4-6)**,** velocities are again lowest in the lowermost ~8 km

of the glacier ranging 1-20 m/yr. From the section of the glacier located ~8 -18 km from the terminus, the velocities are at their maximum and reach ~80-90 m/yr. In the section of the glacier located ~18-28 km from the glacier front, velocities decrease to 60-70 m/yr, before increasing again to 90 m/yr by ~32 km from the terminus. Velocities remain between 90-100 m/yr before decelerating again by ~43 km from the terminus. Upglacier of this point, velocities gradually slow, reaching <10 m/yr beyond ~60 km. In 2018 (Figure 4-5h, Figure 4-6), the final year from which ITS_LIVE data are available, the overall pattern of slowdown of Otto Glacier continues. Velocities range 1-20 m/yr in the lower section of the glacier before reaching a maximum of 70-80 m/yr by ~18 km upglacier from the terminus. Velocities remain in this range between ~18-23 km upglacier of the terminus. Between ~23-28 km from the terminus, velocities decrease to 50-60 m/yr before increasing again, reaching 70-80 m/yr between ~28-43 km. Velocities gradually decelerate upglacier of ~43 km from the terminus, slowing to <10 m/yr upglacier of ~60 km from the terminus.

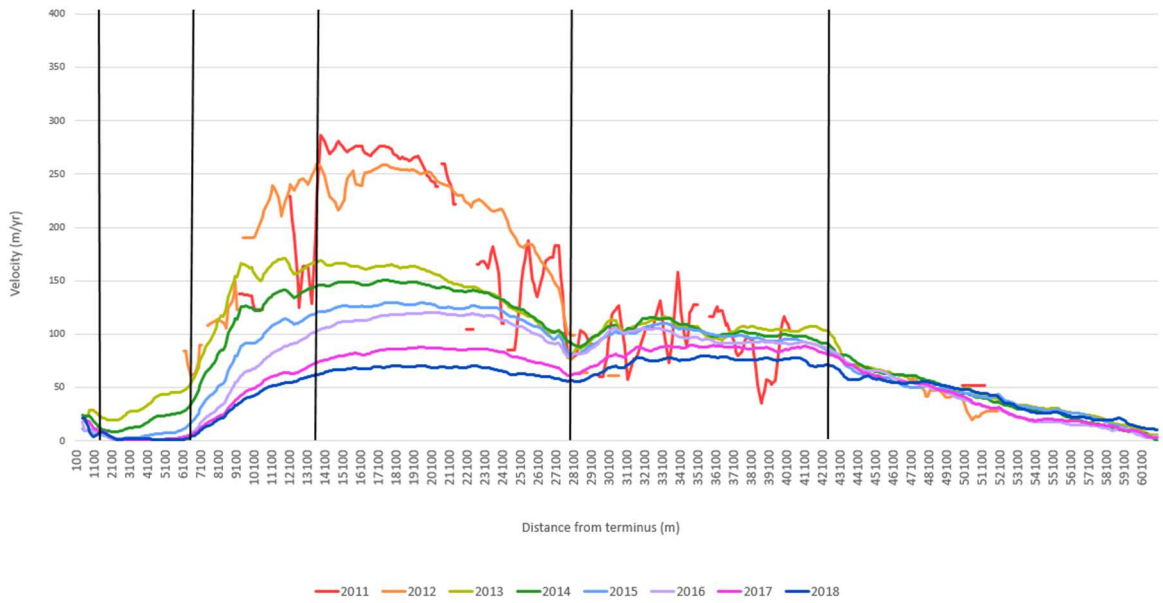

Figure 4-6: Average annual velocities for Otto Glacier from 2011-2018, derived from ITS_LIVE composite velocity products by NASA Jet Propulsion Laboratory (Gardner et al., 2019, https://its-live.jpl.nasa.gov/). Black vertical lines denote important velocity trends based on a qualitative assessment of the data. Velocities are averaged over every 400 m.

Figure 4-6 provides the extracted centerline velocities along the main trunk of Otto Glacier for the years 2011-2018. In general, the lowest velocities for 2011-2018 period occur in the lowermost ~6 km (with small peaks in the lowermost 1 km). Velocities thereafter increase and peak at ~14-15 km and then slow until ~28 km. At ~28 km, velocities slightly increase again and plateau until ~42 km upglacier, beyond which they consistently decline for all years.

4.1.3 2009-2020: R2-Derived Velocities

The R2 dataset provides velocities averaged over 24-day intervals during 2009-2020 and are presented here in three time periods: 2009-2010 where the highest velocities are measured (Figure 4-7), 2011-2017 where notable slowing occurs compared to previous R2 data (Figure 4-8), and 2018-2020 during which the slowest velocities are observed (Figure 4-9). A summary of the R2-derived velocities for all dates are provided in Figure 4-10. In general, the highest velocities occur from January-April 2009 and are observed within the lowermost ~6 km of the glacier as well as in the section located ~8-10 km from the terminus, and gradually slow upglacier of ~10 km from the terminus. Velocities overall begin slowing in August 2009 through January 2011, by which time velocities in the lowermost ~6 km are markedly slower and are either slower, or similar to, velocities in the section immediately upglacier at ~6-14 km from the terminus. In January 2012, there is a subtle increase in velocities in the lowermost ~6 km, slowing in the ~8-10 km section, and slowing upglacier of ~10 km from the terminus. This is followed by a sharp decrease in overall velocities starting in March 2013. The set of slowest velocities begins in April 2018 and persists until the end of the dataset (February 2020). A detailed review of velocity changes in the R2 dataset is provided below.

4.1.3.1 R2 Velocities for 2009-2010

Figure 4-7 provides the R2 extracted centerline velocity structures for Otto Glacier, demonstrating how velocities vary in relation to distance from terminus. The highest velocities of the dataset occur in 2009. The year 2009 includes velocities for the months January to April, and August to November. The

velocities for January to April inclusive are consistent. During these months, the highest velocities (>300 m/yr) occur within the lowermost ~6 km of the glacier. From the section of the glacier located ~6-15 km from the terminus, velocities are slightly lower at 200-300 m/yr. At ~15 km, velocities decline to 150-200 m/yr, and gradually decline with increasing distance to the terminus. Velocities reach a minimum of 40-50 m/yr beyond ~48 km from the terminus. During August 24 to September 17, 2009, velocities slow compared to January-April velocities. Velocities here are 250-300 m/yr in the lowermost ~2 km of the glacier and ~200 m/yr in the section ~2-8 km from the terminus. There is a slight increase in velocities to 400 m/yr in the section ~8-11 km from the terminus, then a decline in velocities to 200-300 m/yr in the section ~11-19 km from the terminus. Data are missing for much of the region upglacier of this section, but the velocities available are as low as 20-50 m/yr upglacier of ~25 km from the terminus, followed by an increase to ~100 m/yr in the section ~39-42 km from the terminus, followed by gradual slowing upglacier of ~42 km from the terminus to a minimum of ~50-60 m/yr. During September 17 to October 11, 2009, velocities are similar to those of August but slightly lower. Velocities are 190-250 m/yr in the lowermost ~10 km before increasing to 300-400 m/yr by ~10-14 km from the terminus. From the location ~15-20 km from the terminus, velocities decrease to 200-300 m/yr, and gradually slow upglacier to <50 m/yr by the ~46 km mark upglacier of the terminus.

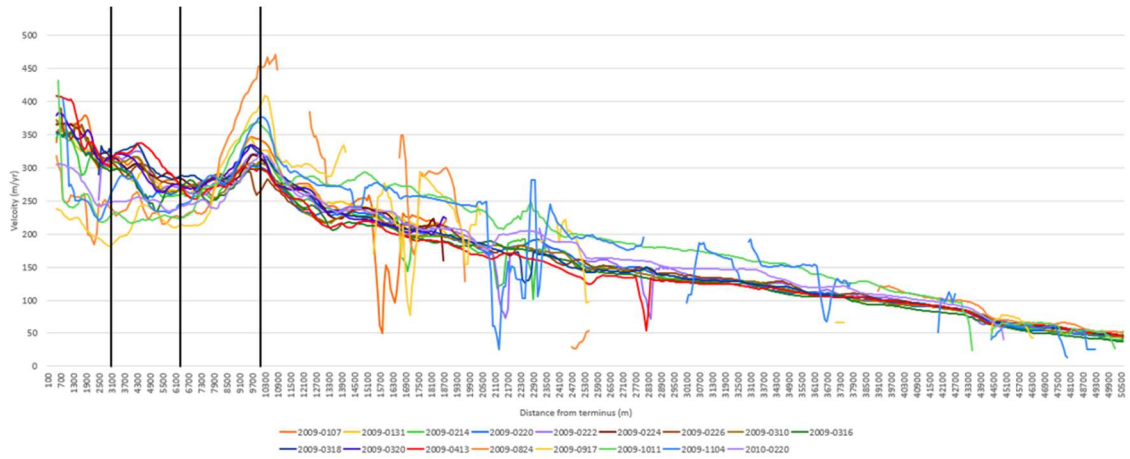

Figure 4-7: R2-derived centerline velocities for Otto Glacier from 2009-2010 in relation to distance from terminus. Only dates of the reference image are provided (repeat images were acquired 24 days following the reference image). Velocities are averaged over every 400 m. Black vertical lines denote important velocity trends based on a qualitative assessment of the data.

Velocities remain similar but slower from October 11 to November 4, 2009. Velocities here are 200-250 m/yr in the lowermost ~7 km of the glacier (highest in the lowermost 2 km), then increase to 200-300 m/yr from this point to ~10 km from the front, then decline again to 200-250 m/yr over the section ~10-25 km from the terminus. Velocities gradually decline upglacier of ~25 km from the terminus, reaching a minimum of <50 m/yr**.** Over November 4-28, 2009, velocities are similar to October. Velocities here are highest in the lowermost ~5 km and range 250-350 m/yr, then gradually decline to 200-250 m/yr until ~6 km from the terminus, at which point they increase to 200-350 m/yr and remain in this range until ~10 km from the terminus. From the section ~10-20 km from the terminus, velocities decline again, ranging 200-300 m/yr, after which point velocities slow to 100 m/yr by ~21 km from the terminus. There is a brief increase in velocities in the section ~21-25 km from the terminus, ranging 150-200 m/yr, then a decline at ~30 km upglacier to 100-150 m/yr. In the region ~30-33 km from the terminus, velocities increase to a maximum of ~180 m/yr, then slow again along the remainder of the glacier reaching <50 m/yr by ~48 km upglacier. The year 2010 only includes a velocity measurement for the period of February 20 to March 26, and velocities are similar to November of 2009, where velocities are highest in the

lowermost ~5 km of the glacier and increase again by ~10 km from the glacier front. Upglacier of ~10 km, velocities gradually slow, with missing data beyond ~46 km.

4.1.3.2 R2 Velocities for 2011-2017

Figure 4-8 provides the R2-derived velocity structure along Otto Glacier Velocities for the years 2011-2017. Velocities from January 26 to February 19, 2011 (the only data available for 2011), are slightly increased from 2010, however data are missing for the lowermost ~10 km of the glacier. Velocities in the region ~10-13 km from the terminus are 300-400 m/yr. Velocities gradually decrease over ~14-45 km from the terminus, reaching a minimum of 50 m/yr. Data are not available upglacier of ~45 km from the terminus. For 2012, velocities are available for January 3-27, January 4-28, January 28 to February 21, and velocities for each period are similar to each other and similar to the 2011 January velocities. During this time, velocities within the lowermost ~10 km of the glacier are 200-300 m/yr and in the section ~10-20 km from the terminus, velocities are slightly lower at 200-250 m/yr. In the region ~20-30 km from the terminus, velocities decrease again to 100-200 m/yr. Upglacier of ~30 km from the terminus, velocities progressively decline reaching <100 m/yr after ~42 km from the terminus.

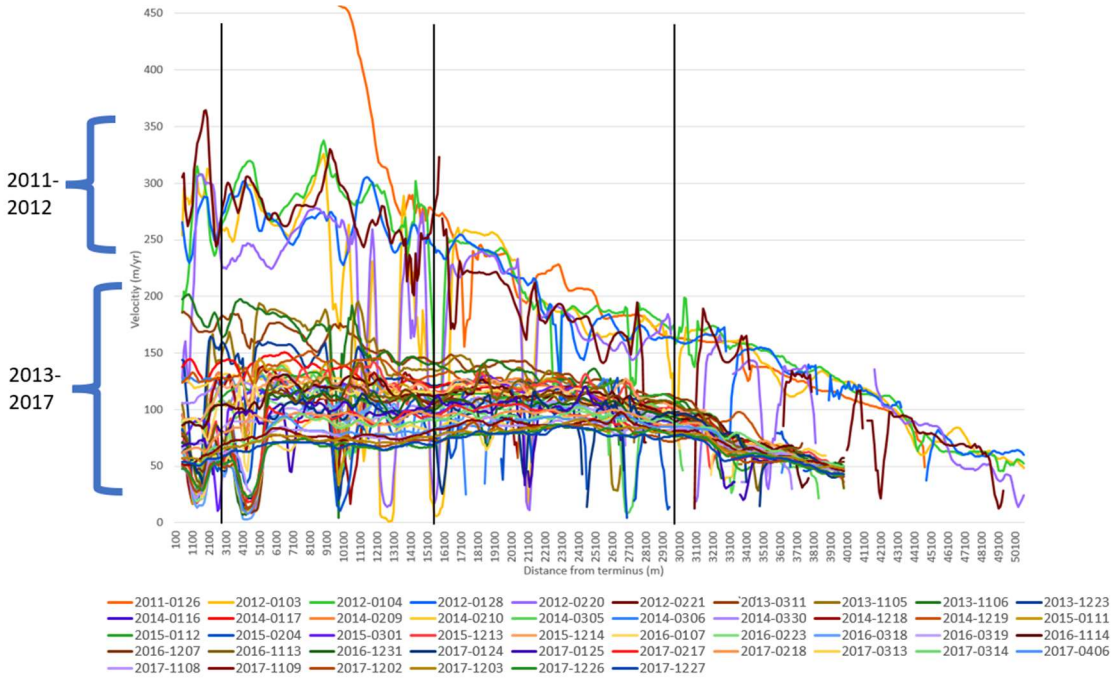

Figure 4-8: R2-derived centerline velocities for Otto Glacier from 2011-2017 in relation to distance from terminus. Only dates of the reference image are provided (repeat images were acquired 24 days following the reference image). Velocities are averaged over every 400 m. Black vertical lines denote important velocity trends based on a qualitative assessment of the data.

In 2013 velocities are available for March 11 to April 4, November 6-30, and December 23 to January 16, 2014. Velocities have notably decreased from February 2012 and are consistent for each of the 2013 dates. Velocities for 2013 are highest in the lowermost ~12 km of the glacier, ranging 150-180 m/yr. In the region ~12-31 km from the terminus, velocities gradually decline to 100 m/yr. Velocities gradually decrease upglacier of this point, reaching a minimum of 70 m/yr by ~37 km from the terminus, and data are not available upglacier of this point. Velocities from 2014 (measured over January 16 to February 9, January 17 to February 10, February 9 to March 5, February 10 to March 6, March 5-29, March 6-31, March 30-April 23, December 18 to January 11, 2016, and December 19 to January 12, 2016) follow a similar pattern to the 2013 velocities. A marked slowing of velocities occurs over February 4-28, 2015. At this time, velocities in the lowermost ~5 km of the glacier ranged 50-100 m/yr. From the section located ~5-15 km from the terminus, velocities are slightly higher ranging 100-120 m/yr. Moving upglacier to the region ~15-17 km from the terminus, there is another slowing to 50-80 m/yr. Much of the data for the

section ~17-20 km from the terminus are missing. In the location ~20-21 km upglacier from the terminus, velocities increase slightly again to 100-110 m/yr, then slow to 70-90 m/yr at ~21-22 km from the terminus, then in the section ~22-23 km upglacier velocities increase to 100-110 m/yr, then vary 60-100 m/yr over the region ~23-27 km from the terminus. Velocities decline to 14 m/yr by ~30 km from the terminus and most data are available upglacier of this point. Velocities for the remainder of 2015 (March 1-25, December 13 to January 6, 2016, and December 14 to January 7, 2016) follow a similar pattern but with more velocity data available for the sections ~15-17 km from the terminus (110-130 m/yr) and ~30-40 km from the terminus (40-70 m/yr). However, data are not available upglacier of ~40 km for any of the 2015 measurements. The velocities measured for 2016 follow a similar pattern to 2015.

Further slowing of velocities is observed over January 24 to February 17, 2017, and this remains consistent over January 25 to February 18, February 17 to March 13, and February 18 to March 14. During these times, velocities in the lowermost ~5 km of the glacier range 30-60 m/yr. From ~5-12 km upglacier, velocities increase from 70 to 100 m/yr. Moving upglacier from here, velocities remain in this range before slowing at ~33 km upglacier from the terminus to 60-80 m/yr. Velocities continue to slow upglacier reaching 40 m/yr at ~40 km from the terminus. Data are not available upglacier of 40 km from the terminus. Another notable slowdown occurs over March 13 to April 6, 2017. Velocities in the lowermost ~2 km of the glacier are consistently <50 m/yr. From the section of the glacier ~2-31 km from the terminus, velocities increase to 70-90 m/yr. Upglacier of ~31 km from the terminus, velocities decrease with progression away from the terminus, reaching a minimum of 40-50 m/yr by ~40 km from the terminus. Data are not available beyond this point. Velocities for the remainder of 2017 (measured over March 14 to April 7, April 6 to April 30, November 8 to December 2, November 9 to December 3, December 2 to 26, December 26 to January 19, 2018, December 27 to January 20, 2018) follow a similar pattern with data missing upglacier of ~40 km from the terminus.

4.1.3.3 R2 Velocities for 2018-2020

Figure 4-9 shows the R2-derived velocity structure of Otto Glacier for the 2018-2020, in which the slowest velocities of the R2 dataset occur. A notable deceleration occurs in early 2018 (measured over January 19 to February 12, January 20 to February 13, February 12 to March 8, February 13 to March 9, March 8 to April 1). During these times, velocities in the lowermost ~2 km of the glacier range 30-50 m/yr. Velocities then increase to 40-60 m/yr in the section of the glacier located ~2-4 km from the terminus, then decrease again in the section ~4-6 km from the terminus to 30-40 m/yr, then increase again to ~60 m/yr in the region ~6-17 km from the terminus. In the region located ~16-32 km from the terminus, velocities increase to 70-80 m/yr. From ~32 km and up the remainder of the glacier, velocities gradually decline reaching 30-40 m/yr by ~40 km from the terminus, beyond which data are not available. Over April 1-25, 2018, velocities subtly decline compared to January to March. In April, velocities in the lowermost ~2 km of the glacier are 20-40 m/yr. Velocities decrease to <10 m/yr over the region ~2-4 km from the terminus, then increase to 40-60 m/yr in the region ~4-32 km from the terminus. Upglacier of ~32 km from the terminus, velocities decline to ~40 m/yr and data are not available upglacier of 40 km from the terminus. Velocities calculated for the remainder of 2018 (November 3 to 27, November 4 to 28, November 27 to December 21, November 28 to December 22, December 21 to January 14, 2019, and December 22 to January 15, 2019) are similar to velocities from April 1-25, 2018.

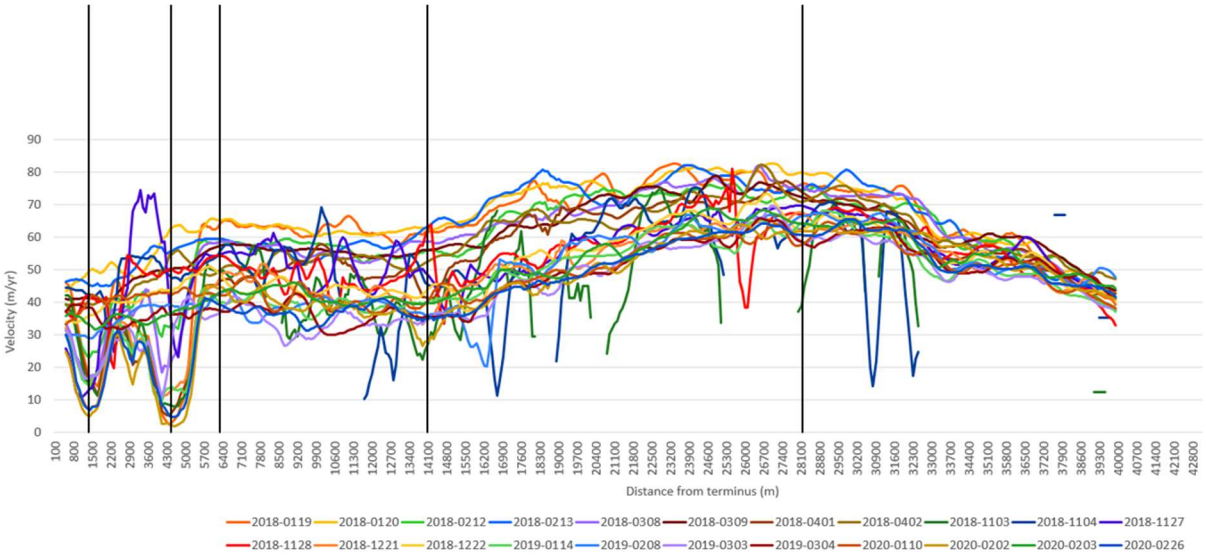

Figure 4-9: R2-derived centerline velocities for Otto Glacier from 2018-2020 in relation to distance from terminus. Only dates of the reference image are provided (repeat images were acquired 24 days following the reference image). Velocities are averaged over every 400 m. Black vertical lines denote important velocity trends based on a qualitative assessment of the data.

Velocities in 2019 (measured over January 14-February 7, February 8 to March 4, March 3-27, March 4-28) are similar but slower in some areas compared to previous data. At these times, velocities in the lowermost ~2 km of the glacier are 15-30 m/yr. In the location ~2-26 km from the terminus, velocities slightly increase to 20-40 m/yr. In the region located ~26-32 km from the terminus, velocities increase to 50-70 m/yr. In the section located ~32-37 km from the terminus, velocities decrease again to 40-60 m/yr. Upglacier of ~37 km, velocities slow to 30-40 m/yr, with data missing upglacier of ~40 km from the terminus.

Velocities for 2020 (measured over January 10 to February 3, February 2-26, February 3-27), are similar to 2019 data. Velocities in the lowermost ~5 km of the glacier are 20-30 m/yr. In the section located ~5-31 km from the terminus, velocities increase to ~30-60 m/yr. Moving upglacier to the section ~31-40 km from the terminus, velocities gradually decline to ~40 m/yr, and data upglacier of this region are not available. Over February 26 to March 21, 2020, the final velocity measurements of the set, velocities are

slightly lower in some sections of the glacier but are overall similar to the previous 2018 data. Velocities in the lowermost ~5 km of the glacier range 10-30 m/yr. Velocities increase to ~30 to 60 m/yr over the section of the glacier that is ~5-31 km from the terminus. Upglacier of ~31 km from the terminus, velocities decrease to ~40m/yr. Data are not available upglacier of ~40 km from the terminus. Figure 4-10 provides a summary of the velocities derived from the entire R2 dataset.

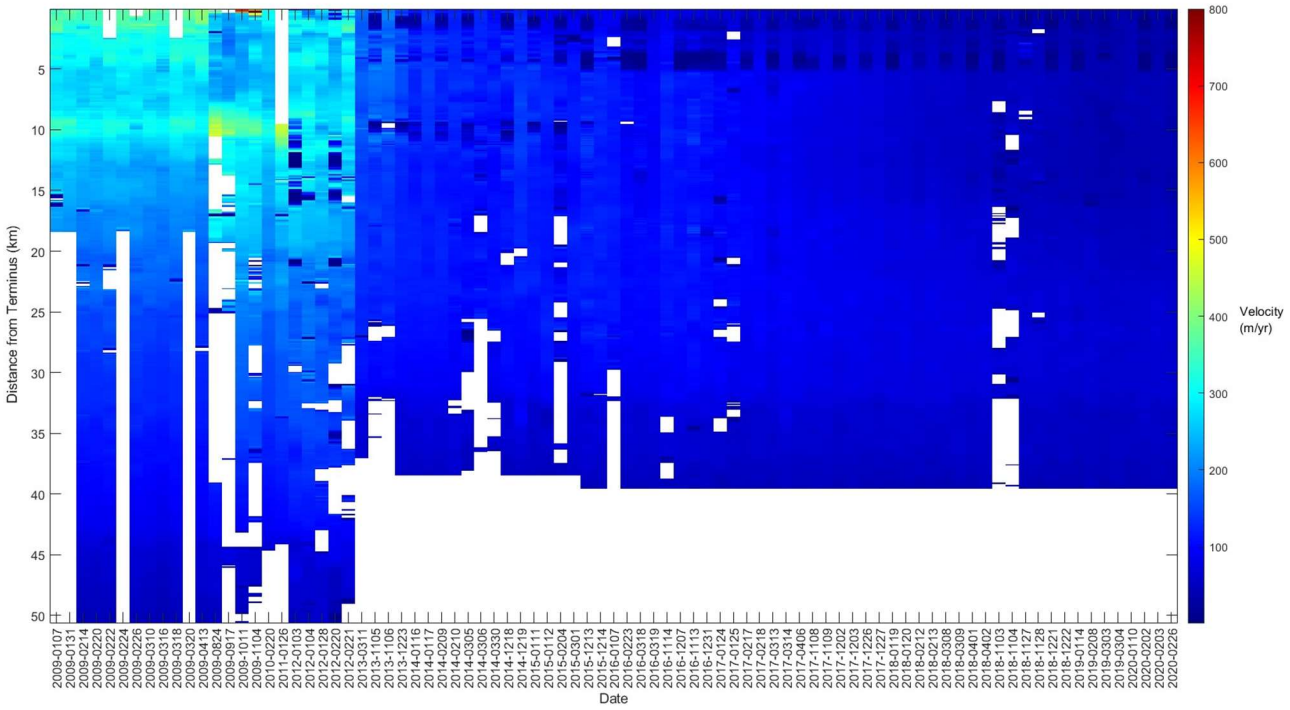

Figure 4-10: Summary of R2 centerline velocities for Otto Glacier over 2009-2020 in relation to distance from terminus. Velocities are presented in chronological order from left to right, where the date provided is the date of the reference image.

4.1.4 Summary of Velocity Trends

Some of the highest velocities occur during 1992-1994 where the lowermost ~2 km of the glacier is flowing at 1000-1200 m/yr. Velocities rapidly slow to 600-800 m/yr in the section of the glacier that is ~2-7 km from the terminus. Velocities then gradually slow with progression upglacier to minima of 10-20 m/yr. Over 1999-2004, 2006, 2008, and 2009, velocities decline each year (exceptions are peaks in the lowermost ~5 km of the glacier in 2005 and 2007). During these years, velocities in the lowermost ~6 km of the glacier are slightly lower than velocities in 1992-1994 but maxima still occur in this region, ranging

600-1000 m/yr. Over the region ~6-14 km from the terminus, velocities decline to 200-600 m/yr. From ~14-28 km upglacier, velocities slow to 150-250 m/yr, then slightly increase by ~20 m/yr before plateauing upglacier of this point to 50-200 m/yr. Velocity peaks occur in 2005 and 2007 where velocities in the lowermost 2 km of the glacier range 1000-1300 m/yr, however velocities upglacier of this section follow similar trends to others from 1999-2009. In 2010, velocities slow further, with notable slowing in the lowermost ~6 km of the glacier where velocities range 400-500 m/yr. The remainder of the 2010 velocities follow a similar trend to previous years where decreases occur at ~14 km from the terminus followed by a minute increase at ~28 km from the terminus, followed by plateauing upglacier from here.

Over 2011-2018, velocities continue to slow each year. A key change is that velocities in the lowermost ~6 km (10-50 m/yr) are now slower or similar to velocities in the section immediately upglacier located ~6-14 km from the terminus. Prior to 2011, maximum velocities occurred within the lowermost ~6 km region. From ~6-14 km upglacier, velocities increase (60-280 m/yr). In the section ~14-28 km from the terminus, velocities decline to 60-100 m/yr. In the region ~28-42 km velocities slightly increase and plateau to 60-120 m/yr before decelerating with progression upglacier of ~42 km from the terminus.

The final most notable slowing is observed over 2018-2020. During these years, velocities remain at minima in the lowermost ~6 km of the glacier (ranging 30-70 m/yr with increases moving upglacier). Velocities plateau over the region ~6-14 km from the terminus, then slightly increase to 30-80 m/yr over the section ~14-28 km upglacier. Upglacier of ~28 km from the terminus, velocities decline to minimum of 30-50 m/yr with no data available upglacier of this point.

4.2 Terminus Extents

Data for terminus extents are available for 1992-1993 (derived from ERS), 1999-2008 (Landsat 7), 2009-2019 (R2), and 2020 (Landsat 8) (Table 4-2). Images are approximately 1 year apart, except February 11, 1992 and December 29, 1993 which are 1.9 years apart. A large data gap occurs from 1993 to 1998 (approximately 5.6 years) as coherent data from these sensors are not available. Terminus advance was

observed over 1992-2010 (Table 4-1) and retreat observed from 2011-2020 (Table 4-2). Terminus extent changes in these tables are provided as absolute changes between images as well as values normalized to m/yr. Detailed terminus extent changes relative to the previous image are presented below.

4.2.1 Terminus Advance for Otto Glacier: 1992-2010

Terminus extent change over 1992-2010 is provided in (Table 4-1). In 1993, the terminus advanced by 543 m relative to 1992. In the next image from 1999, an advance of 500 m relative to 1993 is observed. This was followed by an advance by 484 m in 2000, 18 m in 2001, and no change from 2002-2010.

Table 4-1: Terminus position changes for Otto Glacier from 1992-2010 derived from ERS-1, Landsat 7, Landsat 8, and R2, reported with uncertainty of +/-193 m.

Period of advance: 1992-2010	**Image acquisition date (yyyy-mm-dd)**	**Sensor**	**Terminus advance relative to 1992 position (+/-193 m):**	**Terminus advance relative to previous image (+/-193 m):**	**Change per year (+/- 193 m/yr)**
	1992-02-11	ERS-1	-	-	
	1993-12-29	ERS-1	543	543	289
	1999-07-20	Landsat 7 Band 4	1043	500	90
	2000-06-21	Landsat 7 Band 4	1527	484	525
	2001-07-19	Landsat 7 Band 4	1545	18	17
	2002-07-31	Landsat 7 Band 4	1545	0	0
	2003-07-23	Landsat 7 Band 4	1545	0	0

	2004-06-21	Landsat 7 Band 4	1545	0	0
	2005-07-26	Landsat 7 Band 4	1545	0	0
	2006-07-08	Landsat 7 Band 4	1545	0	0
	2007-07-28	Landsat 7 Band 4	1545	0	0
	2008-06-27	Landsat 7 Band 4	1545	0	0
	2009-01-07	R2	1545	0	0
	2010-02-20	R2	1545	0	0

4.2.2 Terminus Retreat for Otto Glacier: 2011-2020

Terminus extent changes from 2011-2020 are provided in Table 4-2. In 2011, the terminus retreats by 751 m relative to the 2010 position, and this is the first instance where retreat is observed. In 2012 there is no change. In 2013, observed retreat is 44 m relative to 2012. In 2014 no change is observed, and in 2015 the terminus retreats by 56 m relative to 2014. In 2016, terminus retreats by 535 m relative to 2015, and in 2017, retreat of 22 m relative to 2016 is observed. There was no change in 2018, 2019, or 2020, and during these years the terminus was at approximately the same extent as the 1992 extent.

Table 4-2: Terminus position changes for Otto Glacier from 2011-2020, derived from ERS-1, Landsat 7, Landsat 8, and R2, reported with uncertainty of +/-193 m.

Period of retreat: 2011-2020	Image acquisition date (yyyy-mm-dd)	Sensor	Terminus extent change relative to 2010 position (m):	Terminus extent change relative to previous image (m):	Change per year (+/- 193 m/yr)
	2011-01-26	R2	-751	-751	-236
	2012-02-21	R2	-751	0	0
	2013-03-10	R2	-795	-44	-162
	2014-01-16	R2	-795	0	-123
	2015-01-11	R2	-851	-56	-307
	2016-01-07	R2	-1386	-535	-24
	2017-01-24	R2	-1408	-22	-42
	2018-01-19	R2	-1408	0	0
	2019-01-14	R2	-1408	0	0
	2020-01-10	Landsat 8 Band 4	-1408	0	0

4.3 Glacier Surface Elevation Changes

Figure 4-11 and Table 4-3 provides ice surface elevation changes for Otto Glacier over 5-year intervals, from 2000-2019, as determined by Hugonnet et al. (2021). In general, the lowermost ~6 km of the terminus experiences surface lowering (thinning) with the progression of time, while the regions upglacier of ~6 km generally experience increase in surface elevation (thickening). Specific glacier surface elevation changes are discussed below for each epoch.

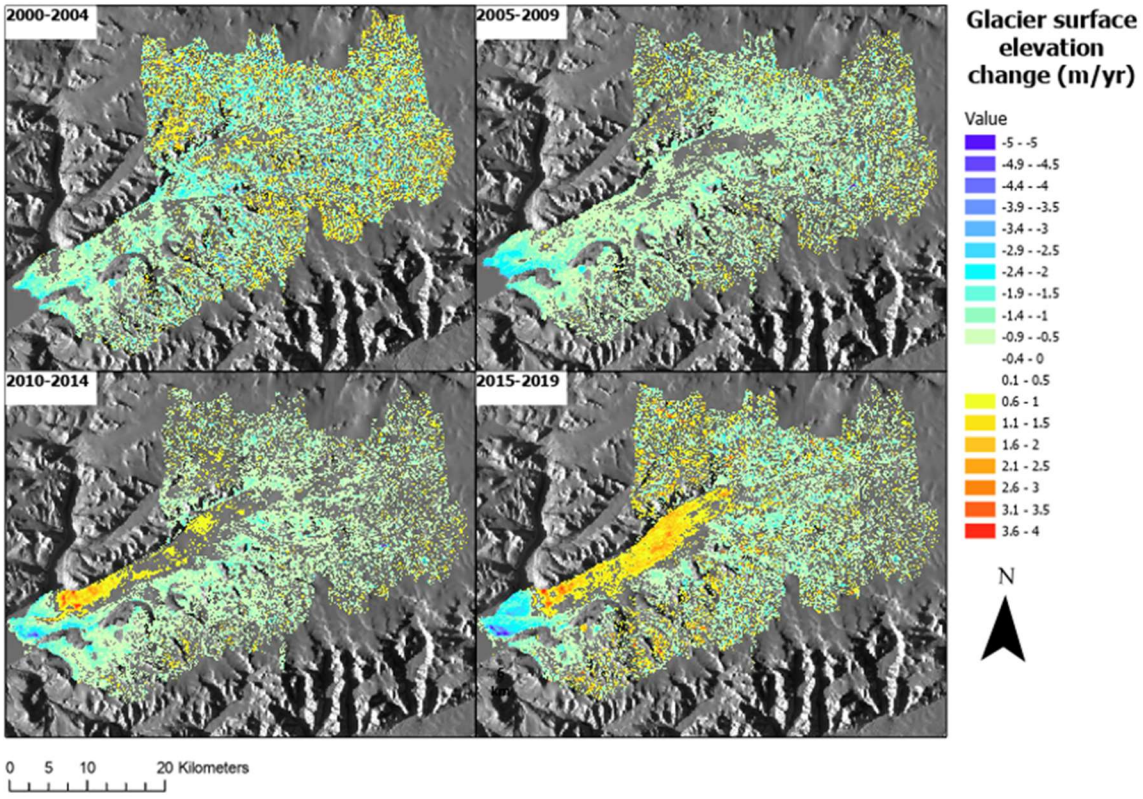

Figure 4-11: Glacier surface elevation changes derived by Hugonet et al. (2021) from 2000-2019, overlying Landsat 8 imagery (acquired April 13, 2020). Elevation changes are clipped to RGI 6.0 Polygon. No-fill areas represent areas within the error bounds for elevation change (-0.5 - +0.5 m/yr).

From 2000-2004, surface elevation lowering of 1.5 to 2.5 m/yr is observed in the lowermost ~3 km of the glacier. Upglacier from here, the data are too noisy to lend confidence to interpretation. From 2005-2009, the lowermost ~6 km experiences surface lowering of 1.5-2.5 m/yr. Again, upglacier from ~6 km from the terminus, the data contain too much noise for interpretation. From 2010-2014, the lowermost ~6 km of the terminus experiences further surface lowering of 1-5 m/yr. Surface elevation increase of 1-4.5 m/yr is observed in the section ~6-14 km from the terminus. Moving upglacier to the section ~14-30 km from the terminus, some areas of elevation gain are noted ranging 1-1.5 m/yr, however much of this section remains unchanged. Upglacier of ~30 km from the terminus, minimal data are available. In the most recent period, from 2015-2019, the lowermost ~6 km of the glacier experiences the most surface lowering of all periods, ranging 2-5 m/yr. In the region ~6-8 km from the terminus, elevation increase of

1-4 m/yr occurs. In the section ~8-14 km from the terminus, surface elevation gain of 2-3.5 m/yr occurs. In the area of glacier that is ~14-21 km from the terminus, slightly less elevation gain occurs ranging 1-1.5 m/yr. From ~21-30 km, elevation gain occurs again ranging 1.5-2 m/yr. Upglacier of 30 km, some surface lowering occurs at 1-2 m/yr, though much of the area remains unchanged.

Table 4-3: Summary of elevation changes for Otto Glacier in 5-year intervals, from 2000-2019. Elevation data obtained from Hugonet et al. (2021).

Time Period	**Distance from terminus**	**Elevation change**
2000-2004	0-3 km	-1.5 - -2.5 m/yr
	>3 km	Minimal
2005-2009	0-6 km	-1.5 - -2.5 m/yr
	>6 km	Minimal
2010-2014	0-6 km	-1 - -5 m/yr
	6-14 km	1-4.5 m/yr
	14-30 km	1-1.5 m/yr
	>30 km	Minimal
2015-2019	0-6-km	-2 - -5 m/yr
	6-8 km	1-4 m /yr
	8-14 km	2-3.5 m/yr
	14-21 km	1-1.5 m/yr
	21-30 km	1.5-2 m/yr
	>30 km	Minimal

4.4 Bedrock Topography

Figure 4-12 shows the bedrock profile for Otto Glacier, clipped to the glacier extent determined in the MLI file from February 11, 1992, which is used as a common terminus point to all velocity image pairs. The lowermost 0.5 km of the glacier is ~100 m below sea level. From ~0.5-2.5 km upglacier from the terminus, elevation of the most central bedrock gradually increases to 50 m below sea level. By ~3 km from the terminus, centrally located bedrock rises to sea level, and remains here (with minute variability) until ~6 km. A notable sill (raised bump in the bedrock) is observed in this region. The sill begins on the northern border of the terminus at ~4 km up glacier, extends toward the southern border of the terminus, and branches back toward the northern border at ~8 km uplgacier in a v-like formation (delineated by solid arrows in Figure 4-12B). Upglacier of the sill, in the area spanning ~8-16 km from the terminus, the most centrally located bedrock areas are 20-30 m above sea level and surrounding areas reach as high as 300 m above sea level. A trough occurs from ~17-21 km upglacier, where centrally located bed elevation declines to 10 m above sea level at ~17 km up glacier and reaches 100 m ablove sea level at ~21 km from the terminus. The outer most regions around this trough are as high as 300-500 m above sea level. A shorter-spanning trough occurs between 22 km and 23 km from the terminus before bed elevation increases to 190 m above sea level at ~28 km from the terminus. At ~28-30 km from the terminus, another small trough occurs, where central areas of bedrock decline to 100 m above sea level and outer areas are as high as 300 m above sea level. Progressing upglacier of ~28 km from the terminus, bed elevation increases from 90 to >300 m above sea level in the upper most region of the glacier.

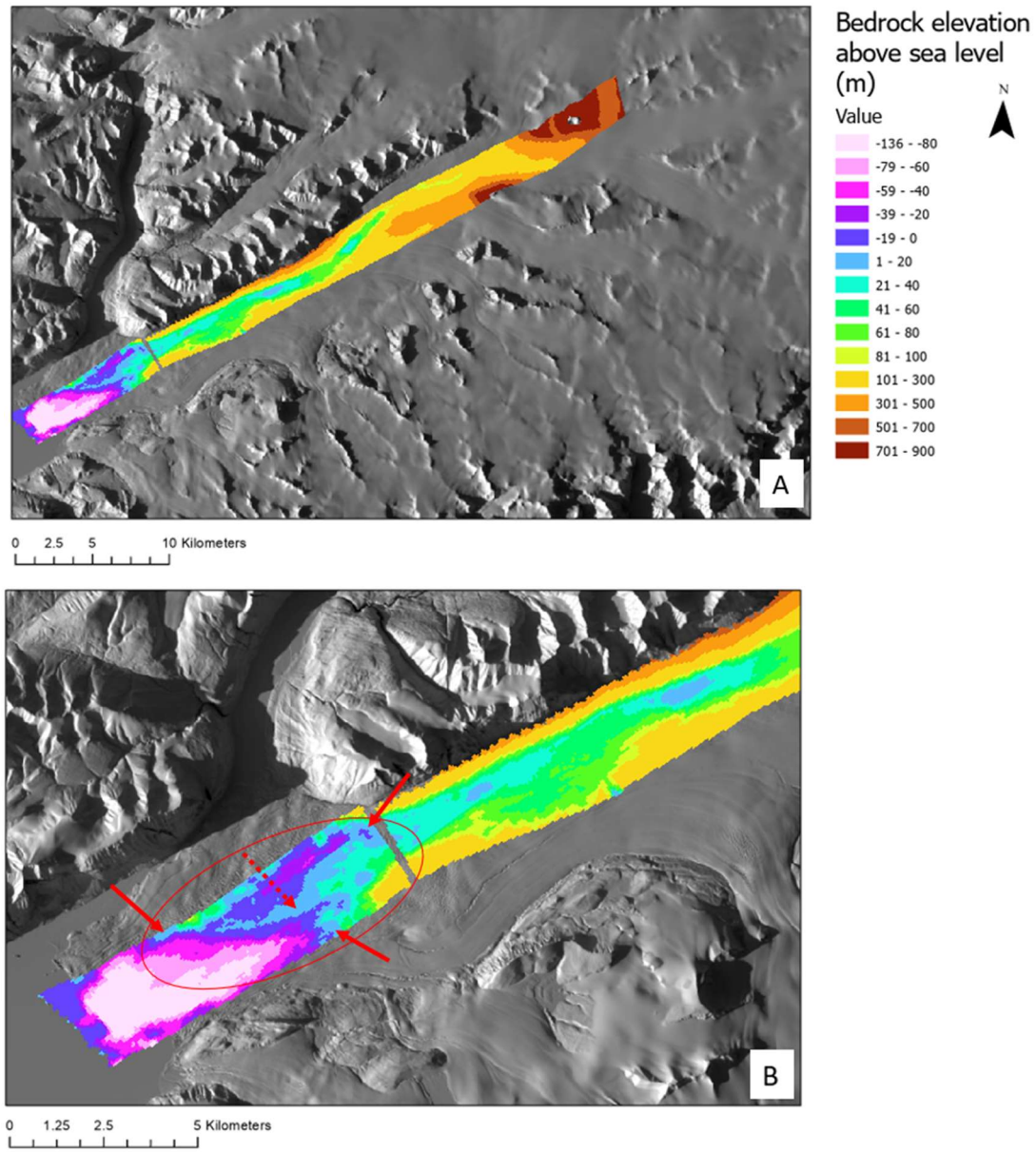

Figure 4-12: Bedrock elevation profile under Otto Glacier, from CReSIS MCoRDS data from 2014, overlying Landsat 8 imagery (acquired in April 2020). (A) shows a view of the entire glacier, while (B) is a close-up view of the lowermost terminal region with a change in scale. The red circle in (B) delineates the sill that extends most of the width of the glacier, represented with light blue colour. Solid arrows indicate the extent of the v-shape of the sill, and the hashed arrow indicates the midpoint of the sill that intersects with the centerline velocity data used in the study (~6 km upglacier from the terminus). A gap in the data occurs at ~10 km from the terminus.

4.5 Comparison of Velocity Changes to Bedrock Topography

Figure 4-13 provides a comparison of bedrock elevation to the variance in centerline velocities that occurred over the entire study as they relate to distance from glacier terminus. The greatest velocity

variability occurs in the lowermost ~6 km of the glacier, where velocity variance is 800-1100 m/yr (first orange line in Figure 4-13). The lowermost ~6 km is the region of bedrock that is either at or below sea level and is also the region of ice that is immediately downglacier of the midpoint of the sill, located at ~6 km (Figure 4-12B), which is the only point on the sill that intersects with the centerline-derived velocities. Velocity variance rapidly declines from ~6-14 km upglacier, where velocity variance is highest near the ~6 km point (800 m/yr, first orange line in Figure 4-12) and lowest at the ~14 km point from the terminus (420 m/yr) (second orange line in Figure 4-12). Velocity variability gradually and consistently declines upglacier, to a minimum of ~10 m/yr in the uppermost regions. The bedrock troughs located at ~6-14 km, ~17-21 km, and ~22-23 km do not appear to impact velocity variability trends, since velocity variability consistently declines with progression upglacier of these features.

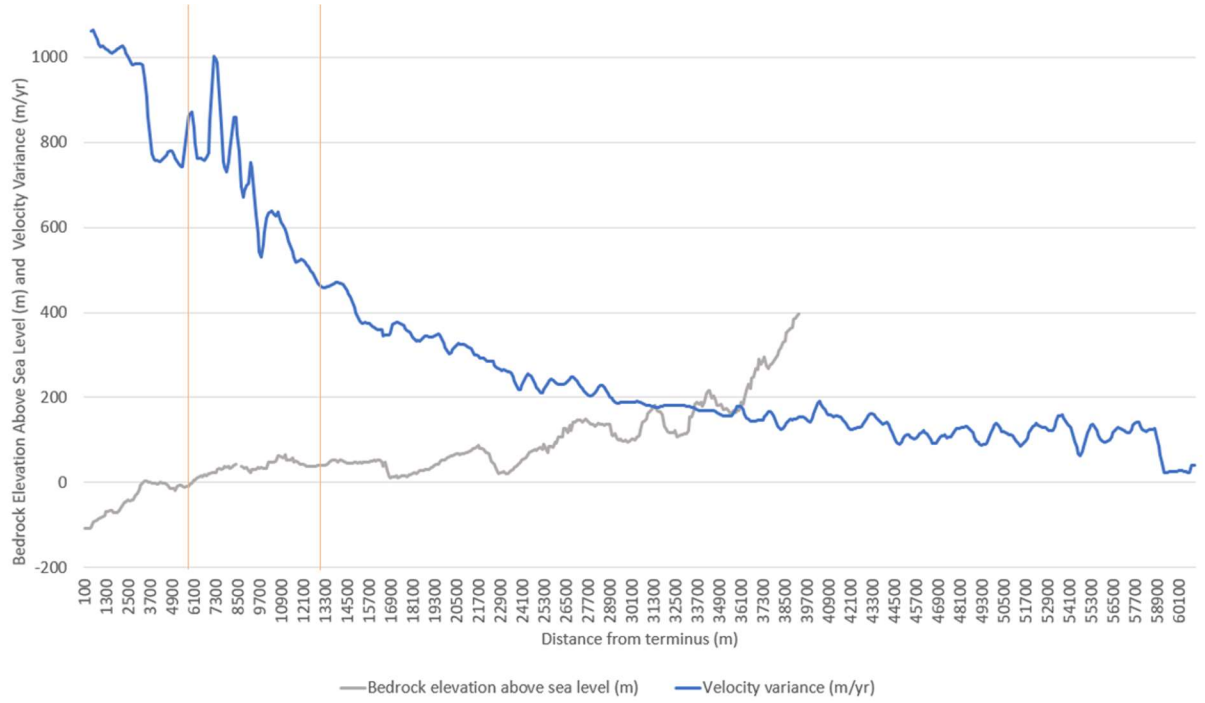

Figure 4-13: Comparison of bedrock profile to centerline velocity range profile. Velocity range is averaged every 400 m. The velocity and bedrock measurements begin at the most retreated terminus position, which occurs in 1992, and is a common reference point for all velocity rasters. Orange vertical lines denote important changes in velocity variance trends.

4.6 Summary of Results

This chapter achieved the first 4 objectives of the study by providing a detailed characterization of the dynamics and surge of Otto Glacier over 1992-2020, using measurements of velocity, terminus extent changes, and glacier surface elevation changes. This chapter also analyzed the bedrock under Otto Glacier in comparison to velocity variance over the study period. Essentially, the entire main trunk of Otto Glacier was flowing at higher speeds during 1992-2008 and progressively slowed from 2009-2020. During years of fast flow, the lowermost terminal regions had the highest velocities, but this region was also the first to start slowing during the years of slow flow. Terminus advance was measured over 1992-2001 and no change in extent was found from 2002-2008, while retreat was measured from 2009-2017. There was no change from 2018-2020. Glacier surface elevation change analyses revealed progressive thinning in the lowermost ~6 km of the terminus and progressive thickening upglacier over 2000-2020. The bedrock profile revealed a v-shaped sill spanning the section of glacier ~4-8 km from the terminus, the midpoint of which, located ~6 km upglacier, intersects with the extracted centerline velocity data. The highest velocity variability (800-1100 m/yr) occurred in the lowermost ~6 km of the terminus, downglacier of the sill midpoint. A drastic decline in velocity variability occurred immediately upglacier in the section ~6-14 km from the terminus, and a more gradual decline in velocity variability with progression upglacier.

Chapter 5 - Discussion

This chapter addresses objective 5, using data from objectives 1-4 to provide a detailed analysis of Otto Glacier's surge event from 1992-2020 in the context of the Canadian Arctic. This chapter will begin with a review of the surge evolution for Otto Glacier and associated geometry changes, including possible mechanisms to explain why these changes may occur. This is followed by a comparison of Otto Glacier to other surge-type glaciers. The chapter concludes with an interpretation of the relationship between bedrock topography and velocity variance and how the data can be used to infer a possible surge mechanism, along with a schematic in Figure 5-3.

5.1 Surge Evolution and Associated Geometry Changes

The dynamic evolution of Otto Glacier over the 1992-2020 period can be divided into three phases: the first two phases are interpreted to be part of the surge. Phase I is the fast flow phase (1992-2008) where terminus advance is observed, and velocities are higher than in other years of the study. Phase II is the deceleration phase (2009-2017), where velocities are still higher than non-surging glacier velocities but are slower compared to phase I, and where the first terminus retreat is observed. Phase III of the cycle is considered the start of the quiescence phase (2018-2020), where the glacier flows at non-surging velocities and minimal change in terminus extent occurs. Each of these phases are described below, along with a summary of velocity and geometry changes over time provided in Figure 5-1. The relationship between velocity variance and bedrock topography is discussed separately and includes a hypothesis for a possible surge mechanism.

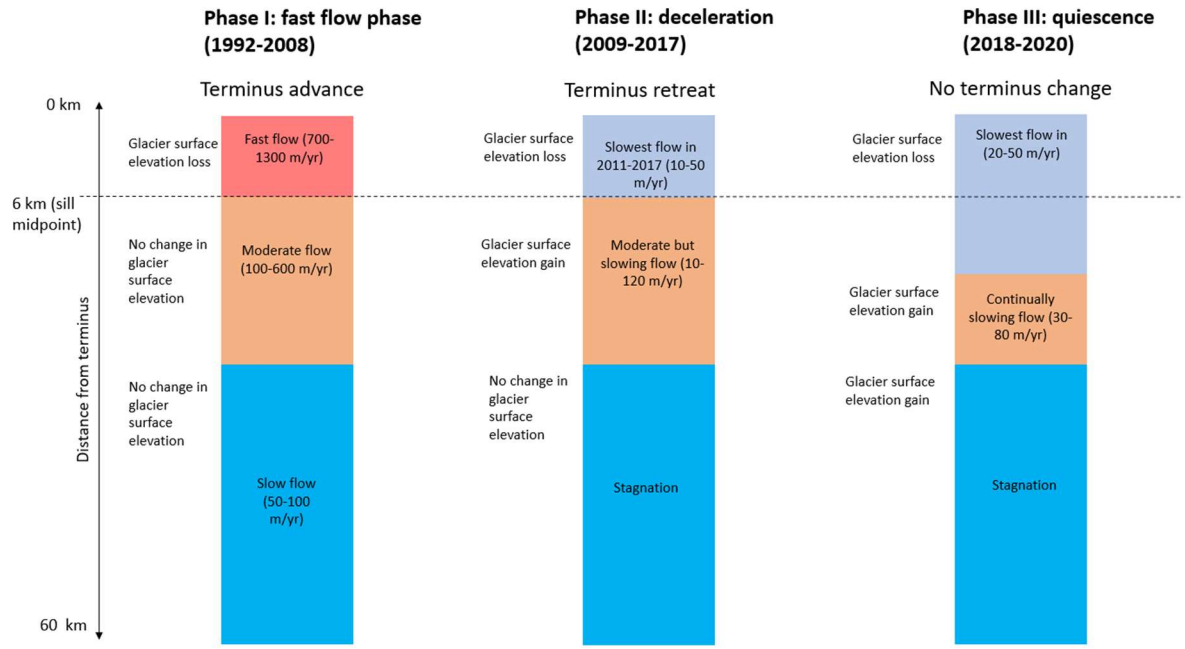

Figure 5-1: Summary of velocity, terminus, and surface elevation changes for Otto Glacier over 1992-2020, shown in relation to distance from the terminus, providing a conceptual framework of three differing phases of glacier flow.

5.1.1 1992-2008: Phase I, Fast Flow Phase

The highest velocities for Otto Glacier occur during 1992-2008, albeit with some variability and gradual slowing over time (Figure 4-1, Figure 4-2, Figure 4-3, Figure 4-4). Terminus advance occurs during 1992-2000 with no change in terminus extent from 2001-2008 (Table 4-1). The coincident net terminus advance and fast velocities are interpreted to comprise the fast flow phase of this surge of Otto Glacier (Figure 5-1). Terminus advance during periods of fast flow is consistent with expected surge behavior, where acceleration results in the transport of mass from upglacier (reservoir area) toward the terminus (receiving area), and the terminus subsequently advances (Benn and Evans, 2010; Van Wychen et al., 2016). This is also evident with the previously observed surge for Otto Glacier, where terminus advance was observed over 1950-1964 along with new crevassing which suggested an intense acceleration event had occurred (Hattersley-Smith, 1964, 1969). Lack of change in terminus extent during 2001-2008 indicates a transition point in the surge behavior, where mass from the regions upglacier (the reservoir

zone) has now been exhausted, and mass is no longer able to be transported to the terminus (the receiving zone), especially with overall slowing velocities during these years.

During phase I, velocities vary along the main trunk of the glacier, with the highest velocities (700-1300 m/yr) observed in the lowermost ~6 km of the terminus (the area at or below sea level) and slowing with progression up glacier (Figure 4-1, Figure 4-2, Figure 4-3, Figure 4-4, Figure 5-1). High speeds in the areas at/below sea level are also reported for pulse type glaciers in the Canadian Arctic (Van Wychen et al., 2016). Though velocities for Otto Glacier are highest in the area at or below sea level, most of the main trunk is flowing at high speeds during the surge, which contrasts the pulse behavior reported for other glaciers within the region (Van Wychen et al., 2016; Van Wychen et al., 2020). This full-trunk activation during the surge phase is more consistent with surge-type glaciers in the Canadian Arctic, such as Mittie Glacier and Chapman Glacier (Van Wychen et al., 2016) and Iceberg Glacier (Lauzon, 2022), lending confidence to the premise that Otto Glacier is a surge-type glacier and not a pulse-type.

Though velocities are relatively high during the fast flow phase, there is overall slowing as the phase progresses. Of note is the fact that the slowing is not consistent over time, but rather includes times of alternating faster and slower flow, particularly in the lower most ~10 km of the glacier (Figure 4-3, Figure 5-2). The first instance where this is apparent is in 2001, where velocities in the lowermost ~10 km of the glacier are lower than in 2000. In 2002, velocities in the lowermost ~10 km increased relative to 2001. Data are missing for the lowermost ~10 km in 2003. In 2004, velocities in this region are similar to 2002, then increase in 2005, then decrease in 2006, and increase in 2007 again. In 2008, velocities slow compared to 2007. After 2008, velocities in the lowermost ~10 km progressively slow in each year.

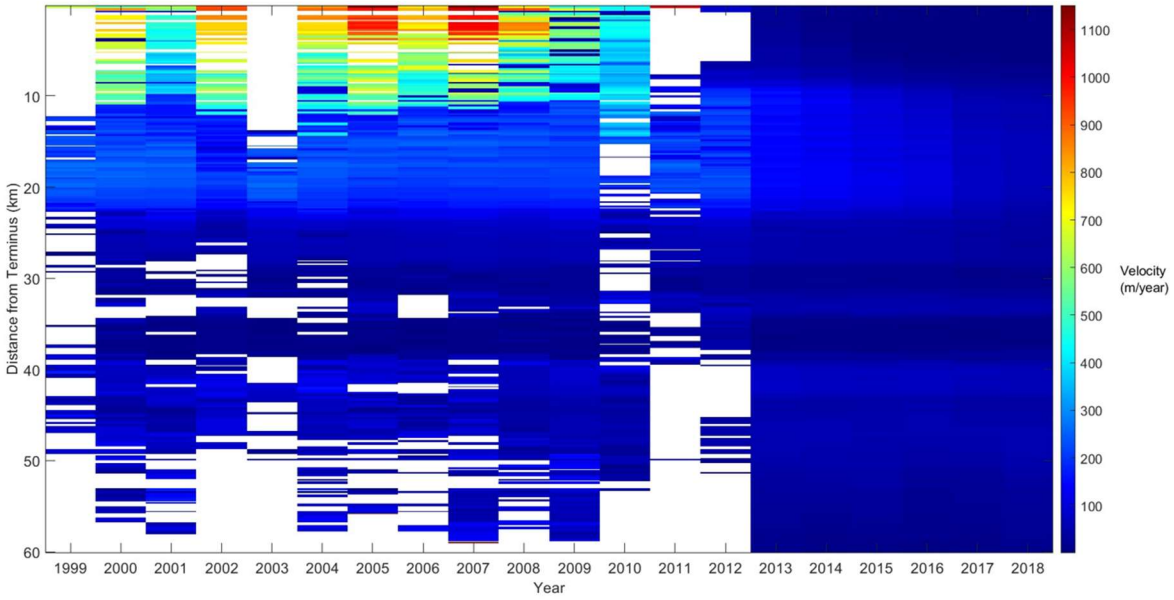

Figure 5-2: ITS_LIVE-derived centerline velocities for Otto Glacier from 1999-2018, in relation to distance from terminus.

Glacier surface elevation data for 2000-2004 showed thinning of 1.5-2.5 m/yr in the lowermost ~3 km of the terminus and minimal change upglacier from this point (Figure 4-11). Then, from 2005-2009, the area of thinning expands upglacier and now occurs in the lowermost ~6 km (Figure 4-11). This association of thinning during fast flow is again consistent with surge theory: prior to a surge, mass typically accumulates up glacier (reservoir area), resulting in an area of thickening and steepening surface slope, and subsequent increase in driving stress which triggers the surge (Benn and Evans, 2010; Raymond, 1987). During the surge, mass from the area that had been thickening is rapidly transported to lower regions of the glacier (receiving area) (Benn and Evans, 2010; Raymond, 1987). During this process, the faster flowing ice that has moved downglacier is restrained by the slower flowing ice upglacier, and at the same time, the slower moving ice upglacier is pulled by the faster flowing ice downglacier. The propagation of this longitudinal stress, in a region of low basal drag, can result in dynamic thinning and eventual velocity increase further upglacier due to the pulling effect from downglacier (Cuffey and Paterson, 2010). The thinning in the lowermost ~6 km of Otto Glacier is coincident with the area of glacier that flows at the highest velocities during phase I. This, along with slower velocities upglacier of this region, suggest that the thinning is due to the surge process.

5.1.2 2009-2017: Phase II, Deceleration Phase

Consistent slowing of the velocity structure of Otto Glacier (Figure 4-4, Figure 4-5, Figure 4-6, Figure 4-7, Figure 4-8) as well as terminus retreat (Table 4-1, Table 4-2) and glacier thickening (Figure 4-11) take place over the 2009-2017 period. Hence, this is interpreted as a new phase of the surge and is identified here as Phase II, the deceleration phase of the surge (Figure 5-1). The progressive slowing and coincident terminus retreat are consistent with what is seen in other thermally-controlled surge-type glaciers as they transition to quiescence, such as Monacobreen Glacier (Murray et al., 2003). The first terminus retreat for Otto Glacier is observed in 2011, where it retreats by 751 (+/-193 m) from the 2010 position. In 2012, no change in terminus extent is observed, and from 2013-2015, terminus change is within the error bounds and therefore change cannot be confidently determined. Retreat of 535 m (+/-193 m) is observed in 2016 and no certain extent changes are measured in 2017. Overall terminus retreat during phase II occurs in response to slowing velocities, where there is reduction in the transport of mass from upglacier (reservoir area) to the lower regions (receiving area), and therefore terminus position cannot be maintained as the glacier calves ice to the ocean. The sill spanning ~4-8 km upglacier from the terminus could be exacerbating the reduced transfer of mass to the area downglacier of the sill, where ice flowing in from upglacier is obstructed as velocities slow. With sustained deceleration over time, the above processes result in terminus retreat. The obstruction of the sill may also act a pinning point that controls how far the terminus retreats, where ice accumulates over and upglacier of the sill and thus continuously replenishing mass lost in these areas.

In phase II, velocities continue to slow each year, however the entire main trunk remains non-stagnant during this phase (Figure 4-4, Figure 4-5, Figure 4-6, Figure 4-7, Figure 4-8). In 2009-2010, velocities are still highest in the lowermost ~6 km of the terminus (500-600 m/yr) compared to any other location on the glacier, as in phase I (Figure 5-1). Then, over 2011-2017, velocities along the glacier continue slow, but the pattern of velocity variability along the glacier changes compared to previous years.

Importantly, the lowermost ~6 km of the glacier now flows at slower velocities (10-50 m/yr) than the ice in the section immediately upglacier at ~6-14 km from the terminus (Figure 4-8), whereas in previous years, the lowermost ~6 km flowed at higher speeds than this section upglacier. The marked slowing of the lowermost region during 2011-2017 is possibly a response to a reduction in mass transfer from upglacier to the lowermost regions following a surge, which would act to reduce driving stress. The marked slowing of the lowermost region is also consistent with other surges observed in the Canadian Arctic, such as Iceberg Glacier, where fast flow was observed along the entire main trunk in 2000, and subsequent slowing observed to have initiated in the lowermost terminus region, spreading upglacier until 2010, at which time the entire main trunk was stagnant (Van Wychen et al., 2016; Lauzon, 2022).

In 2010-2014, thinning rates increase in the lowermost ~6 km (1-5 m/yr). The increased thinning in the lowermost ~6 km of the terminus is likely due to the progressive slowing of glacier velocities in this area and subsequent reduced incoming mass downglacier of the sill to replace mass lost here. During this period, a notable switch to thickening (4.5 m/yr) occurs at ~6-14 km from Otto Glacier's terminus (Figure 4-11, Figure 5-1). Thickening to a lesser degree (1-1.5 m/yr) occurs in the section upglacier of ~14 km from the terminus however much of the data in this section show no change. This switch to thickening in the section ~6-14 km from the terminus is a major identifier of the new surge phase. The thickening is likely partially a result of the faster flowing ice in this section becoming obstructed by the newly slower flowing ice in the lowermost ~6 km of the glacier, which impedes the fast-flowing ice upglacier, resulting in ice accumulation and thickening in this section (Cuffey and Paterson, 2010). The switch to thickening in the section ~6-14 km from the terminus is also coincident with the sill spanning the section ~4-8 km upglacier from the terminus (Figure 4-12, Figure 4-13), which likely impedes glacier flow, resulting in accumulating mass upglacier of the sill especially as speeds slow. Bedrock topography is known to modulate glacier surface geometry, where bedrock bumps act as obstacles to flow and subsequently impose gradients in basal drag along the glacier, resulting in glacier thickening over the bump (Cuffey and Paterson, 2010; Van

Wychen et al., 2016) The sill at ~4-8 km from the terminus of Otto Glacier likely acts in this way, and the midpoint of the sill (~6 km from the terminus) is the point that separates areas of glacier thickening and thinning as well as areas of faster and slower velocities. Raised areas of bedrock (bumps) have been observed to be coincident with areas of thickening in other glaciers, such as Good Friday Bay Glacier on Axel Heiberg Island in the Canadian Arctic. Good Friday Bay Glacier overlies a nunatak located at ~9 km from the terminus where glacier thickening was observed (Medrzycka et al., 2019). A similar process has been reported for Dobbin and Parish Glaciers which are pulse-type glaciers in the Canadian Arctic, each overlying a bedrock sill. The sills are thought to obstruct the flow of these glaciers which resulted in thickening over each glacier's respective sill, and thinning downglacier of the sill (Van Wychen et al., 2016). The effect of bedrock bumps on velocity variability in addressed in section 5.1.5.

5.1.3 2018-2020: Phase III, Quiescence

In 2018-2020, velocities at all points along Otto Glacier are <80 m/yr (Figure 4-5, Figure 4-9, Figure 4-10, Figure 5-1) which is consistent with speeds observed in surge-type glaciers transitioning to quiescence (Van Wychen et al., 2016; Van Wychen et al., 2020). In the lowermost ~6 km of the terminus, velocities remain slower than other locations on the glacier (5-50 m/yr). This observation can be considered a continued manifestation of the process described in phase II, where reduction in mass transfer results in reduced driving stress and slower velocities but to a more severe degree in this quiescent period. No change in terminus extent is observed during this phase (Table 4-2), again due to the reduced transfer of mass to the terminus (Benn and Evans, 2010). The sill located ~4-8 km upglacier (Figure 4-12) may continue to act as a pinning point in this phase, where it prevents further terminal retreat by obstructing the incoming ice from upglacier, resulting in mass accumulation that replenishes any mass lost in the area over and upglacier of the sill. The area of thinning during this phase remains in the lowermost ~6 km of the glacier (Figure 4-11), which is downglacier of the sill (Figure 4-12). Thickening spreads further upglacier of the sill during this phase. The greatest thickening still occurs over the section ~6-14 km from the

terminus (Figure 4-11), which is partially due to the thickening process described in phase II, where the faster flowing ice in the ~6-14 km section is obstructed by the slower flowing ice downglacier, resulting in flow impedance and thickening. The sill itself likely exacerbates the impedance, as in phase II.

5.1.4 Summary of the Surge Cycle

The evolution of the surge for Otto Glacier is summarized in Figure 5-1. To summarize, the earliest phase (fast flow phase, 1992-2008) is characterized by fastest flow in the lowermost ~6 km of terminus. Moderate flow occurs in the lower-mid section spanning ~6-14 km upglacier, and slower flow upglacier from here. Terminus advance occurs during this period, as well as glacier thinning in the lowermost ~6 km and no change in glacier surface elevation upglacier. The thinning is a result of the dynamic thinning process, where the lower part of the glacier is flowing faster than ice upglacier, and is in turn pulled back by the slower region upglacier, resulting in ice extension and surface lowering.

In phase II (deceleration, 2009-2017), velocities are slower than in phase I, and the lowermost ~6 km of the glacier now flows at slower velocities than the region upglacier located ~6-14 km from the terminus (whereas in phase I, the lowermost ~6 km flowed at velocity maxima). The first terminus retreat is observed in 2011, attributable to slowing velocities and reduced transportation of mass to the terminus to replace what is lost. Glacier thickening occurs in the lower-mid section at ~6-14 km from the terminus. The thickening is partially a result of the now faster flowing lower-mid section flowing into the slower ice downglacier (Cuffey and Patterson, 2010) and is a key signature of the transition to quiescence. Additionally, the sill spanning ~4-8 km from the terminus likely also impedes flow here, causing a pile-up and further ice thickening on the upglacier side of the sill.

In phase III (quiescence, 2018-2020), the slowest velocities occur, with the lowermost ~6 km still flowing at slower speeds compared to flow upglacier. No change in terminus extent occurs due to the exhaustion of mass from upglacier and possibly also due to stabilization provided by the sill. The area ~6-

14 km upglacier continues to thicken, in a continued manifestation of the thickening processes described in phase II. Thickening now spreads up glacier as the obstruction of ice flow continues over time.

5.1.5 Possible Surge Mechanism: Bedrock and Velocity Variance

As discussed in the preceding sections, the sill spanning the region ~4-8 km from the terminus likely impedes glacier flow. Bedrock bumps can impede glacier flow by creating variations in basal drag, with subsequent glacier thickening over and upglacier of the bump (Cuffey and Paterson, 2010) (Figure 5-3A). Eventually, so much mass accumulates at the impedance that glacier driving stress increases until a pressure threshold is reached, at which point acceleration is triggered over the impedance (Cuffey and Paterson, 2010; Van Wychen et al., 2016). The subsequent propagation of longitudinal stress gradients (fast flowing ice downglacier of the impedance pulls on slow flowing ice upglacier of the impedance) eventually increases velocity further upglacier (Cuffey and Paterson, 2010) (Figure 5-3B). On the downglacier side of the impedance, the fast-flowing ice eventually flows into an area of slower flowing ice and subsequently slows down (Sergienko, 2012). The sill under Otto Glacier may induce a similar obstructing effect, where oscillations between low and high velocities in this area explain the high degree of velocity variability seen over and downglacier of the sill (Figure 4-13). It is the thickening upglacier of the sill during quiescence that will probably trigger the next surge phase (Figure 5-3C). The next surge phase will again lead to dynamic thinning and terminus advance until transportation of mass from upglacier to the lower region is exhausted. The dynamic thinning will then reduce driving stress, causing further slowing, and eventual thickening again over the impedance, until the cycle repeats (Cuffey and Paterson, 2010; Van Wychen et al., 2016).

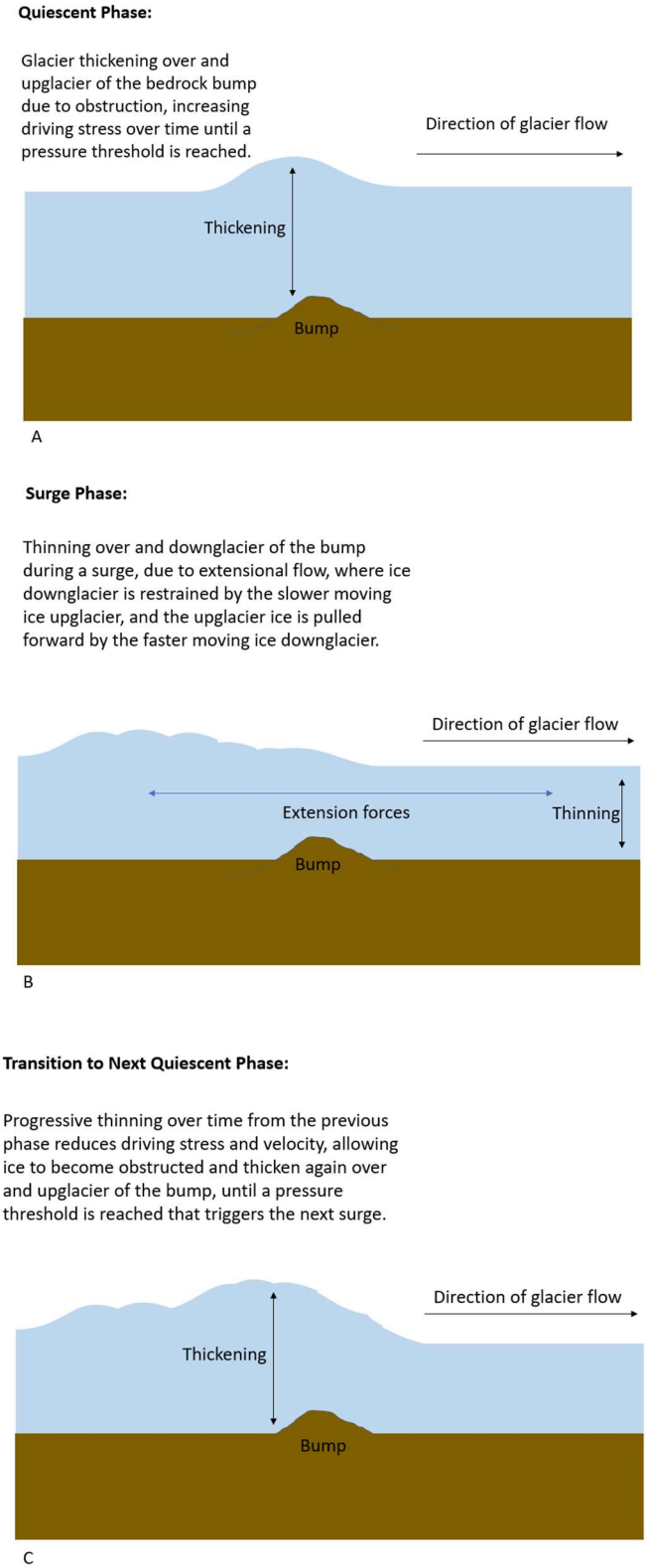

Figure 5-3: Schematic of suggested glacier geometry changes during the surge cycle of Otto Glacier.

Similar processes have been reported for Good Friday Bay Glacier on Axel Heiberg Island, which is hypothesized to have been in a slow surge since 1960 (Medrzycka et al., 2019). Velocities have remained consistently high since 1960 (250-470 m/yr) in the location immediately downglacier of the nunatak located at ~9 km upglacier from the terminus, and these velocity peaks are inferred to be a result of thickening/steepening over the bump and increased driving stress toward the downglacier side of the bump (Medrzycka et al., 2019; Müller, 1969). The sill under Otto Glacier may have the same effect on glacier flow and geometry as the nunatak did for Good Friday Bay Glacier. This effect of bedrock bumps on glacier flow variability has also been reported for the pulse-types Dobbin and Parish Glaciers (eastern Ellesmere Island). Though each are located on different ice caps, both pulse-type glaciers had near identical surface elevation profiles before and after their pulse events (Van Wychen et al., 2016). Both glaciers are grounded below sea level for most of their ~20 km lengths, but each glacier overlies a sill that rises above sea level (~4.5 km upglacier for Dobbin Glacier and ~8-12 km upglacier for Parish Glacier) (Van Wychen et al., 2016). A common pattern of glacier thickening was observed over the sill and thinning in the region between the sill and where the bed goes back down below sea level (Van Wychen et al., 2016). Thickening occurred again in the lowermost region of the terminus (Van Wychen et al., 2016). It was inferred that the acceleration resulted from thickening/steepening over the sills that exceeded a pressure threshold, and subsequent, rapid transfer of mass from the regions above the sill to the lower regions (Van Wychen et al., 2016). The sill under Otto Glacier likely plays a role in the regulation of flow speeds, similar to that of the sills under Parrish and Dobbin Glaciers, since similar changes in flow and geometry are observed. It is possible that Otto Glacier experiences a pulse that is superimposed on a surge, where the greatest velocity variability is restricted to the areas below sea level (as occurs with pulse-types), however, the entire main trunk is also flowing at higher-than-normal speeds (as occurs with surging).

5.1.6 Surge Timing

A summary of observations for Otto Glacier's surge cycle to date is presented in Figure 5-4. In terms of surge duration, it is confirmed that Otto Glacier's surge lasts for a minimum of 26 years, starting at least as early as 1991 and continuing until 2017. Although this study only presents observations as far back as 1992, Millan et al. (2017) reported frontal speeds >800 m/yr in 1991 for Otto Glacier, which are similar to the speeds found in 1992-1994 in this thesis. The surge ends by 2018, at which time it enters quiescence. Otto Glacier was last observed surging in 1950-1964 (Hattersley-Smith, 1964, 1969). The next study that included Otto Glacier was by Copland et al. (2003), who noted that Otto Glacier was surging in 1999, but could not determine whether this was a new surge or continued from the surge observed over 1950-1964. Because no observations are reported between 1965-1990, it is not possible to pinpoint exactly when the most recent surge began. The surge phase may have initiated before 1991 or even before the first observation in 1950, and in the latter case, the surge would be a minimum of 67 years long. The quiescent phase can also not be definitively quantified but has two possible scenarios: a maximum of 25 years (from 1965 and until 1990 or earlier) or an indeterminable amount of time, since a quiescent phase may not have even occurred during 1965-1990 and a full quiescent phase has not been reported for any other time period.

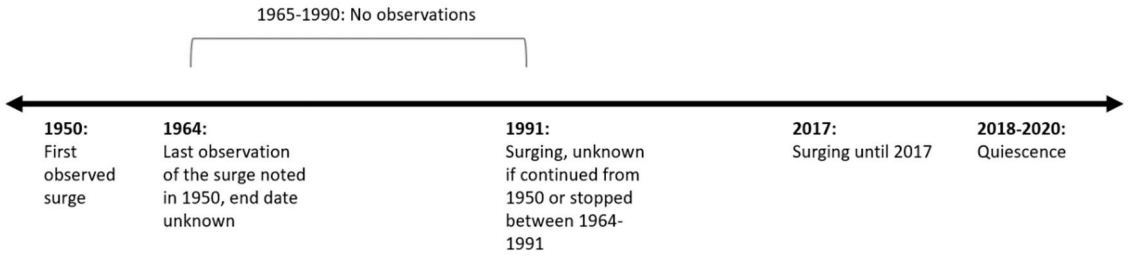

Figure 5-4: Timeline of observations of surging for Otto Glacier.

A surge phase of at least 26 years, regardless of the exact duration, is noteworthy because even this minimum surge duration is longer than that of Alaskan and Svalbard-type surges. Alaskan-type surges have a surge duration of only months-4 years (Benn and Evans, 2010; Kamb et al., 1985). Bakaninbreen Glacier, a Svalbard surge-type, was observed surging for only 10 years (1985-1995) (Murray et al., 1998). Monacobreen Glacier, another Svalbard-type, had an estimated surge phase of only 7-11 years (Murray et al., 2003). If Otto Glacier's surge phase is longer than 26 years, it is even more dissimilar to these classic surge-type classifications. An even more unique scenario is if Otto Glacier's surge and quiescent duration are both ~25-26 years long, as this near-equal ratio has not been reported elsewhere and especially not in the Canadian Arctic, where much longer quiescent phases are expected due to the cold and dry climate (Van Wychen et al., 2016). A comparison of Otto Glacier's possible surge cycle durations to those of other surge-type glaciers in the Canadian Arctic follow in sections 5.1.6.1 and 5.1.6.2.

5.1.6.1 Comparison of Minimum Surge Phase Duration to those of Other Surge-Type Glaciers

Most other studies of surge-type glaciers in the Canadian Arctic have not been able to capture a complete surge or quiescent phase due to the long surge cycles reported for this region. Though observations might begin during a surge or quiescent phase, the exact start of the phase cannot be confirmed if observations prior to the study are not available. Therefore, most studies report minimum phase durations, which are compared to the minimum surge phase of Otto Glacier in this section.

If Otto Glacier's active phase is closer to ~26 years long, this would be most similar to the minimum surge phase of Chapman Glacier, located adjacent to Otto Glacier. Chapman Glacier was observed accelerating over 2000-2011, reaching 200 m/yr in the lowermost 20 km of the main trunk (Van Wychen et al., 2016). From 2011-2015, velocities in the section ~5-20 km up glacier from the terminus deceased each subsequent year while velocities in the lowermost ~5 km of the glacier increased (Van Wychen et al., 2016). After 2016, velocities generally increased each subsequent year for the remainder of observations which stopped in 2020 (Van Wychen et al., 2020). The studies that report the velocity

behavior for Chapman Glacier only offer brief descriptions, but it is possible that Chapman Glacier had a surge phase of at least ~20 years (2000-2020). If Chapman Glacier's surge phase is closer to ~20 years, this would be similar to the possible scenario where Otto Glacier's surge phase is ~26 years. Estimates for the quiescent phase of Chapman Glacier are not available, and the studies do not discern whether the slow-down in 2011-2015 was the start of the quiescent phase. Since Chapman and Otto Glaciers are so close in proximity and have similar surge cycles, external factors common to both glaciers could control their velocity changes, such as local climate, bedrock morphology, or bedrock lithology.

A surge phase duration closer to ~26 years would also be similar to that of Iceberg Glacier on Axel Heiberg Island, which was observed surging for at least ~22 years (at least as early as 1981 until 2003) (Lauzon, 2022). From 1972-1980, Iceberg Glacier's mean centerline velocity trunk was ~89 m/yr. Velocities in the terminus region drastically increased in 1981 to >1700 m/yr with associated terminus advance of 100-400 m, suggesting that surging initiated at that time. The highest velocities were observed in 1991 (~2000 m/yr) in the terminus region (Lauzon, 2022). Velocities then slowed each subsequent year until near stagnation in 2003. It was noted that Iceberg Glacier's surge phase may have begun even earlier than 1981, since the velocities from 1972-1980 were much higher than those during surge termination in 2003 (Lauzon, 2022). The duration of Iceberg Glacier's quiescent phase is also uncertain, but it is at least 17 years long, since the glacier has been nearly stagnant from 2003-2020 when the last observations ended (Lauzon, 2022; Van Wychen et al., 2020).

Mittie Glacier on southern Ellesmere Island is another known surge-type glacier in the Canadian Arctic. Mittie Glacier was observed to be un-crevassed in 1959 and extensively crevassed along the main trunk in 1999 and 2000, with maximum velocities of 1000 m/yr measured at ~20 km of upglacier from the terminus (Copland et al., 2003). Coincident surface lowering of 10-25 m in the section 15-20 km from the terminus was also observed along with terminus advance of >4 km relative to its position in 1959 (Copland et al., 2003). Short and Gray (2005) later reported deceleration to 700 m/yr at the terminus in 2004, and

in 2012, the glacier decelerated to stagnation (Van Wychen et al., 2014). These reports suggest a surge phase of at least 13 years (at least as early as 1999 until 2012) with a quiescent phase of at least 40 years (at least as early as 1959 until 1999). The minimum duration of the surge phase is shorter than the minimum surge duration suggested for Otto Glacier, however, limited analysis is available to confirm the phase durations for Mittie Glacier.

Pulses or "partial surges" involve velocity changes that occur only in the area of the glacier that is below sea level (Van Wychen et al., 2016). Milne Glacier, a likely pulse type Glacier located on northern Ellesmere Island, was reported to have slowed over 2000-2005 and accelerated between 2005-2020 in the lowermost 15 km of the terminus, reaching speeds of 80-100 m/yr, with no observations available after 2020 (Millan et al., 2017; Van Wychen et al., 2020). Most of the velocity variability was confined to the section 15-20 km from the terminus (Van Wychen et al., 2020). Milne Glacier's minimum fast flow phase of ~15 years is shorter than Otto Glacier's minimum surge phase of 26 years. However, Jeffries (1984) identified that Milne Glacier had advanced by 4 km between 1959 and 1983 and showed distorted moraines on its surface, indicating fast flow. This implies a possible active phase of 24 years for Milne Glacier which would be similar to the minimum possible surge phase of Otto Glacier.

Overall, Otto Glacier's minimum surge phase duration is similar to those reported for the surge-types Chapman and Iceberg Glaciers, but this comparison is difficult to confirm since observations have not definitively captured a complete surge or a complete quiescent phase for any of these glaciers. Otto Glacier's minimum surge duration could also be similar to the pulse-type Milne Glacier, however, because it is a pulse-type, different processes could be controlling its velocity variability. At the very least, this analysis of Otto Glacier adds to this growing body of literature that finds long surge lengths in the Canadian Arctic.

5.1.6.2 Comparison of longer surge phases

It is widely accepted that dynamic instabilities can range across a spectrum of flow patterns, where character and duration of acceleration varies between glaciers and geographic regions (Medrzycka et al., 2019; Van Wychen et al., 2016; Van Wychen et al., 2022). Good Friday Bay Glacier on Axel Heiberg Island, for example, is theorized to have been in a slow surge since the 1950s, which would be the longest active phase ever documented (Medrzycka et al., 2019). The terminus of this glacier was observed to have advanced by ~9 km over 1948-2018, with frontal velocities of 350 m/yr from 2006-2018 that were similar to those found in the 1960s by Müller (1969).

Split Lake Glacier in southeast Ellesmere Island is another glacier in the Canadian Arctic hypothesized to be in an unusually prolonged surge phase (Van Wychen et al., 2022). It is thought that Split Lake Glacier has been surging since the 1970s, as evidenced by acceleration and terminus advance since this time. However, velocities during acceleration were slower than for Otto Glacier, where 500 m/yr was the maximum speed observed on Split Lake Glacier (Van Wychen et al., 2022). If Otto Glacier's surge phase began in 1950 or earlier (and ended in 2017), its surge phase duration would align more with the hypothesized prolonged surges of Good Friday Bay and Split Lake Glaciers. The range of dynamic patterns in the Canadian Arctic support the idea that surging/acceleration can be considered a spectrum of behavior, rather than fitting into two discreet classes of either Alaskan or Svalbard type surging (Medrzycka et al., 2019; Van Wychen et al., 2022).

Considering the surge phase of Otto Glacier is at least 26 years, the surge could possibly be classified as a slow surge in which the surge phase is defined to last at least 20 years (Jiskoot, 2011). However, Otto Glacier differs from the definition of a slow surge, since slow surging frontal speeds are only 5-10 times higher than speeds observed during quiescence. This is a much slower speed than what is observed for Otto Glacier, where frontal speeds are up to ~60 times higher in the fast flow phase compared to quiescence.

In summary, it is difficult to compare Otto Glacier's surge cycle duration to other glaciers since data from 1965-1990 has not been analyzed for Otto Glacier. Further complicating the comparison is that most studies of other surge-type glaciers in the Canadian Arctic have not been able to definitively quantify surge or quiescent phases due to the tendency of quiescent phases in the region to be longer than the study periods (Copland et al., 2003; Lauzon, 2022; Van Wychen et al., 2016). If Otto Glacier's surge phase is closer to the minimum 26 years, this would be most similar to Chapman Glacier's surge phase, which lies adjacent to Otto Glacier, and also Iceberg Glacier on Axel Heiberg Island. It is possible that Otto and Chapman Glaciers' surges are controlled by common external mechanisms since they are so close in proximity. If a longer surge phase of at least 67 years is the case for Otto Glacier, this would be most similar to Good Friday Bay and Split Lake Glaciers in the Canadian Arctic, which may have similar surge phase durations. In either scenario, Otto Glacier's minimum surge phase is longer than both Alaskan and Svalbard-type surges. The above analysis supports the argument that surges likely do not fit into one of two discreet classes, and likely pertain to a spectrum of dynamic instability globally but especially in the Canadian Arctic, albeit with some similarities (Medrzycka et al., 2019; Van Wychen et al., 2016; Van Wychen et al., 2022).

5.2 Summary of Discussion

The detailed analysis of Otto Glacier's surge cycle has better characterized the dynamic phases for Otto Glacier over 1992-2020. All previous studies of glacier dynamics that include Otto Glacier have only been able to offer brief descriptions of the glacier's speed changes during this time (Copland et al., 2003; Millan et al., 2017; Short and Gray, 2005; Van Wychen et al., 2016; Van Wychen et al., 2020). Specifically, this analysis included suggestions for quiescent and surge phase duration, as well as characterization of how flow speeds change along the glacier in relation to distance from the terminus over time. Additionally, associated geometry changes were discussed, which strengthened the conclusion that Otto Glacier's speed changes are likely related to surging as opposed to other dynamic processes. The analysis also led

to the hypothesis that bedrock sills may regulate speed and geometry changes. The only study that analyzed the bedrock topography under Otto Glacier was Hattersley-Smith (1969), though this analysis was brief and did not make comparisons to velocity variance. This current study went further and demonstrated how velocity changes for Otto Glacier might be regulated by bedrock features. The speed and geometry changes observed over the sill spanning ~4-8 km upglacier are similar to those reported for pulse-types Dobbin and Parish Glaciers (Van Wychen et al., 2016) and Good Friday Bay Glacier (Medrzycka et al., 2019). Lastly, the revelation that Otto Glacier's surge cycle could be unique in the Canadian Arctic and globally adds to the emerging literature claiming that surge behavior consists of a spectrum, rather than discrete classes of dynamic patterns (Medrzycka et al., 2019; Van Wychen et al., 2022).

Chapter 6 - Conclusion

6.1 Thesis Overview

The mass loss observed in glaciers in the Canadian Arctic is unprecedented over recent decades (Hugonnet et al., 2021) and is the third largest contributor to global sea level rise (Derksen et al., 2019). Air temperature is expected to increase under all emission scenarios, and continued glacier mass loss is virtually certain (Derksen et al., 2019). Sea level rise adversely impacts coastal community infrastructure and agriculture (Gingerich et al., 2017) as well as marine ecosystems (Frainer et al., 2017). Sea level rise has accelerated over recent decades (Dieng et al., 2017), and glacier mass loss is estimated to have contributed ~21% of the sea level rise measured over 2000-2019, after the Greenland and Antarctic Ice Sheets (Hugonnet et al., 2021). Dynamic discharge from glaciers (calving of ice into the ocean) is a primary way through which glaciers lose mass to the ocean (Gardner et al., 2018; Mouginot et al., 2014a). As such, understanding the dynamic patterns through which glaciers discharge ice to the ocean is essential for understanding how these patterns might contribute to sea level rise. Glacier surging is one particular motion pattern that is not well studied, especially in the Canadian Arctic. Studies dedicated to individual glaciers provide detailed characterization of velocity changes, associated glacier geometry changes, and possible surge mechanisms, are particularly lacking. Otto Glacier is one surge-type glacier that has been little studied. Hence, the purpose of this study was to provide a detailed analysis of the surge cycle of Otto Glacier over 1992-2020. The research objectives were:

1. characterize Otto Glacier's velocity changes,
2. determine changes in the terminus position,
3. report and compare changes in glacier height over time,
4. map bedrock features under Otto Glacier and determine if/how bedrock features control velocity changes,

5. use the above information to provide a detailed analysis of the Otto Glacier's surge event from 1992-2020 in the context of the Canadian Arctic.

6.2 Thesis summary

6.2.1 Objective 1

Objective 1 was to characterize Otto Glacier's centerline velocity changes using satellite imagery. Specifically, RADAR images from ERS-1 and R2 were used in an offset tracking code to determine glacier velocities, and pre-derived optical velocity products from NASA's ITS_LIVE collection were also used. The period 1992-2008 was considered the fast flow phase of the surge since the fastest velocities (700-1300 m/yr) as well as terminus advance were observed during this time. The next period of 2009-2017 was considered the deceleration phase of the surge, where consistent velocity slowing as well as terminus retreat were observed. During this phase, from 2011-2017, the lowermost ~6 km of the glacier flowed at slower speeds (10-50 m/yr) than the section located ~6-14 km from the terminus (10-120 m/yr). This contrasts with the first phase, where velocity maxima were observed in the lowermost ~6 km. Velocity slowing continued over 2018-2020 and by this time reached values consistent with the quiescent phase of surge-type glaciers, hence this period was termed the quiescent phase.

An important observation was that over the entire study period, the greatest centerline velocity variability was restricted to the region of ice that is downglacier of the sill's midpoint (~6 km upglacier of the terminus). This area of maximal velocity variability is also the area of glacier that lies at or below sea-level, as seen in pulse-type glaciers. However, unlike pulse-type glaciers, the entire main trunk of Otto Glacier was flowing at higher-than-normal speeds during the surge. This combination of findings could be evidence of a pulse superimposed on a surge.

6.2.2 Objective 2

Objective 2 was to assess changes in terminus extent over the study period, using manually delineated terminus extents from ERS-1, R2, and Landsat imagery. The terminus was determined to have

advanced 1527 m over 1992-2001. No change was observed over 2001-2010. The first terminus retreat was observed in 2011 which persisted into 2016, retreating a total of 1286 m since 2010 (excludes values within the error bounds). From 2017-2020, no change was observed. The advance from 1992-2001 coincides with times of the highest flow speeds, suggesting that mass was rapidly transferred to the terminus as occurs during surges (Benn and Evans, 2010). The lack of change observed over 2002-2010 could be related to exhaustion of the transfer of mass to the terminus following the years of faster flow. Eventually, so little mass was transferred to the terminus that it began retreating due to ocean and atmospheric-induced melting. Regarding why no further retreat was observed in 2018-2020, this could be due to the bedrock sill located at ~4-8 km from the terminus, which may act a pinning point that stabilizes the glacier from further retreat by obstructing flow over and upglacier of the sill, in turn causing an accumulation of ice upglacier that continually replenishes mass ablated in this area.

6.2.3 Objective 3

Objective 3 was to analyze changes in glacier height over time using already-differenced elevation time series products from Hugonnet et al. (2021). The elevation data were only available for 2000-2019. Thinning was progressive in the lowermost ~6 km of the glacier throughout this period, while thickening upglacier of ~6 km from the terminus was progressive from 2010 to the end of the study period. Initial thinning in the lower region was inferred to be a result of dynamic thinning during the surge. The persistent thinning into the later years was concluded to have been caused by the exhaustion incoming mass from upglacier after the surge, which is a consequence of slowing velocities. Furthermore, the obstruction of incoming mass over the sill likely exacerbated the thinning. The progressive thickening upglacier of ~6 km from the terminus is a result of faster flowing ice from the lower-mid section of the glacier (~6-14 km from the terminus) flowing into the slower flowing ice downglacier, which began in phase II when the lowermost ~6 km of the glacier became slower than the ice upglacier. The obstruction of the faster flowing ice results in mass accumulation and thickening upglacier (Cuffey and Paterson,

2010). It is also likely that the sill spanning the region ~4-8 km from the terminus exacerbated the obstruction and thickening upglacier, as seen in other glaciers in the Canadian Arctic such as Good Friday Bay Glacier (Medrzycka et al., 2019) and Dobbin and Parish Glaciers (Van Wychen et al., 2016).

6.2.4 Objective 4

Objective 4 was to map bedrock features under Otto Glacier and determine how this might control velocity variability. The v-shaped bedrock sill spanning the region ~4-8 km upglacier from the terminus was identified as the most important bedrock feature that likely influenced centerline velocity variability. The main finding supporting this idea is that centerline velocities intersect the sill at its midpoint, located ~6 km from the terminus, and the greatest velocity variability was found downglacier of this point (800-1100 m/yr). The key effect of the sill would be ice thickening over the sill. The thickening then likely increases glacier surface slope and driving stress until a pressure threshold was reached, at which time a surge is triggered over the impedance. The surge results in fast flowing ice over and downglacier of the impedance, which is restrained by the slower flowing ice upglacier of the impedance. The resulting extension leads to dynamic thinning in the area downglacier of the impendence. The thinning here reduces driving stress in this section, and in turn, velocity slows in this section over time. The progressive slowing leads to quiescence, until the cycle repeats as mass re-accumulates over the impedance and a pressure threshold is reached again (Cuffey and Paterson, 2010; Van Wychen et al., 2016). A similar process has been described in the Canadian Arctic for Good Friday Bay Glacier on Axel Heiberg Island (Medrzycka et al., 2019). For Good Friday Bay Glacier, the highest velocities were measured immediately downglacier of the nunatak located at ~9 km from the terminus and thickening over and upglacier of the nunatak. Other reports include the pulse-types Dobbin and Parish Glaciers, which are underlaid by sills that are hypothesized to have a similar effect on geometry and velocity changes (Van Wychen et al., 2016). Based on these studies and the findings for Otto Glacier, there is growing evidence that bedrock bumps may control oscillating velocity patterns.

6.2.5 Objective 5

Objective 5 was to use the findings from objectives 1-4 to provide a detailed analysis of the Otto Glacier's surge event from 1992-2020 in the context of the Canadian Arctic. The exact start of the surge and quiescent phases were unable to be confirmed since observations are not available from 1965-1990. In terms of possible phase durations, Otto Glacier's surge phase has been confirmed to be a minimum of 26 years, starting at least as early as 1991 when including data from Millan et al. (2017) and ending in 2017. The quiescent phase may have lasted either a maximum of 25 years (1965 until 1990 or earlier) or an indeterminable amount of time, since a quiescent phase may not have occurred during the observation gap over 1965-1990, and a full quiescent phase has not been observed at any other time. Regardless of the exact surge duration, the cycle for Otto Glacier is noteworthy, since the minimum surge phase of 26 years is longer than surge phases of Alaskan or Svalbard-types.

Unfortunately, it is difficult to compare Otto Glacier's surge duration to other surge-type glaciers in the Canadian Arctic since observations for Otto Glacier from 1965-1990 are not available to quantify the exact surge duration. The comparison is also complicated by the issue that many studies of other surge-type glaciers in the Canadian Arctic do not capture a complete surge cycle, due to the tendency of glaciers in this region to have surge cycles that are longer than the study periods (Copland et al., 2003; Lauzon, 2022; Van Wychen et al., 2016). If Otto Glacier's surge is closer to 26 years, its surge would be most similar to that of its neighbor Chapman Glacier which has an estimated active phase of at least 20 years (Van Wychen et al., 2016), and would also be similar to Iceberg Glacier on Axel Heiberg Island with a surge phase of at least 22 years (Lauzon, 2022). It is possible that Otto and Chapman Glaciers' surges are driven by common external factors, such as bedrock features or local climate. If Otto Glacier's surge began earlier than 1950 and continued until 2017, Otto Glacier would have an active phase of surge phase of at least ~67 years (1950-2017) and this scenario aligns more with the prolonged surges observed for Good

Friday Bay Glacier (fast flow since the 1950s) (Medrzycka et al., 2019) and Split Lake Glacier (fast flow since the 1970s) (Van Wychen et al., 2022).

6.3 Limitations

One of the greatest limitations of the study is that velocity and geometry data from 1965-1990 were not included in the analysis and have not been analyzed elsewhere. This precludes a precise estimation of the surge and quiescent phases for Otto Glacier, though it is certain that the surge duration is at least 26 years based on the results of this thesis. The lack of observations during 1965-1990 hinder comparison to other glaciers in the Canadian Arctic, which in turn hinders understanding of surge mechanisms in the region. For example, if surge-type glaciers in the Canadian Arctic were known to have similar cycle durations, this could support a hypothesis that surges within defined regions are regulated by common external variables, such as climate, as suggested by Sevestre and Benn (2015). However, if surge-type glaciers within the region were known to have dissimilar cycle durations, the above hypothesis could be refuted, and surge mechanisms could then be attributed to internal factors unique to each glacier, such as glacier geometry (Sevestre and Benn, 2015), hydrology (Kamb et al., 1985), thermal gradients (Murray et al., 2003), and bedrock bumps (Medrzycka et al., 2019; Van Wychen et al., 2016). It is also possible that both external and individual internal factors regulate surging. More studies on surge cycle durations in the Canadian Arctic are needed to better ascertain the influence of these mechanisms on surging. Another limitation is that the association between bedrock features and velocity variability does not necessarily equate to causation. To more definitively determine that bedrock features control oscillatory velocities, statistical studies would be needed to determine the degree of correlation between these two variables, whilst also including a large sample size of glaciers (discussed further in Section 6.4).

The analysis also did not include data for bedrock lithology or basal hydrology, both of which are known to impact glacier surging (Benn and Evans, 2010; Kamb et al., 1985; Murray et al., 2003). While the study did conclude that a bedrock sill likely controlled speed changes, this is just one of many factors that

may regulate surging. Another limitation is that few summer data were usable, i.e., the offset tracking produced erroneous results during summer months. This is likely because melt water on the glacier surface can distort backscatter leading to large errors (Short and Gray, 2005). This constraint prevented correlation of velocity changes with seasonal changes, which may have led to insights into how basal melt water controls surging for Otto Glacier. Air temperature data would offer similar insights but were not included. Air temperature analyses could have also supported hypotheses on how climate change affects surging in the Canadian Arctic. Such analyses would build on the work of Sevestre and Benn (2015), who proposed that surge behavior is correlated with climate characteristics (i.e., surge-type glaciers exist in either a cold-dry or temperate climate and are rare in warmer wetter climates).

6.4 Future work

Future studies should analyze velocity and geometry data for Otto Glacier from 1965-1990 to clarify the question of how long the surge phase really is. If imagery covering Otto Glacier is available for this period (such as from ERS, Landsat, RADARSAT1, or aerial imagery from the Royal Canadian Air Force), it could be used to determine whether Otto Glacier's first observed surge in 1950-1964 continued until 1991, or if the 1950-1964 surge ended prior to the next observed surge in 1991, or if the 1950-1964 surge started earlier than 1950. Otto Glacier's surge duration could then be better quantified, and this would help comparison of its behavior to other glaciers in the Canadian Arctic. Further to this point, more studies that capture full surge and/or quiescent phases of other glaciers should be conducted for this region. Comparisons of surge/quiescent phase durations here would enhance hypotheses on whether external or individual internal factors, or both, regulate surging in the Canadian Arctic (as discussed in Section 6.3).

In terms of factors that control the surge of Otto Glacier, this study only considered bedrock topography as a possible control for the surge. However, analysis of the hydrology system of Otto Glacier would help support or rule out other potential hypotheses. This could be approached in several ways. One option is to use remotely sensed data to measure changes in glacier surface melt lake area and correlate

this to velocity changes. Reduction in surface lake area can be an indicator of drainage of surface water to the base of the glacier, which would then facilitate basal sliding (as in Nikolić, 2023). Another option would be to use either remotely sensed or field data to measure any basal water output and correlate this with velocity changes (as in Kamb et al., 1985). Additionally, bedrock lithology, specifically deformability, has not been analyzed for Otto Glacier, but has been implicated in surging of Svalbard-type glaciers (Murray et al., 2003). One way to measure bedrock deformability would be to measure changes in bedrock elevation profiles over time. This thesis only used bedrock data captured in 2014. Changes in bedrock deformability could then be compared to velocity changes over time and along the length of the glacier. Finally, seasonal changes of Otto Glacier's velocity would also give insight into factors that control the surge cycle. Analysis of seasonal velocity changes and seasonal climate could support hypotheses on how air temperature and precipitation changes impact surge timing. Optical imagery would be particularly useful for this analysis, since feature tracking algorithms are not impacted by summer surface melt in the way that offset tracking is negated by this issue (Short and Gray, 2005). NASA's ITS_LIVE data base can be used to obtain images at user-determined dates starting in 1985, accessible through the ITS_LIVE widget at https://itslive-dashboard.labs.nsidc.org/.

To strengthen the argument that bedrock topography may modulate oscillatory velocity changes, statistical studies such as tests for statistical significance, correlation, and regression studies could be conducted. It is possible that bedrock bumps underlie normal-type glaciers without affecting their velocity variability, and this could disprove the hypothesis that bedrock features control surging. To prove or disprove the hypothesis, studies that compare bedrock under surge-type glaciers to bedrock under normal glaciers (the control group) are required. These studies would use statistical tests (e.g. a chi-square test) to determine if there is a statistically significant difference in the presence of bedrock bumps under surge-type and normal glaciers. If a significant difference is confirmed (that bedrock bumps occur more often under surge-type glaciers), correlation studies would be the next step to determine if there is a correlation

between bedrock and velocity variability. Finally, if correlation is confirmed, a regression analysis of bedrock bumps and velocity variability would determine the degree of the correlation. Large sample sizes of glaciers would strengthen the reliability of these analyses.

In terms of multidisciplinary application, this thesis contributes a foundation for glacier dynamics modelling, which can predict how glaciers behave globally. This becomes very useful for more remote locations, such as the Antarctic Ice Sheet, which is difficult to access for field data. Specifically, velocity data can be used to build models of dynamic changes over time, as well as models for ice discharge to the ocean. Ice discharge to the ocean increases as velocity and glacier surface height increase, as in Equation 6-1 (Van Wychen et al., 2016):

Equation 6-1: Ice discharge calculation.

$$\text{Ice discharge} = (V + V_{error}) \times (H + H_{error})$$

where V is velocity, and H is height.

Therefore, the timing of glacier velocity changes directly affects ice discharge to the ocean over time. Models for ice discharge can then be used for projections of sea level rise, which is important in the context of climate change. Furthermore, firm evidence that surge and pulse-type glaciers have varying phase durations within the same region would improve the accuracy of ice discharge calculations on a regional level, since this evidence would prevent models from assuming that all glaciers in one region undergo the same dynamic changes.

6.5 Thesis Significance

This thesis has both clarified and identified outstanding issues regarding the quantification of Otto Glacier's surge cycle duration by providing a detailed analysis of velocity changes over 1992-2020. Most previous studies that included Otto Glacier were only able to provide brief reports in this regard, as these were regional studies that provided an overview of multiple glaciers (Copland et al., 2003; Millan et al., 2017; Short and Gray, 2005; Van Wychen et al., 2016; Van Wychen et al., 2020). Furthermore, this study

has also characterized how velocity varies along the main trunk of the glacier and even identified that both pulsing and surging may be co-occurring, where the greatest velocity variability occurs in the area below sea level (as in pulsing), but the entire main trunk is flowing at higher than normal speeds.

Analysis of changes in terminus extent and glacier surface elevation affirmed that Otto Glacier's dynamic changes were likely related to surging, as evidenced by terminus advance coincident with acceleration, terminus retreat coincident with deceleration, and glacier thickening during quiescence. Perhaps most importantly, the analysis of bedrock topography and velocity variance is relatively novel and has only been done for a few other glaciers in the Canadian Arctic: the pulse-types Dobbin and Parish Glaciers (Van Wychen et al., 2016) and Good Friday Bay Glacier (Medrzycka et al., 2019). Discussion of bedrock under Otto Glacier was initially presented by Hattersley-Smith (1969), however, this analysis was limited and did not compare bedrock features to velocity changes. This thesis addressed the gap by comparing bedrock features and velocity variance. The results add to the growing body of literature that suggests bedrock bumps may modulate surging and pulsing, where the glacier thickens over the bump, increases driving stress, surges over the bump, until enough dynamic thinning occurs that driving stress is reduced and quiescence ensues (Cuffey and Patterson, 2010). Finally, the uniqueness of Otto Glacier's minimum surge phase duration (compared to Alaskan and Svalbard-types), supports emerging ideas that oscillatory dynamic changes are better conceived of as a spectrum, rather than consisting of discrete classes (Medrzycka et al., 2019; Van Wychen et al., 2022). However, longer study periods are required for Otto Glacier as well as other surge-type glaciers in the Canadian Arctic to capture full surge and/or quiescent cycles and thus support comparison between glaciers.

References

Arctic Monitoring and Assessment Programme (AMAP) (2017): Adaptation Actions for a Changing Arctic: Perspectives from the Bering-Chukchi-Beaufort Region. *Arctic Monitoring and Assessment Programme (AMAP),* Oslo, Norway, xiv + 255.

Benn, D., and Evans, D. (2010). *Glaciers and Glaciation*. 2nd Ed. Routledge: Taylor and Francis Group, London and New York.

Benn, D. I., Fowler, A. C., Hewitt, I., and Sevestre, H. (2019a). A general theory of glacier surges. *Journal of Glaciology*, *65*(253), 701–716. https://doi.org/10.1017/JOG.2019.62

Benn, D. I., Jones, R. L., Luckman, A., Fürst, J. J., Hewitt, I., and Sommer, C. (2019b). Mass and enthalpy budget evolution during the surge of a polythermal glacier: a test of theory. *Journal of Glaciology*, *65*(253), 717–731. https://doi.org/10.1017/JOG.2019.63

Bindschadler, R., Harrison, W. D., Raymond, C. F., Gannet, C. (1976). Thermal Regime of a Surge-Type Glacier. *Journal of Glaciology*, *16*(74), 251–259. https://www.cambridge.org/core.

Bindschadler, R., Harrison, W. D., Raymond, C. F., and Crosson, R. (1977). Geometry and Dynamics of a Surge-type Glacier. *Journal of Glaciology*, *18*(79), 181–194. https://doi.org/10.3189/S0022143000021298

Brown, L. and Duguay, C. (2010). The response and role of ice cover in lake-climate interactions; Progress in Physical Geography, *34*(5). https://doi.org/10.1177/0309133310375653

Brown, R., Schuler, D., Bulygina, O., Derksen, C., Luojus, K., Mudryk, L., Wang, L. and Yang, D. (2017): Arctic terrestrial snow; in Snow Water Ice and Permafrost in the Arctic (SWIPA) 2017 Assessment, Arctic Monitoring and Assessment Programme, Oslo, Norway, p. 40.

Clarke, G. K. C., Collins, S. G., and Thompson, D. E. (1984). Flow, thermal structure, and subglacial conditions of a surge- type glacier. *Canadian Journal of Earth Sciences*, *21*(2), 232–240. https://doi.org/10.1139/E84-024

Cuffey, K. M. and Paterson, W.S.B. (2010). The physics of glaciers. Butterworth-Heinemann/Elsevier: Burlington, MA.

Copland, L., Sharp, M. J., and Dowdeswell, J. A. (2003). The distribution and flow characteristics of surge-type glaciers in the Canadian High Arctic. *Annals of Glaciology*, *36*, 73–81. https://doi.org/https://doi.org/10.3189/172756403781816301

Dalton, A., Van Wychen, W., Copland, L., Gray, L., and Burgess, D. (2022). Seasonal and Multiyear Flow Variability on the Prince of Wales Icefield, Ellesmere Island: 2009–2019. *Journal of Geophysical Research: Earth Surface*, *127*(4). https://doi.org/10.1029/2021JF006501

Dibike, Y., Prowse, T., Bonsal, B., de Rham, L. and Saloranta, T. (2012). Simulation of North American lake-ice cover characteristics under contemporary and future climate conditions. *International Journal of Climatology*, *32*(5), 695–709. https://doi:10.1002/joc.2300

Dieng, H. B., Cazenave, A., Meyssignac, B., and Ablain, M. (2017). New estimate of the current rate of sea level rise from a sea level budget approach. *Geophysical Research Letters*, *44*(8), 3744–3751. https://doi.org/10.1002/2017GL073308

Dowdeswell, J., Hamilton, G. S., and Hagen, J.O. (1991). The duration of the active phase on surge-type glaciers: contrasts between Svalbard and other regions. *Journal of Glaciology*, *37*(127), 388–400. https://doi.org/10.3189/S0022143000005827

Echelmeyer, K., Butterfield, R., and Cuillard, D. (1987). Some Observations on a Recent Surge of Peters Glacier, Alaska, U.S.A. *Journal of Glaciology*, *33*(115), 341–345. https://doi.org/https://doi.org/10.3189/S0022143000008935

Eisen, O., Harrison, W. D., Raymond, C. F., Echelmeyer, K. A., Bender, G. A., and Gorda, J. L. D. (2005). Variegated Glacier, Alaska, USA: a century of surges. *Journal of Glaciology*, *51*(174), 399–406. https://doi.org/10.3189/172756505781829250

Enderlin, E. M., Carrigan, C. J., Kochtitzky, W. H., Cuadros, A., Moon, T., and Hamilton, G. S. (2018). Greenland iceberg melt variability from high-resolution satellite observations. *Cryosphere*, *12*(2), 565–575. https://doi.org/10.5194/TC-12-565-2018

European Space Agency. (n.d.). *SAR (ERS) Overview - Earth Online*. Retrieved April 2, 2023, from https://earth.esa.int/eogateway/instruments/sar-ers/description

European Space Agency. (2012). *ERS-1 (European Remote-Sensing Satellite-1)*. https://www.eoportal.org/satellite-missions/ers-1#mission-capabilities

Fowler, A. C., Murray, T., and Ng, F. S. L. (2001). Thermally controlled glacier surging. *Journal of Glaciology*, *47*(159), 527–538. https://doi.org/10.3189/172756501781831792

Frainer, A., Primicerio, R., Kortsch, S., Aune, M., Dolgov, A. V, Fossheim, M., and Aschan, M. M. (2017). Climate-driven changes in functional biogeography of Arctic marine fish communities. *Proceedings of the National Academy of Sciences of the United States of America*, *114*(46), 12202–12207. https://doi.org/10.2307/26486550

Gardner, A. S., M.A. Fahnestock, and T. A. Scambos. (2019). *ITS_LIVE Regional Glacier and Ice Sheet Surface Velocities. Data archived at National Snow and Ice Data Center. doi:10.5067/6II6VW8LLWJ7*. https://its-live.jpl.nasa.gov/

Gardner, A. S., Moholdt, G., Scambos, T., Fahnstock, M., Ligtenberg, S., van den Broeke, M., and Nilsson, J. (2018). Increased West Antarctic and unchanged East Antarctic ice discharge over the last 7 years. *Cryosphere*, *12*(2), 521–547. https://doi.org/10.5194/TC-12-521-2018

Gingerich, S. B., Voss, C. I., and Johnson, A. G. (2017). Seawater-flooding events and impact on freshwater lenses of low-lying islands: Controlling factors, basic management and mitigation. *Journal of Hydrology*, *551*, 676–688. https://doi.org/10.1016/J.JHYDROL.2017.03.001

Government of Canada. (2015). *Radar Basics*. https://natural-resources.canada.ca/maps-tools-and-publications/satellite-imagery-and-air-photos/tutorial-fundamentals-remote-sensing/microwave-remote-sensing/radar-basics/9355

Government of Canada. (2021). *RADARSAT satellites: Technical comparison*. https://www.asc-csa.gc.ca/eng/satellites/radarsat/technical-features/radarsat-comparison.asp

Hamilton, G. S., and Dowdeswell, J. A. (1996). Controls on glacier surging in Svalbard. *Journal of Glaciology*, *42*(140), 157–168. https://doi.org/10.3189/S0022143000030616

Harrison, W. D., Echelmeyer, K. A., Chacho, E. F., Raymond, C. F., and Benedict, R. J. (1994). The 1987-88 Surge of West Fork Glacier, Susitna Basin, Alaska, U.S.A. *Journal of Glaciology*, *40*(135), 241–254. https://doi.org/10.1017/S0022143000007334

Hattersley-Smith, G. (1964). Rapid Advance of Glacier in Northern Ellesmere Island. *Nature*, *201*, 176–176. https://doi.org/10.1038/201176A0

Hattersley-Smith, G. (1969). Recent observations on the surging Otto Glacier, Ellesmere Island. *Canadian Journal of Earth Sciences*, *6*(4), 883–889. https://doi.org/10.1139/E69-090

Herzfeld, U. C., and Mayer, H. (1997). Surge of Bering Glacier and Bagley Ice Field, Alaska: an up-date to August 1995 and an interpretation of brittle-deformation patterns. *Journal of Glaciology*, *43*(145), 427–434. https://doi.org/https://doi.org/10.3189/S0022143000035012

Hugonnet, R., McNabb, R., Berthier, E., Menounos, B., Nuth, C., Girod, L., Farinotti, D., Huss, M., Dussaillant, I., Brun, F., and Kääb, A. (2021). Accelerated global glacier mass loss in the early twenty-first century. *Nature*, *592*(7856), 726–731. https://doi.org/10.1038/s41586-021-03436-z

Iken, A. (1981). The Effect of the Subglacial Water Pressure on the Sliding Velocity of a Glacier in an Idealized Numerical Model. *Journal of Glaciology*, *27*(97), 407–421. https://doi.org/10.1017/S0022143000011448

IPCC. (2019). *IPCC SROCC Summary For Policy Makers*. Hamish Pritchard.

Jeffries, M. O. (1984). Milne Glacier, Northern Ellesmere Island, N.W.T., Canada: A Surging Glacier? *Journal of Glaciology*, *30*(105), 251–253. https://doi.org/10.3189/S0022143000006043

Jiskoot, H. (2011). Glacier surging. *Encyclopedia of Earth Sciences Series*, *Part 3*, 415–428. https://doi.org/10.1007/978-90-481-2642-2_559

Jiskoot, H., Boyle, P., and Murray, T. (1998). The incidence of glacier surging in Svalbard: evidence from multivariate statistics. *Computers and Geosciences*, *24*(4), 387–399. https://doi.org/10.1016/S0098-3004(98)00033-8

Kamb, B. (1987). Glacier surge mechanism based on linked cavity configuration of the basal water conduit system. *Journal of Geophysical Research*, *92*(B9), 9083–9100. https://doi.org/10.1029/JB092iB09p09083

Kamb, B., Raymond, C. F., Harrison, W. D., Engelhardt, H., Echelmeyer, K. A., Humphrey, N., Brugman, M. M., and Pfeffer, T. (1985). Glacier Surge Mechanism: 1982-1983 Surge of Variegated Glacier, Alaska. *New Series*, *227*(4686), 469–479. https://doi.org/10.1126/science.227.4686.469

Lauzon, B. (2022). *Glacier Surge Dynamics on Western Axel Heiberg Island, Nunavut*.[Master's thesis, University of Ottawa]. University of Ottawa Research.

Medrzycka, D., Copland, L., Van Wychen, W., and Burgess, D. (2019). Seven decades of uninterrupted advance of Good Friday Glacier, Axel Heiberg Island, Arctic Canada. *Journal of Glaciology*, *65*(251), 440–452. https://doi.org/10.1017/jog.2019.21

Millan, R., Mouginot, J., and Rignot, E. (2017). *Mass budget of the glaciers and ice caps of the Queen Elizabeth Islands, Canada, from 1991 to 2015*. https://doi.org/10.1088/1748-9326/aa5b04

Mortimer, C. A., Sharp, M., and Van Wychen, W. (2018). Influence of recent warming and ice dynamics on glacier surface elevations in the Canadian High Arctic, 1995-2014. *Journal of Glaciology*, *64*(245), 450–464. https://doi.org/10.1017/jog.2018.37

Motyka, R. J., Hunter, L., Echelmeyer, K. A., and Connor, C. (2003). Submarine melting at the terminus of a temperate tidewater glacier, LeConte Glacier, Alaska, U.S.A. *Annals of Glaciology*, *36*, 57–65. https://doi.org/10.3189/172756403781816374

Mouginot, J., Rignot, E., and Scheuchl, B. (2014a). Sustained increase in ice discharge from the Amundsen Sea Embayment, West Antarctica, from 1973 to 2013. *Geophysical Research Letters*, *41*(5), 1576–1584. https://doi.org/10.1002/2013GL059069

Mouginot, J., Rignot, E., and Scheuchl, B. (2014b). Sustained increase in ice discharge from the Amundsen Sea Embayment, West Antarctica, from 1973 to 2013. *Geophysical Research Letters*, *41*(5), 1576–1584. https://doi.org/10.1002/2013GL059069

Mudryk, L., Derksen, C., Howell, S., Laliberté, F., Thackeray, C., Sospedra-Alfonso, R., Vionnet, V., Kushner, P. and Brown, R. (2018). Canadian snow and sea ice: historical trends and projections. *The Cryosphere, 12*, 1157–1176. https://doi:10.5194/tc-12-1157-2018

Müller, F. (1969). Was the Good Friday Glacier on Axel Heiberg Island surging? *Canadian Journal of Earth Sciences*, *6*(4), 891–894. https://doi.org/10.1139/E69-091

Murray, T., Dowdeswell, J. A., Drewry, D. J., and Frearson, I. (1998). Geometric evolution and ice dynamics during a surge of Bakaninbreen, Svalbard. *Journal of Glaciology*, *44*(147), 263–272. https://doi.org/10.1017/S0022143000002604

Murray, T., Strozzi, T., Luckman, A., Jiskoot, H., and Christakos, P. (2003). Is there a single surge mechanism? Contrasts in dynamics between glacier surges in Svalbard and other regions. *Journal of Geophysical Research: Solid Earth*, *108*(B5). https://doi.org/10.1029/2002JB001906

NASA. (2021). *What is Synthetic Aperture Radar?* https://www.earthdata.nasa.gov/learn/backgrounders/what-is-sar

National Snow and Ice Data Centre. (2013). *IceBridge MCoRDS L3 Gridded Ice Thickness, Surface, and Bottom, Version 2 | National Snow and Ice Data Center*. https://nsidc.org/data/irmcr3/versions/2

Noël, B., van de Berg, W. J., Lhermitte, S., Wouters, B., Schaffer, N., and van den Broeke, M. R. (2018). Six decades of glacial mass loss in the Canadian Arctic Archipelago. *Journal of Geophysical Research: Earth Surface*, *123*(6), 1430–1449. https://doi.org/10.1029/2017JF004304

Ødegård, R. S., Hagen, J. O., and Hamranw, S.-E. (1997). Comparison of radio-echo sounding (30–1000 MHz) and high-resolution borehole-temperature measurements at Finsterwalderbreen, southern

Spitsbergen, Svalbard. *Annals of Glaciology*, *24*, 262–267. https://doi.org/10.3189/S0260305500012271

Olefeldt, D., Goswami, S., Grosse, G., Hayes, D., Hugelius, G., Kuhry, P., Mc - Guire, A., Romanovsky, V., Sannel, A., Schuur, E. and Turetsky, M. (2016). Circumpolar distribution and carbon storage of thermokarst landscapes. *Nature Communications*, *7*(1), 1–11. https://doi:10.1038/ncomms13043

Paden, J., Li, J., Leuschen, C., Rodriguez-Morales, F., and Hale, R. (2013). IceBridge MCoRDS L3 Gridded Ice Thickness, Surface, and Bottom, Version 2. *Boulder, Colorado USA. NASA National Snow and Ice Data Center Distributed Active Archive Center*. https://doi.org/10.5067/YP1PVPR72IHG

Pizzolato, L., Howell, S., Dawson, J., Laliberté, F. and Copland, L. (2016): The influence of declining sea ice on shipping activity in the Canadian Arctic. *Geophysical Research Letters*, *43*(23). https://doi:10.1002/2016GL071489

Qiu, J. (2017). *Why slow glaciers can sometimes surge as fast as a speeding train—wiping out people in their path | Science | AAAS*. https://www.science.org/content/article/why-slow-glaciers-can-sometimes-surge-fast-speeding-train-wiping-out-people-their-path

Raymond, C.F. (1987) How do glaciers surge? A review. *Journal of Geophysical Research, 92*(B9), 9121–9134. https://doi: 10.1029/JB092iB09p09121

Romanovsky, V., Smith, S., Isaksen, K., Shiklomanov, N., Streletskiy, D., Kholodov, A. Christiansen, H., Drozdov, D., Malkova, G. and Marchenko, S. (2017): Terrestrial Permafrost; in Arctic Report Card 2017, (ed.) J. Richter-Menge, J.E. Overland, J.T. Mathis, and E. Osborne.

Rothlisberge, H. (1972). Water Pressure in Intra- and Subglacial Channels. *Journal of Glaciology*, *11*(62), 177–203. https://doi.org/10.3189/S0022143000022188

Sergienko, O. (2012) The effects of transverse bed topography variations in ice-flow models. *Journal of Geophysical Research, 117*(F3), https://doi: 10.1029/2011JF002203

Sevestre, H., and Benn, D. I. (2015). Climatic and geometric controls on the global distribution of surge-type glaciers: implications for a unifying model of surging. *Journal of Glaciology*, *61*(228), 646–662. https://doi.org/10.3189/2015JOG14J136

Sharp, M. (1988). Surging glaciers: behaviour and mechanisms. *Progress in Physical Geography*, *12*(3), 349–370. https://doi.org/10.1177/030913338801200302

Short, N. H., and Gray, A. L. (2004). Potential for RADARSAT-2 interferometry: glacier monitoring using speckle tracking. *Canadian Journal of Remote Sensing, 30*(3), 504-509. https://doi.org/10.5589/m03-071

Short, N. H., and Gray, A. L. (2005). Glacier dynamics in the Canadian High Arctic from RADARSAT-1 speckle tracking. *Canadian Journal of Remote Sensing*, *31*(3), 225–239. https://doi.org/10.5589/m05-010

Sturm, M., Goldstein, M., Huntington, H. and Douglas, T. (2016). Using an option pricing approach to evaluate strategic decisions in a rapidly changing climate. *Climatic Change, 140*, 437–449. https://doi:10.1007/s10584-016-1860-5

Sturm, M., Goldstein, M. and Parr, C. (2017). Water and life from snow: A trillion-dollar science question. *Water Resources Research*, *53*(5), 3534–3544. https//doi:10.1002/2017WR020840

Strozzi, T., Luckman, A., Murray, T., Wegmüller, U., and Werner, C. L. (2002). Glacier motion estimation using SAR offset-tracking procedures. *IEEE Transactions on Geoscience and Remote Sensing*, *40*(11), 2384–2391. https://doi.org/10.1109/TGRS.2002.805079

Van Den Broeke, M. R., Enderlin, E. M., Howat, I. M., Munneke, P. K., Noël, B. P. Y., Van De Berg, W. J., Van Meijgaard, E., and Wouters, B. (2016). On the recent contribution of the Greenland ice sheet to sea level change. *The Cryosphere*, *10*, 1933–1946. https://doi.org/10.5194/tc-10-1933-2016

Van Wychen, W., Burgess, D., Kochtitzky, W., Nikolic, N., Copland, L., and Gray, L. (2020). RADARSAT-2 Derived Glacier Velocities and Dynamic Discharge Estimates for the Canadian High Arctic: 2015–2020. *Canadian Journal of Remote Sensing*, *46*(6), 695–714. https://doi.org/10.1080/07038992.2020.1859359

Van Wychen, W., Burgess, D. O., Gray, L., Copland, L., Sharp, M., Dowdeswell, J. A., and Benham, T. J. (2014). Glacier velocities and dynamic ice discharge from the Queen Elizabeth Islands, Nunavut, Canada. *Geophysical Research Letters*, *41*(2), 484–490. https://doi.org/10.1002/2013GL058558

Van Wychen, W., Davis, J., Burgess, D. O., Copland, L., Gray, L., Sharp, M., and Mortimer, C. (2016). Characterizing interannual variability of glacier dynamics and dynamic discharge (1999–2015) for the ice masses of Ellesmere and Axel Heiberg Islands, Nunavut, Canada. *Journal of Geophysical Research: Earth Surface*, *121*, 39–63. https://doi.org/10.1002/2015JF003708

Van Wychen, W., Hallé, D. A. M., Copland, L., and Gray, L. (2022). Anomalous surface elevation, velocity, and area changes of Split Lake Glacier, western Prince of Wales Icefield, Canadian High Arctic. https://doi.org/10.1139/AS-2021-0039

Wu, X., Jezek, K. C., Rodriguez, E., Gogineni, S., Rodriguez-Morales, F., and Freeman, A. (2011). Ice Sheet Bed Mapping with Airborne SAR Tomography. *IEEE Transactions on Geoscience and Remote Sensing*, *49*(10). https://doi.org/10.1109/TGRS.2011.2132802